Fault Simulator

For Proportional Solenoid Valves

A Thesis Submitted to the

College of Graduate Studies and Research

in Partial Fulfillment of the Requirements

for the Degree of Master of Science

in the

Department of Mechanical Engineering

University of Saskatchewan

Saskatoon, Saskatchewan

By

Amit Bhojkar

July 2004

Permission to Use

In presenting this thesis in partial fulfillment of the requirements for a Postgraduate degree from the University of Saskatchewan, I agree that the Libraries of this University may make it freely available for inspection. I further agree that permission for copying this thesis in any manner, in whole or in part, for scholarly purposes, may be granted by the professors who supervised my thesis work or, in their absence, by the Head of the Department or Dean of the College in which my thesis work was done. It is understood that any copying, publication or use of this thesis or parts thereof for financial gain shall not be allowed without my written permission. It is also understood that due recognition shall be given to me and to the University of Saskatchewan in any scholarly use which may be made of any material in my thesis.

Requests for permission to copy or to make other use of material in this thesis, in whole or in part, should be addressed to:

Head of the Department of Mechanical Engineering

University of Saskatchewan

Engineering Building

57 Campus Drive

Saskatoon, Saskatchewan, S7N 5A9

Canada

Abstract

Proportional Solenoid Valves (PSV) have been successfully used in the hydraulic industry for many years due to the benefits associated with higher accuracy compared to on/off solenoid valves, and the robustness and cost compared to servo valves. Because the PSV plays an important role in the performance of a hydraulic system, a technique commonly referred to as Condition Monitoring Scheme (CMS) has been used extensively to monitor the progress of faults in the PSV. But before any CMS can be implemented on a system, it needs to be thoroughly tested for its reliability of fault detection since, a failure of the CMS to detect any potential fault can be economically disastrous, and dangerous in terms of the safety of personnel. The motivation of this research was to develop a fault simulator which could reliably and repeatedly induce user defined faults in the PSV and thereby aid in testing the efficacy of the CMS for monitoring such simulated faults.

Industry research has revealed that the most common mode of failure in spool valves is an increase in the friction between the spool and valve, due to wear, contamination and dirt, which renders the valve inoperable. In this research, a non-destructive fault simulator was developed which induced artificial friction faults in the PSV. The PSV consisted of two solenoids on the opposite sides of the valve spool by virtue of which, bi-directional position control could be achieved.The PSV with the spool and one of the solenoids was used as the system in which the faults were simulated, and the second solenoid was used an a fault simulator for inducing the desired friction characteristics in the system.

The friction characteristics induced in the valve were similar to those in the classical friction curve, i.e., stiction at low velocities and Coulomb and viscous friction at higher velocities. By employing a closed loop position control scheme, one of the solenoids was used to generate a linearly increasing velocity profile by virtue of which the desired friction characteristics could be induced in different velocity regimes. The other solenoid was used to generate the desired friction force. A closed loop force control strategy,

which used the feedback from a force transducer, allowed for the accurate control of the friction characteristics. stiction was induced at low velocities by passing the required current in both the solenoids that resulted in no net force on the valve spool. Due to the absence of any driving force the spool was stalled at the desired location, thus achieving the same effect of stiction at low velocities. The coulomb and viscous friction were induced at higher velocities by employing an algorithm which was a function of the spool velocity. Different magnitudes of static, coulomb and viscous friction were induced to achieve the friction characteristics represented by the classical friction curve. Since the change in force characteristics of the valve results in a corresponding change in the current drawn by the position control solenoid, a rudimentary CMS for monitoring the current characteristics is presented. Based on the experimental results and validation using the CMS it was concluded that the fault simulator was able to accurately produce the desired frictional loading on the valve spool and was able to do so with a high degree of repeatability.

Acknowledgements

The author would like to express his gratitude to his supervisors, Dr. R. T. Burton and Dr. G. J. Schoenau, for their invaluable guidance, advice and encouragement throughout the course of this research and the writing of this thesis. Also, the author would like to express his sincere appreciation to Mr. D. V. Bitner for his consistent help throughout the project.

The author acknowledges the financial assistance provided in the form of research assistantship from the supervisors.

Dedication

To my beloved parents, Smt. Archana Bhojkar and Sri. Arvind Bhojkar.

Table of Contents

Permission to Use ..... **I**

Abstract ..... **II**

Acknowledgements ..... **IV**

Dedication ..... **V**

Table of Contents ..... **VI**

List of Figures ..... **VIII**

List of Tables ..... **XI**

Nomenclature ..... **XII**

Chapter 1 Introduction **1**

1.1 Condition monitoring for fault diagnosis 1

1.2 Validation of condition monitoring: How reliable is the CMS? 2

1.3 Fault simulation in hydraulic components 5

1.4 Research Objective 11

1.5 Thesis Outline 12

Chapter 2 System Design and Experimental Setup **13**

2.1 Proportional Solenoid Direction Control Valve 13

2.2 Common Faults in Proportional Solenoid Valve 16

2.3 Experimental System 21

2.4 Summary 23

Chapter 3 Friction Modeling and Control System Design **25**

3.1 Friction characteristics 25

3.2 Control System for Position Control 32

3.3 Control System for Force Control 35

3.4 Friction Model 36
3.5 Control system interaction 40
3.6 Summary 43

Chapter 4 Experimental Results 44

4.1 General 44
4.2 Controller Design for Position and Velocity Control 50
4.3 Controller Design for Force Control 58
4.3.1 Removing Bias of Force Transducer 58
4.3.2 Static Friction /Stiction 61
4.3.2.1 Force-Current-Displacement characteristics of a PSV 62
4.3.3 Sliding Friction 72
4.3.3.1 Coulomb Friction 73
4.3.3.2 Viscous Friction 76
4.3.3.3 Combined friction 78
4.4 Evaluation using a simple condition monitoring technique 80
4.5 Summary 86

Chapter 5 Conclusions and Recommendations 88

5.1 General 88
5.2 Conclusions 89
5.3 Recommendations 91

References 92

Appendix A 96

List of Figures

Figure 1.1 Reliability evaluation of a CMS using fault simulation 5

Figure 1.2 Oil contaminant monitor (BHRA), (Raw and Hunt [1986]) 6

Figure 1.3 Hydraulic Test Rig for Fault Simulation 9

Figure 2.1 Electro hydraulic Proportional Valve 14

Figure 2.2 Proportional Solenoid Assembly 15

Figure 2.3 Force-Displacement characteristics of conventional and proportional solenoid 16

Figure 2.4 Forces acting on the valve spool 18

Figure 2.5 Test System coupled to (a) Conventional load and (b) Load simulator 19

Figure 2.6 Fault Simulator to provide add on force ΔF 20

Figure 2.7 Experimental setup for Fault Simulator 23

Figure 3.1 Velocity profile and Friction force for a sliding mass 28

Figure 3.2 Normal and simulated increase in Friction 31

Figure 3.3 Spool position, velocity and friction force profile 34

Figure 3.4 Closed loop position control system 35

Figure 3.5 Closed loop force control system 36

Figure 3.6 Fault Simulator algorithm 39

Figure 4.1 Solenoid force measurement using force transducer 46

Figure 4.2 Coulomb friction estimation 48

Figure 4.3 Viscous friction estimation 49

Figure 4.4 Closed loop system with only proportional control 51

Figure 4.5 Critical gains for different spool positions 53

Figure 4.6 Spool position and velocity profile using a PI controller..... 55

Figure 4.7 Measured spool displacement and velocity profile 57

Figure 4.8 Normal force characteristics before fault simulation 60

Figure 4.9 Force conditioning algorithm 60

Figure 4.10 Fault simulator employing force conditioning in feedback loop 61

Figure 4.11 Force -Current- Displacement characteristics of Proportional Solenoid 64

Figure 4.12 Experimental setup for main spring current-displacement characteristics.. 67

Figure 4.13 Main spring Current-Displacement characteristics 67

Figure 4.14 Current-displacement map of main spring for generating stiction..... 68

Figure 4.15 Maximum static friction induced in a PSV 70

Figure 4.16 Different magnitudes of stiction induced in a PSV [(a) 10N, (b) 5N, (c) 2N] 71

Figure 4.17 Effect of different magnitudes of static friction on spool displacement 72

Figure 4.18 Simulation of increased coulomb friction in a PSV using Fault Simulator 75

Figure 4.19 Desired and measured values of coulomb friction [(a) 1N (b) 1.25 N (c) 0.5 N] 75

Figure 4.20 Simulation of increased damping co-efficient in a PSV using Fault Simulator 77

Figure 4.21 Simulation of increased coulomb and viscous friction in a PSV 79

Figure 4.22 Static, Coulomb and viscous friction induced in a PSV..... 80

Figure 4.23 Effect of increase in static friction on the current drawn by Solenoid A 82

Figure 4.24 Effect of increased coulomb friction on the current drawn by Solenoid A. 84

Figure 4.25 Effect of increased viscous friction on the current drawn by Solenoid A... 84

Figure 4.26 Effect of simulated increase in coulomb and viscous friction on the current drawn by Solenoid A..... 85

Figure 4.27 Effect of combined friction on current in Solenoid A..... 86

Figure A.1 Calibration of analog input..... 97

Figure A.2 Calibration of analog output..... 98

Figure A.3 Calibration of force transducer..... 99

Figure A.4 Current Meter Calibration 100

Figure A.5 Calibration of LVDT..... 101

List of Tables

Table 4.1 Controller gains using Zeigler Nichols method.....53

Nomenclature

F_{fric}	Total friction in the valve (N)
F_s	Inherent static friction in the valve (N)
F_c	Inherent coulomb friction in the valve (N)
F_v	Inherent viscous friction in the valve (N)
ΔF	Increased friction force induced by fault simulator (N)
F_T	Output from force transducer (N)
F_{solA}	Force developed by Solenoid A (N)
F_{solB}	Force developed by Solenoid B (N)
F_{sa}	Static friction of solenoid armature (N)
F_{ca}	Coulomb friction of solenoid armature (N)
F_{va}	viscous friction of solenoid armature (N)
i_{SolA}	Current through the coil of Solenoid A (A)
$i_{Sol\mathbf{B}}$	Current through the coil of Solenoid B (A)
i_{2K_ax}	Current required in overcoming the effective spring force of the valve (A)
K_a	Solenoid spring coefficient (N/m)
K_{ca}	Coulomb friction co-efficient of solenoid armature (N)
K_{va}	Viscous friction co-efficient of solenoid armature (N-m/sec)

K_p	Proportional gain of PID Controller
K_i	Integral gain of PID Controller
K_d	Derivative gain of PID Controller
K_v	Spring co-efficient of main spring in the valve (N/m)
M_v	Mass of spool (kg)
x	Spool displacement (m)
$\frac{dx}{dt}$	Spool velocity (m/sec)
PSV	Proportional Solenoid Va lve
CMS	Condition Monitoring System/Scheme

Chapter 1

Introduction

1.1 Condition monitoring for fault diagnosis

Hydraulic systems are widely employed in many industrial applications due to their ability to economically convert mechanical energy into fluid energy, which can be regulated to provide speed, force and direction control with the help of some simple components. In industries like construction, aircraft, mining, etc., hydraulic systems provide the high force requirements with considerably greater power/weight ratio than other power transmission systems. No other type of power transmission system provides the range of control over speed, force and direction that could be obtained through fluid power. However, undiagnosed faults in hydraulic systems can result in gradual degradation of plant performance, and if not fixed in time could damage the expensive equipment as well as endanger human life.

The ability to anticipate a fault in a system/ system components by monitoring certain parameters and/or state variables is commonly referred to as condition monitoring and diagnosis. Condition Monitoring Systems (CMS) have been used extensively to monitor hydraulic components employed in high risk applications like nuclear power plants and aircraft industry, which places a high demand on the reliability of components, in order to predict their time to failure so that the component can be replaced before any catastrophic failure occurs. In industrial applications such as process, chemical, manufacturing, etc., condition monitoring brings in a third dimension to the two most common methods of maintenance, (break down and preventive /scheduled maintenance), by predicting the need for maintenance/replacement of particular components. Modern predictive maintenance techniques utilize various condition monitoring approaches to predict unplanned equipment failures thereby reducing the cost associated with system down time, increased life of the system components and increased safety of human life.

Techniques like 'vibration analysis' [Badi, 1996], 'contaminant monitoring' [Raw and Hunt, 1986] and 'model based approach' [Azzam and Hazell, 1996], are used to provide a reliable health diagnosis of the system.

One very important component in a hydraulic system is the proportional solenoid valve. Proportional Solenoid Valve (PSV) is an electro-hydraulic valve, which employs a proportional solenoid to accurately meter the flow of hydraulic fluid, (i.e. oil), to an actuator or a motor thereby controlling the motion. PSV have been successfully used in the hydraulics industry for many years due to the benefits associated with higher accuracy as compared to conventional solenoid valves, and the robustness and economy compared to servo valves. Because the PSV plays an important role in the performance of a hydraulic system, any deterioration in their performance can directly affect the overall performance of the system. This has led to a considerable amount of research being directed towards different parameter based condition-monitoring schemes applied to proportional solenoid valves. Techniques like Neural Networks [Rosa et al., 2000] Ordinary Least Square [Ansarian et al., 2001] and Extended Kalman Filtering [Wright et al., 2000] have been used to estimate some valve parameters, with varying degrees of success. Another method developed by Mourre et al., [2001] combines Neural Networks with statistical methods which allows the friction and spring characteristics to be identified as a norm from which the deviations could be used to detect faults as they propagate in the valve.

1.2 Validation of condition monitoring: How reliable is the CMS?

Even though many Condition Monitoring Systems (CMS) have been developed and serve as powerful tools for fault diagnosis and prognosis, one question still remains unanswered: how reliable is the CMS? A study by Inerny and Hardman [2002], on the fault detection algorithms applied to a bearing supporting the main-gearbox input pinion shaft of a helicopter rotor, indicated that the existing CMS did not indicate any change in the bearing's health until the bearing started to disintegrate. The health monitoring system using the vibration spectra to monitor faults, failed to show the progression of the fault

with no change in the power spectrum until the bearing had failed, which raised questions regarding the reliability of the existing CMS. This eventually resulted in modifying the CMS to yield better diagnostic capabilities. It is apparent that any failure on the part of CMS to quickly detect the fault at initial stages could lead to a catastrophic failure, since an undiagnosed fault in any of the critical components can propagate throughout the system leading to overall system damage. Kumar and Hazra [1996], in their study of monitoring techniques for gas turbines, have indicated how vibration monitoring used on these systems failed to envisage the failure of a turbine blade, which had a cascading effect, resulting in damage to several other stages of the turbine blades. This translated into severe economic losses due to equipment downtime and the loss of expensive equipment.

From the foregoing discussion it is quite clear that any CMS needs to be thoroughly tested before being commissioned, since the failure of a CMS to detect any potential fault can be economically disastrous, and dangerous in terms of the safety of personnel. "The reliability of fault detection is the most important criterion for the success of a condition monitoring system, and the challenge always, is to develop algorithms and systems that can diagnose fault conditions more accurately than those available at present" [Nandi, 2002].

An important question then is "how should a CMS be assessed for its reliability in fault detection"? Consider the system in Figure.1.1. It is assumed that any fault will affect the system process and its control. Generally, a fault is to be understood as a "non-permitted deviation of a characteristic property of the process itself, the actuators, the sensors and the controllers" [Isermann, 1984]. As shown in Figure 1, the CMS constantly processes the measurable data to extract useful quantities, which are indicative of the current health of the system. This information is compared against certain norms or predetermined values and eventually fault or failure indicative signals are generated. Fault detection and diagnosis are comprised of processing the fault/failure indicative signals through some decision-making mechanism to determine the nature and type of the fault.

Hence, the most effective way of testing a CMS is to induce a deliberate/ artificial fault in the system, such that it manifests itself in one or more of the parameters being monitored, and then check to see if the CMS is able to detect it. This can be achieved by developing a fault simulator, as shown in Figure 1.1, which can induce user-defined faults in the system in a controlled manner and also simulate the progress of such faults over time. A comparison of the faults identified by the CMS and those actually implanted into the system by the simulator will reveal the efficacy of the CMS. Any significant error in identifying the fault would indicate to the operator/ engineer, that the existing CMS is unreliable for detecting any potential faults and that the operator/engineer should consider a modification of the CMS or use better diagnostic algorithms for developing a robust CMS.

As mentioned previously the PCV is a critical component in many hydraulic systems. Many CMS discussed previously have been developed for monitoring the states or parameters of this valve but the literature review indicates that the issue of reliability of CMS has largely gone unaddressed. This research attempts to fill this void by developing a non-destructive fault simulator, which can induce user defined faults in the valve and thereby aid in testing the efficacy of the CMS for monitoring such simulated faults. If the CMS is able to diagnose such simulated faults, it can be inferred with a certain level of confidence that it will be able to diagnose the progression of the real faults as well.

The following section considers some typical hydraulic components and the fault simulation techniques adopted to evaluate the reliability of CMS developed for these systems.

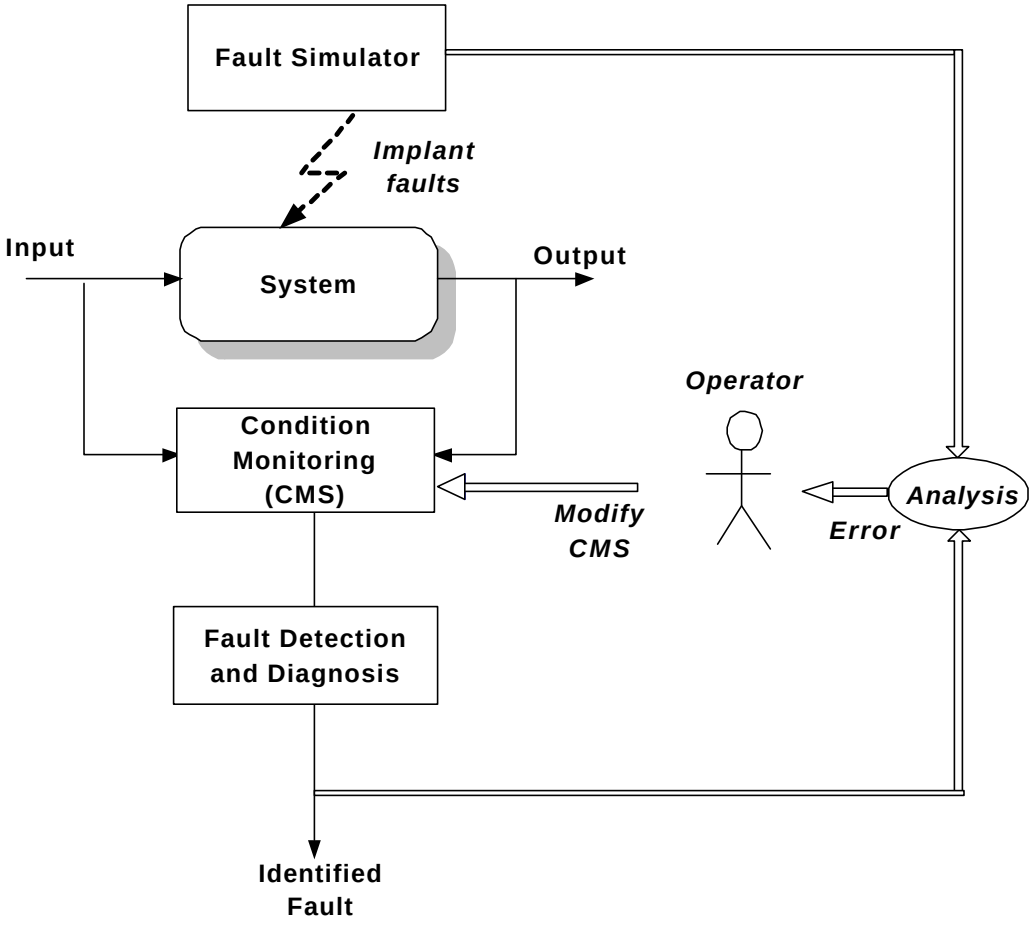

Figure 1.1 Reliability evaluation of a CMS using fault simulation

1.3 Fault simulation in hydraulic components

In fluid power transmission systems, hydraulic fluid (oil, water or air) is used to transmit power and utilizes different combinations of pumps, valves and actuators for converting energy from one form to another. Typical faults in hydraulic systems include, oil contamination, component degradation due to excessive wear, overheating, increased friction, etc. One way of simulating the faults due to oil contamination is by adding contaminants to the oil and running the oil through the system to check the system behavior in presence of debris or contaminated oil. Heron and Huges [1986] developed a novel contaminant monitor to check the cleanliness level of fluid in a hydraulic system. The monitor puts to use the well-known problem of silting of spool valves. Fine solid

contaminant present in hydraulic systems can accumulate around the small clearances in precision spool valves, thereby increasing the friction in the valve and causing erratic operation. In essence, the monitor is a precision spool valve deliberately arranged to be exposed to contamination in the hydraulic system. To simulate the fault, the oil was added with various level of contaminants and was passed through the hydraulic system and finally through the contaminant monitor.

Consider Figure 1.2. The contaminated oil enters the instrument through an orifice meant to provide a near constant flow rate, and passes through the small clearance between the spool and valve body. As the contaminant builds up, the cylindrical clearance is gradually blocked causing the pressure upstream to rise thereby triggering a pressure switch. This causes the solenoid to attract the piston, which allows more flow of hydraulic fluid through the gap thereby flushing away the contaminant build up.

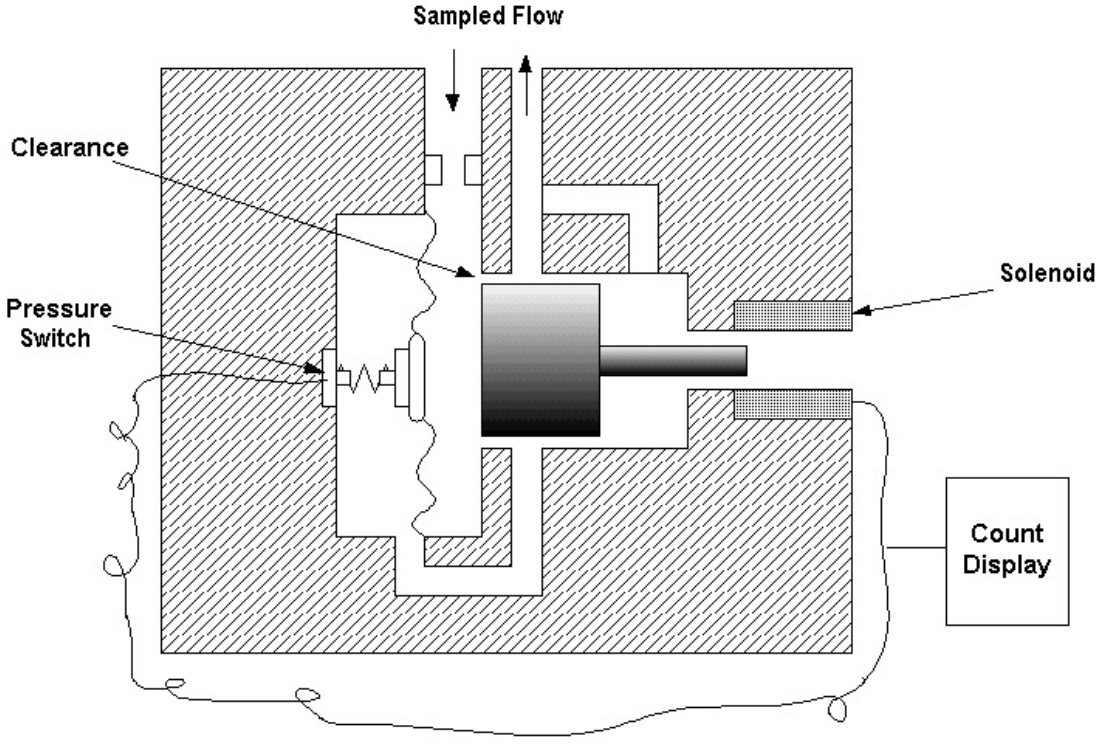

Figure 1.2 Oil contaminant monitor (BHRA), (Raw and Hunt [1987])

The PSV used in this research is a spool type solenoid valve which is often plagued

with the problem of silting as mentioned above. The operating principle of the contaminant monitor could also be used to simulate friction faults in the PSV. Silting normally causes the valve spool to stick at some location, which is also the effect of one of the friction properties namely, stiction. By passing oil with varying levels of contaminants it is possible to simulate stiction of different magnitudes. But the potential problem with this method of fault simulation is that the contaminated oil can damage the pumps and other accessories of the hydraulic system, thereby rendering the system useless after testing. Moreover, producing the exact amount of stiction cannot be easily controlled and must be done by trial and error. Since the underlying principle for Heron's research is to use a destructive form of fault simulation technique, developing an alternative non destructive method is explored in this research.

In order to simulate component faults like degradation due to wear etc, Tan et al [2003] have tried to induce possible real-life faults into a water hydraulic cylinder and an axial piston motor. Vibration analysis and leakage flow analysis were used to identify the induced faults. Different types of faults in the cylinder such as a reduction of piston diameter, wear of the cylinder rod and rod seal, were implemented by replacing the new seals with worn out seals. Similarly, motor faults such as worn piston shoes, reduction of the outside diameter of piston were implemented by replacing the new pistons with worn capstans and shoes. This methodology was used as an arrangement to test any potential CMS for hydraulic actuators and required the availability of worn out pistons and bearings. Again, this would mean damage to the existing system components if the worn components are used, hence constitutes a destructive and therefore an unacceptable form of fault simulation technique.

It was observed that in many of the applications reviewed, fault simulation was carried out by physically modifying the properties of the system or by employing some form of destructive testing. In many applications it maybe un-economical and impractical to use destructive tests by implanting the faults directly in the system being monitored,

since this could alter the system characteristics and render the system useless after fault simulation. For example in the nuclear and aircraft industry in which CMS are used to detect incipient faults, it may not be possible to implant the faults in their systems for obvious reasons of safety and economy. An alternative is to build a test system or create a software model of the system, which represents the original system as closely as possible and then mimic the faults. This can be achieved by simulating the fault conditions in the system such that the original system cannot differentiate between actual and simulated faults.

In a research carried out by Martin [2000], simulated fault tests were performed on a robot hydraulic drive in order to extract failure indications from the test data and to develop a reliable fault diagnostic technique. Since the hydraulic robots used in this study were used for cleanup of hazardous and radioactive waste, any undetected faults could damage the waste containment facilities due to a faulty robot. Since it was not practical to implant the faults on an actual robot, a test rig as shown in Figure 1.3, was constructed. This system was comprised of a hydraulic motor and power system along with several other components, (similar to that used in the actual robot). Some of the important faults introduced/ simulated in the system were:

1. Plugged high-pressure filter: This fault was simulated by inserting a restriction in pressure feed line to the test rig. Reduced load capacity of the hydraulic power system at higher loads and rise in oil temperature were the expected results.
2. Loss of casing oil: This fault was simulated by bleeding the casing oil from the motor prior to the start of the test.
3. Open control valve winding: A computer-controlled relay was used to simulate this fault, by interrupting the command signal to the valve. Inability to operate the motor was the expected result.
4. Sticking Control Valve: This fault was simulated by modifying the command signal

from the PID controller. The "normal condition" command profile was a 10 sec ramp whereas the faulted command profile was a staircase comprised of ten 1-second stick-slip intervals. This resulted in pressure, and flow fluctuations and motor vibrations. Manifestations of the faults were analyzed to determine the type and location of instrumentation needed to detect them. For most of the faults, pressure, flow, temperature, current and vibration signals provided the required information to classify the fault.

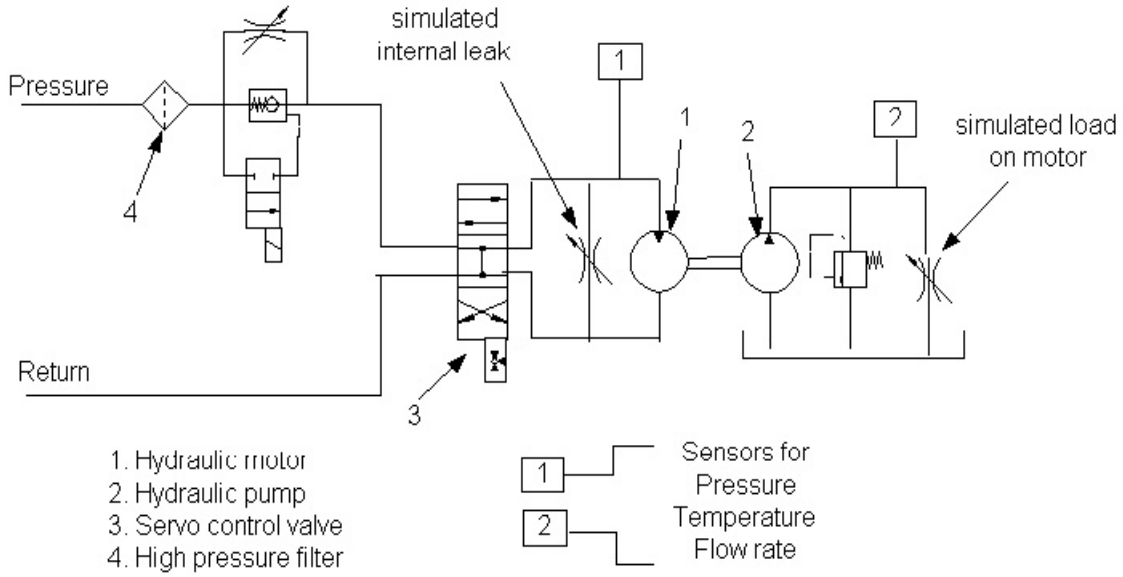

Figure 1.3 Hydraulic Test Rig for Fault Simulation [Martin, 2000]

Though the central idea of this system is close to the principles of the present research which is of non-destructive fault simulation, the main drawbacks of Martin's system are the extra cost associated with the test system and the simplifications and assumptions associated with the test system, which may not represent the fault effects correctly. Hence, it would be of interest to develop a non-destructive fault simulation technique, which can reliably and repeatedly produce the conditions representative of a real life fault in the original system at minimal cost. This approach would not only cause minimal damage to the original system but would prove economical as well.

Load simulators have been used extensively in the aircraft and automotive industries

to test a prototype under various laboratory-loading conditions. These simulators are similar in their working principle to that of non-destructive fault simulators, except that the programmed disturbance introduced on the system using an "add on" load in the load simulator, is considered as a fault in the fault simulator system. In hydraulics, load simulators have been developed for testing system and component performance under varying loading conditions.

Martin [1992] and Nimegeers et al., [1996] developed a load simulator for a proportional valve and actuator using an external hydraulic loading system which could be connected to a test system in order to create different types of loads like friction, damping, spring and mass. They could successfully create other types of loads but were limited in their success to simulate the friction characteristics, due to the non-linear and complex dynamics of the friction.

Ramden et al., [2000] has theoretically analyzed a load simulator using both dynamic simulation and linear analysis by using a technique referred to as dynamic "Hardware in Loop Simulation" (Haibin [2001]). In this technique some complicated components of the system are simulated in software, and other components are introduced physically in the simulation loop using a suitable interface. This makes it possible to simulate an actual system without the need to carry out physical testing on the components. For this to be accomplished, both experiments and simulations must be carried out simultaneously. Though this approach had the potential to successfully simulate the loading pattern using the model of two servo valves, validation using an actual system had not been reported in the literature.

Ohuchi and Ikai [1989] have developed a load simulator by coupling the load system to the test system and then providing the necessary pressure disturbance on the load system, which could cause the desired effects of actual load. They have employed feedback as well as feed forward control techniques to compare the improvement in the load pressure, but for simplicity, have assumed no loading effects due to friction.

The load simulators discussed above, essentially added some programmed disturbance to the system. In reality, this behavior is also what is required for a fault simulator and hence was deemed to be an approach, which could be pursued in this thesis.

1.4 Research Objective

As mentioned, a particularly important component in modern hydraulic systems is the PSV. From the literature, the most common fault reported in proportional valves is the increase in friction between the spool and valve housing, due to wear, scuffing and contaminant buildup, etc., that alters the frictional characteristics in the valve [Fey, 1987]. This can cause the valve to have a stick-slip motion that can result in a jerky motion of the device being controlled. Due to the criticality and frequency of occurrence of this fault, a device that could accurately simulate an increase in friction characteristics (static and sliding friction) of spool type valves was desirable, and was the motivation to develop a fault simulator in this study.

The objective of this research is the development of a fault simulator to induce artificial friction in the PSV to simulate the case of increased friction in the proportional solenoid valve, in a non-destructive manner. It is envisaged that the development of the fault simulator will facilitate future reliability evaluations of several CMS developed for these valves, which utilize friction as one of the parameters to monitor the health

Based on the literature review described in the previous sections, no load simulator has been designed to induce user defined friction characteristics in a PSV. The work described in this thesis achieves the research objective achieved through the following tasks.

1. Design a experimental system which gives the flexibility to induce the friction faults at any desired location in the valve, and at the same time does not produce any superfluous friction due the arrangement, other than that induced by the simulator algorithm.

2. Design a suitable fault simulation algorithm that offers the flexibility to induce any or all of the friction components repetitively (static and sliding).
3. Validate the fault simulator through experimental testing.

1.5 Thesis Outline

The research carried out to meet the above objective will be presented in following order. Chapter 2 introduces the working of a proportional solenoid valve and experimental setup for the fault simulator to induce the desired frictional loads. In Chapter 3, the fault simulator algorithm and the control system architecture for position and force control will be discussed. Chapter 4 elaborates on the design of the position and force controllers experimentally and the results achieved for the proposed introduction of the faults in the PSV. Chapter 5 discusses some views on the ability of the fault simulator to produce the desired frictional loads along with some conclusions and recommendations for future work.

Chapter 2

System Design and Experimental Setup

In this chapter, the experimental setup used for fault simulation is introduced. First, a general description of the proportional solenoid valve is presented followed by the modification of the valve to incorporate the components for fault simulation. The physical components used to implement the fault simulator are presented and the control system for computer control is discussed.

2.1 Proportional Solenoid Direction Control Valve

As mentioned in Chapter 1, a Proportional Solenoid Valve (PSV) forms an important part of modern hydraulic systems. In position control applications where the accuracy of positioning the load is to be matched with the cost of achieving it, proportional valves provide a much cheaper alternative than the costlier but more accurate servo valves. This is mainly due to reduced manufacturing tolerances and lesser control electronics required for the proportional valves. Also PSV are more robust and contaminant tolerant than servo valves, which makes them a preferred choice in industrial applications.

Figure 2.1 depicts a 4-way, 3-position, closed center PSV typically used in a circuit powered by a pressure-compensated or load-sensing pump. Current through the solenoid coil windings generates a magnetic potential difference across the air gap. This creates an attractive force between the armature and stator, which causes the armature to move and close the air gap thereby minimizing the reluctance in magnetic circuit. A pushpin connected to the center of the armature acts directly on the spool, causing the displacement of the spool. The spool slides back and forth within the limits of maximum and minimum permissible spool displacement, throttling fluid across the metering lands. For $x>0$ load port B connects to the source, P_s, and load port A connects to tank, P_t. When $x<0$ the roles are reversed with port A connected to source and B to tank. When $x=0$ all ports are blocked. An LVDT connects to one end of the spool providing feedback to a control

loop that accurately positions the spool as desired. Solenoid A provides the axial force required to move the spool when $x > 0$. Similarly, Solenoid B provides the force when $x < 0$. The two mainsprings assure the centering of the spool.

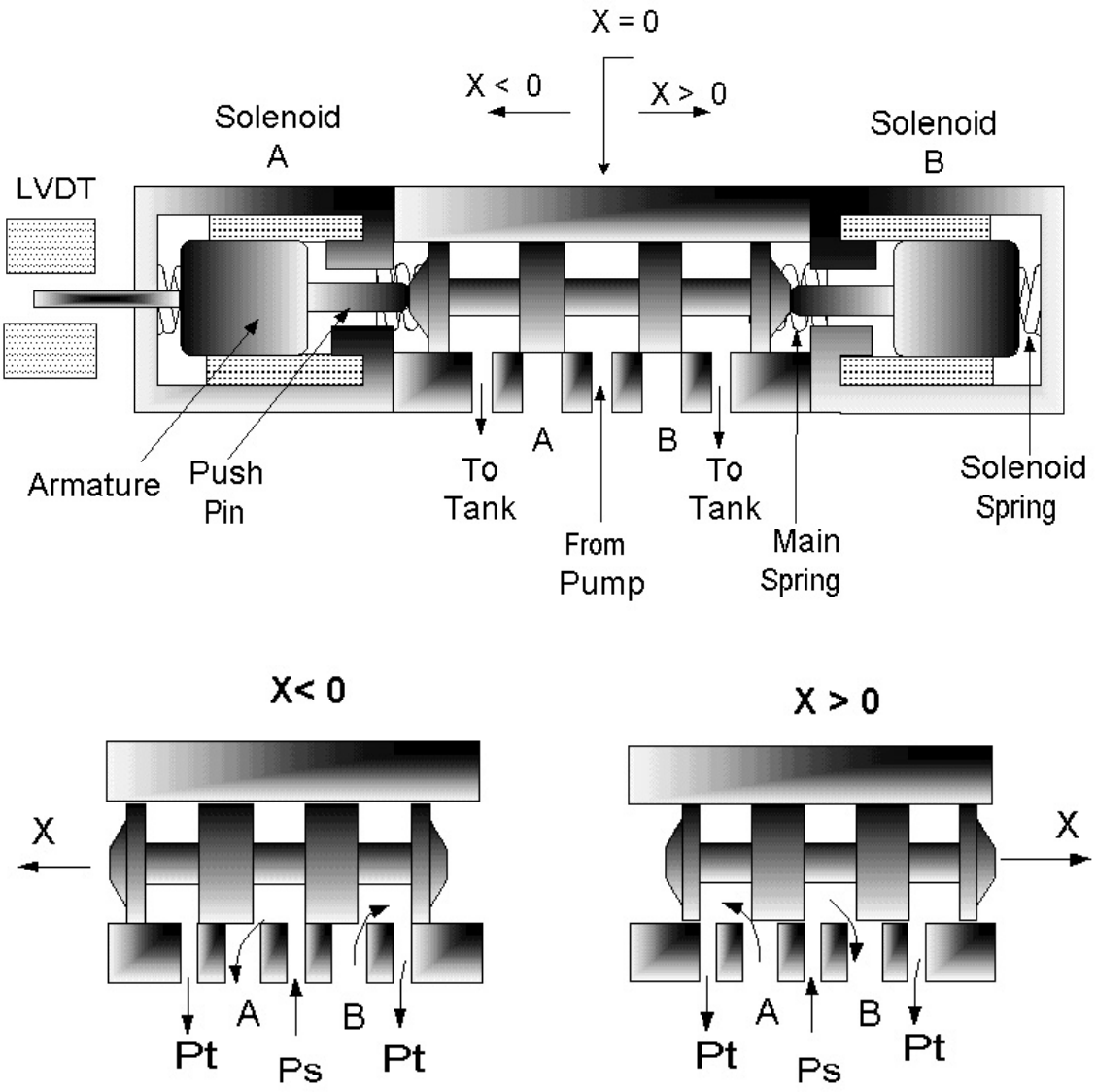

Figure 2.1 Electro hydraulic Proportional Valve

PSV differ in operation from that of direct acting on/off valves in terms of the accuracy of flow metering. Unlike on/off solenoid valves, the current in a proportional solenoid can be varied to move the spool variable distances, which under certain circumstances can result in the output flow being proportional to the input signal. The major difference between a proportional solenoid and a conventional on/off solenoid is the

design of the armature and pole piece assembly as detailed in Figure 2.2. The air gap in a proportional solenoid is shaped in such a manner as to give constant force throughout the working range of its stroke.

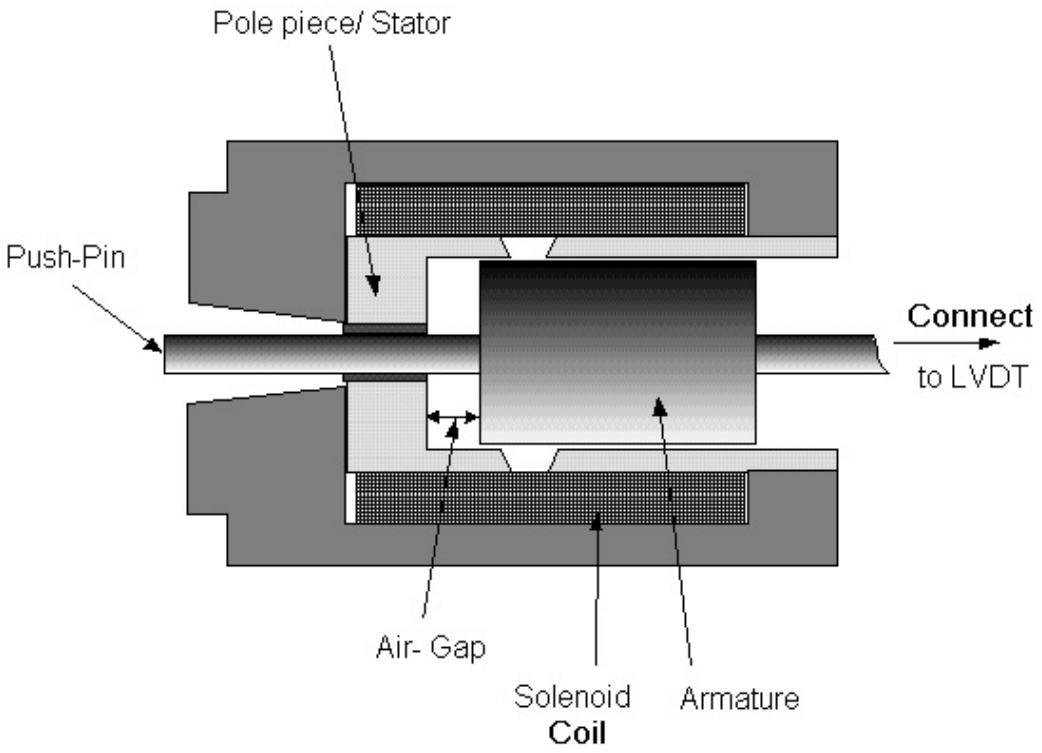

Figure 2.2 Proportional Solenoid Assembly

As shown in Figure 2.3, the proportional solenoid delivers a constant force irrespective of the armature position. In the conventional solenoid as the armature moves towards the pole piece, the inductance in the solenoid coil increases as more lines of magnetic flux cut the solenoid coil thereby reducing the rate at which current rises in the solenoid. This results in a decrease in the force as the armature completes its stroke, as shown in Figure 2.3 (a). In contrast, the armature and pole piece of the proportional solenoid are modified to give a constant force for a particular value of current, over a certain range of armature displacement as shown in Figure 2.3 (b). The coil current is the main factor by which the force developed by the solenoid can be modulated. The solenoid force moves the spool until a balance is achieved between the solenoid force and the

valve's spring force.

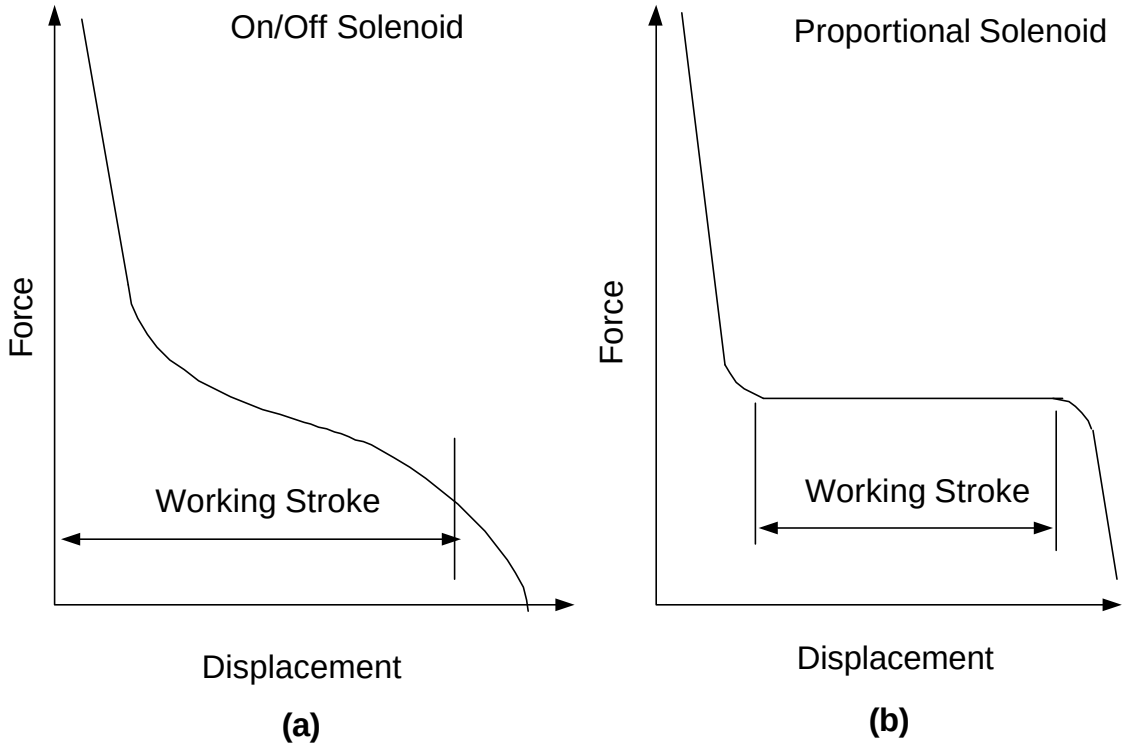

Figure 2.3 Force-Displacement characteristics of conventional and proportional solenoid

2.2 Common Faults in Proportional Solenoid Valve

Some typical faults that occur in a spool valve and their effects on the valve performance are summarized as follows:

Fault 1: Spool sticking in the valve body due to local increase in friction force, which may be due to wear, scuffing, contaminants, etc.

Effect: Solenoid coil not capable of generating enough force to dislodge the spool, which may eventually lead to coil burnout.

Fault 2: Increased sliding friction between spool and valve body.

Effect: Increase in the force required to move the spool, resulting in an increased current drawn by the solenoid.

Fault 3: Coil magnetic saturation.

Effect: Coil not capable of generating the desired force to move the spool.

Fault 4: Spring Breakage or Drift.

Effect: Valve instability.

Fault 5: Change in area gradient of spool due to abrasion and silting.

Effect: Affects the pressure sensitivity and flow gain of the valve.

The effect of most of the faults is an increase in the force required to move the spool. This increase in force can be thought of as an "add on" load on the valve spool, which tends to oppose the motion of the spool. As mentioned in Chapter 1, the most common fault in a proportional valve is the increase in force required by the solenoid to move the spool due to the contaminant build up, wear or scuffing in the valve spool thereby increasing the friction and possible stalling of the spool if the frictional force becomes excessive. During the normal operation of the valve the force characteristics of the solenoid driving the spool are given by

$$F_{sol} = M_v \ddot{x} + K_v x + F_{fric} \tag{2.1}$$

Equation 2.1, gives a certain minimum value of force above which any force acting on the valve is perceived as a fault by the system. An increase in the force by ΔF , assuming only the friction faults is shown in Figure 2.4 and can be represented by an equation of the form

$$F_{sol\Delta F} = M_v \ddot{x} + K_v x + F_{fric} + \Delta F \tag{2.2}$$

where, ΔF is the induced force to simulate the effect of friction faults and

$F_{sol\,\Delta F}$ is the increase in solenoid force to overcome the induced force ΔF .

Generally the friction force comprises of two components; static and sliding friction. It is the objective of this research to develop a fault simulator, which can accurately simulate the effect of increased static and sliding friction (including viscous friction) in the valve represented by ΔF in the Equation 2.2 above. A detailed discussion of the friction characteristics and the simulation model for introducing the additional friction ΔF, will be presented in Chapter 3.

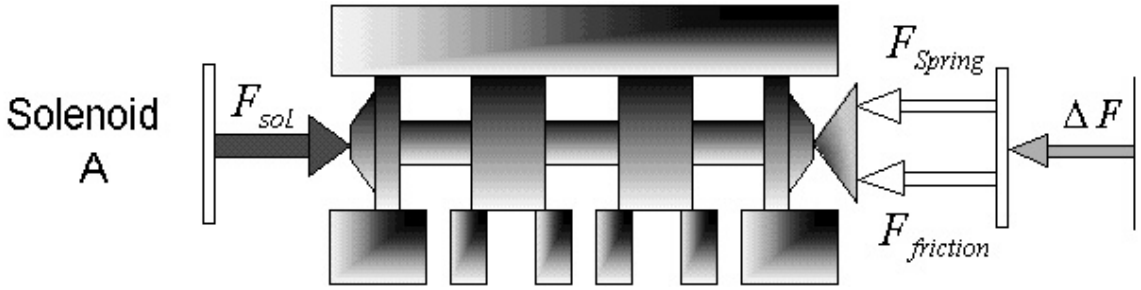

Figure 2.4 Forces acting on the valve spool

From the foregoing discussion it is evident that the most effective representation of the friction faults in the valve could be achieved by developing a loading device, which can produce the "add on" force, ΔF on the valve spool as illustrated in Equation 2.2. As mentioned in Chapter 1, load simulators utilize a loading system to simulate the desired loading conditions on the test system, such that the test system cannot differentiate between the actual physical loads and the simulated loads.

Consider Figure 2.5 (a). A test system is connected to a typical operating load comprising of a Mass (M), Spring (K) and Damper (B), in order to test the response of the test system to different loading conditions, i.e. physically changing the mass, spring constant and damping in the system. Since this method can be quite cumbersome and impractical for larger loads, an equivalent loading system programmed to supply different values of the load [Nimegeers, 1996] can be used to simulate the same dynamic effects of the load as shown in Figure 2.5 (b). Moreover, this arrangement of load simulation is non

intrusive to the test system since no modification of the original test system is required. But due to the requirement of an additional loading system, this arrangement might be a less attractive option where cost and space limitations are important.

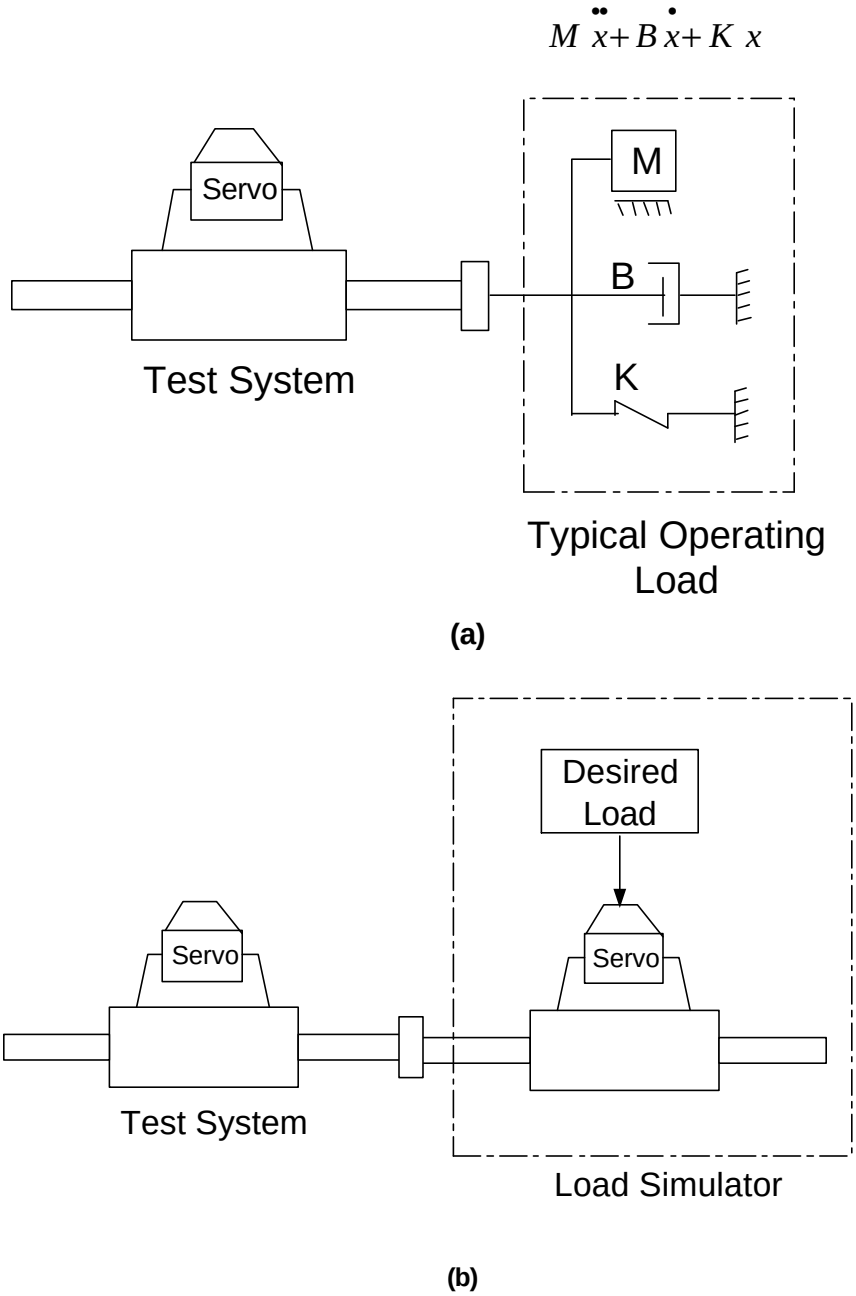

Figure 2.5 Test System coupled to (a) Conventional load and (b) Load simulator

It is proposed in this research to create loading conditions on the PSV representing artificial faults in a similar manner as outlined for the load simulator. The PSV has two

solenoids driving the spool as shown previously in Figure 2.1. Solenoid A drives the spool to the right ($x>0$) and Solenoid B to the left ($x<0$). Similar to the concept of load simulator, it was decided that the attachments of Solenoid B should be redesigned so as to be the fault simulator. This concept is illustrated in Figure 2.6.

The effect of increased friction force can be produced by developing a resistive force from solenoid B to accurately produce the desired friction force characteristics. Since the loads being simulated represent the varying levels of friction experienced by the system in the event of a fault, the loading arrangement is referred to as a "Fault Simulator". The effect should be such that any external system connected to the fault simulator is not able to differentiate between the simulated fault and the actual fault.

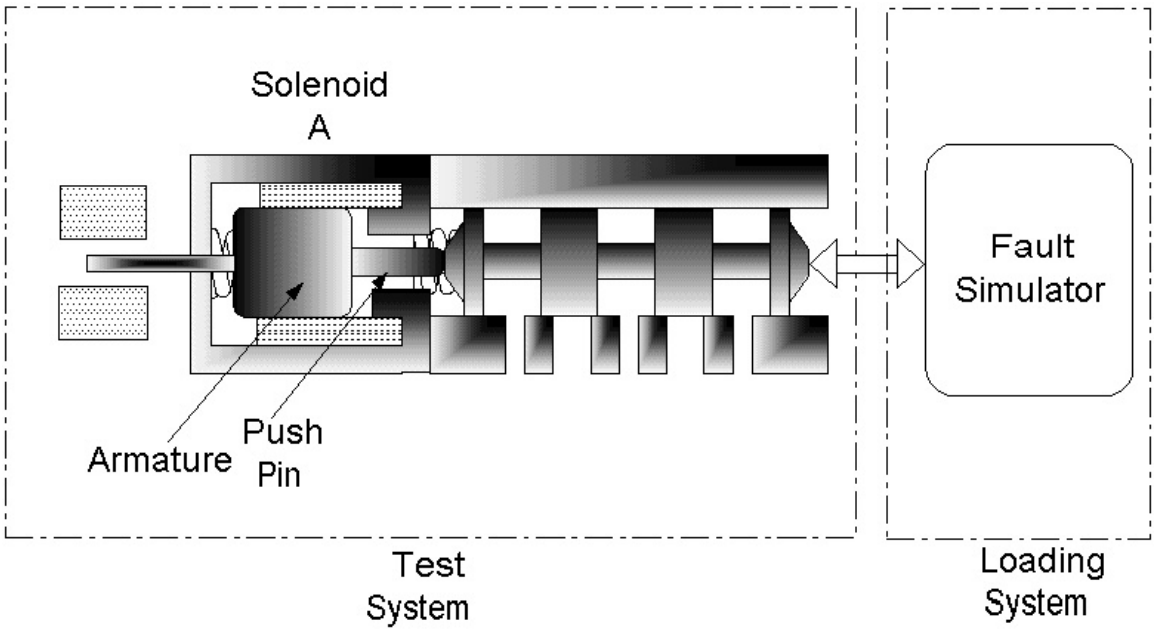

Figure 2.6 Fault Simulator to provide add on force ΔF

In simulating friction faults, it was assumed that other faults do not occur simultaneously in the valve. In other words, only one type of fault would be simulated at a time assuming other conditions to be normal.

It was a major objective of this research to ensure that the fault simulation procedure

should be non-destructive and should not harm any of the critical components in the valve. Also the arrangement was required be cost effective, requiring few additional components for fault simulation. The following section then considers the design of a load simulator based on the approach illustrated in Figure 2.3 with the aforementioned constraints and would be simple enough to introduce the friction faults using a computer-controlled system.

2.3 Experimental System

The PSV used a push type solenoid, which can produce force only in one direction. During the normal operation of the valve, only one of the solenoids is energized, so that the solenoid at the other end can be used to simulate the faults. This arrangement has two benefits:

- There is no requirement of an additional experimental set up to induce the faults in the valve.
- By using closed loop simulation better control over the fault characteristics can be achieved.

The experimental system is illustrated in Figure 2.7, and was primarily comprised of a Vickers proportional valve with solenoids on each end. Each solenoid had a coil resistance of 2.07 ohms and a current limit of 2.5 amperes. Solenoid A was used to drive the spool using a special waveform, which enhanced the friction forces on the valve spool. The waveform of the spool position could be controlled using the feedback signal from the LVDT via Solenoid A. Solenoid B was used to create the additional force ΔF described by Equation 2.2. To compensate for disturbances due to spool displacement, a controller employing force feedback using a strain gauge type force transducer was used. A spring cap was placed on the valve end of Solenoid B to accommodate the main spring with the original pre-compression. The force transducer was connected to the pushpin of Solenoid B on one side and the spool on the other side using self-aligning rods that were not fixed at

the ends.

As the spool moves along the desired waveform, the fault simulator algorithm uses a lookup table relating the velocity of the spool to the corresponding friction force desired by the user to output the desired friction force. Since the conditions most conducive for stiction occur at very low velocities, the spool is made to slow down to zero velocity and reverse its direction, creating optimal conditions for enhancing friction. The fault simulator algorithm outputs a stiction force near zero velocity, which momentarily stops the spool at the reversal position. As the position controller increases the current to Solenoid A, the force developed by Solenoid A increases and overcomes the stiction force, thereby increasing the velocity of the spool. At higher velocities, the fault simulator algorithm switches from a static to dynamic friction model, introducing a force on the valve spool proportional to Coulomb and viscous friction force. The Fault Simulator algorithm is developed in Chapter 3.

One of the main challenges in constructing the experimental setup was minimizing any additional friction due to the arrangement other than that introduced by the fault simulator. This required that the force generated by Solenoid B be transmitted directly to the spool, without being obstructed by the setup. For example, since the force transducer was connected on one side to Solenoid B and on other side to the valve spool, the weight of the transducer could result in a bending moment on the edge of spool causing it to skew in the body. This was highly undesirable as it would induce superfluous friction and could also damage the valve spool during the experiments. To ensure that no external friction effects were introduced as a result of adding the force transducer, a thin cable of about 0.5 meters was used to suspend the transducer, as shown in Figure 2.7. The cable offsets the weight permitting free motion in the axial direction.

A data acquisition system (DAQ) with 12-bit resolution and a sampling frequency of 500 Hz was used for all experiments. Two power op-amps, one for each solenoid, were used to amplify the signal from the controller. Instead of using the valve controller

provided by the manufacturer, a PI controller was designed in Matlab/Simulink for force and position control. An LVDT integral to the valve was used to measure the displacement of the spool, while a force transducer was used to measure the change in force due to Solenoid B. The calibrations of the amplifiers, force and position transducer are elaborated in Appendix A.

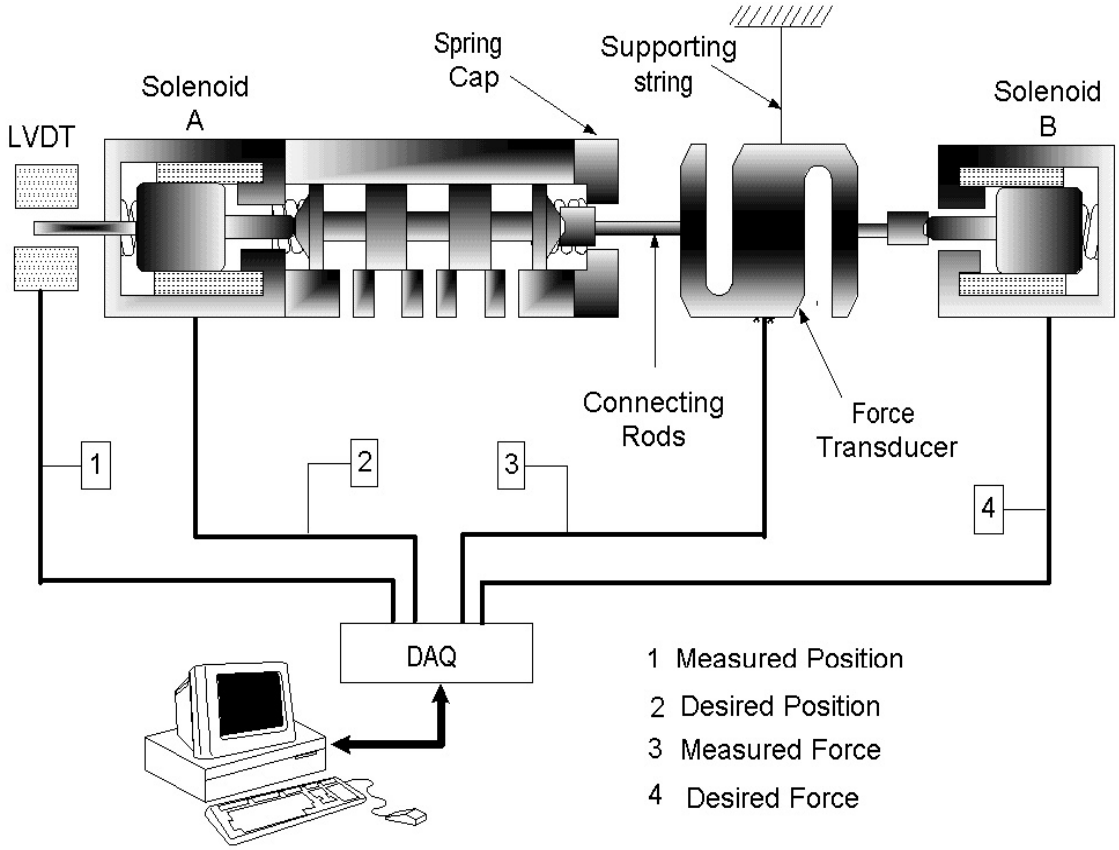

Figure 2.7 Experimental setup for Fault Simulator

2.4 Summary

This chapter presented the basic operating principle of a proportional solenoid valve and introduced the proposed fault simulator and its similarity to the load simulator. The principle of load simulator leading to the development of the fault simulator was described.

The experimental setup to implement the fault simulator was described along with some of the constraints associated with it. The next chapter discusses in detail the development of the control system for inducing friction faults in the valve, which is implemented using the Matlab/Simulink Real Time software.

Chapter 3

Friction Modeling and Control System Design

The previous chapter introduced the concept behind the fault simulator, the basic experimental setup to realize the simulator and the hardware components required to implement it. In this chapter, an overview of the classical friction models is presented followed by the development of a friction model appropriate for this research. The control system for simulating friction faults in a proportional valve is presented which was developed using the Matlab/Simulink ® software environment

3.1 Friction characteristics

Friction is present in all moving bodies in some form or the other. From basic applications to high tech automation industry, friction affects the dynamic as well as the steady state performance in their working range. The problem of controlling mechanical systems in the presence of friction has seen been an area of active research for many years now and has witnessed a surge of interest due to advances in industrial automation (CNC machines), robotic systems and recently MEMS.

Friction is a widely researched topic, yet despite being studied by numerous researchers [Dahl, 1977, Armstrong et al., 1990, just to name a few] it does not readily yield to rigorous mathematical treatment. This is mainly due to the highly non-linear behavior of friction at the very low velocities, (called stick-slip friction) and due to its dependence on various factors like temperature, and lubrication between sliding surfaces, etc. Modeling of the friction characteristics in a particular system generally involves finding the appropriate model which best fits the experimental data. In many situations though this is true, most designers prefer the use of readily available steady state friction models without giving much consideration to the dynamics of friction. For control

engineers the consideration of dynamic friction characteristics during motion reversal or at zero velocity is of particular importance as a host of dynamic effects have been observed and subsequently many friction models have been developed [Dahl, 1977 and Haessig and Friedland, 1990]. Unlike the traditional use of friction models for designing compensation, the friction model developed in this research is used for simulating increased friction in a PSV. Since the classical friction model forms the foundation for friction modeling it would be worthwhile to consider the characteristics of this model based on which a friction model suitable for this research was developed.

Consider a mass sliding on a surface with hydrodynamic lubrication prevailing between the sliding surface and the friction forces acting on the body as shown in Figure 3.1 (a, b, c). The typical friction characteristics between the two sliding surfaces as the applied force displaces the mass with a linearly increasing velocity is shown Figure.3.1 (a). The friction force can be divided into two distinct regions with reference to the velocity; i.e. static and sliding friction. To initiate any motion of the mass the applied force must overcome a certain force threshold called the static friction or stiction. This implies that the applied force will continue to increase until it reaches a magnitude sufficiently greater than the static friction force, at which point motion is initiated.

As soon as the mass starts to move, the total friction force drops and only the viscous and Coulomb friction force play a dominant role, as indicated in Figure 3.1 (c). The Coulomb friction is independent of the relative velocity between the sliding surfaces and is only dependent on the material properties at the contact surfaces. The component of friction which is dependent on the velocity of the sliding surface as well as the viscosity of fluid film is the viscous friction force. viscous friction is characterized by an increase in the friction force as velocity of the sliding surfaces increases linearly. The transition from the low velocity regime to higher velocity is characterized by a decrease in friction with increasing velocity. This region of negative viscous friction is due to the Stribeck effect, which is characterized by boundary lubrication and partial fluid lubrication between the

surfaces. As soon as the mass begins to slide, the velocity is not high enough to build fluid film between the surfaces causing shear of the solid junction between the sliding surfaces giving boundary lubrication. Since the shear strength at the junction is not high enough the friction force decreases, giving negative friction characteristics. As the velocity increases more fluid is drawn in between the sliding surfaces and partial lubrication exists in the junction. If the mass travels in the opposite direction of travel, the velocity profile would increase linearly in the negative direction, and the friction characteristics would be similar to those explained above except that it would be reversed in the negative direction.

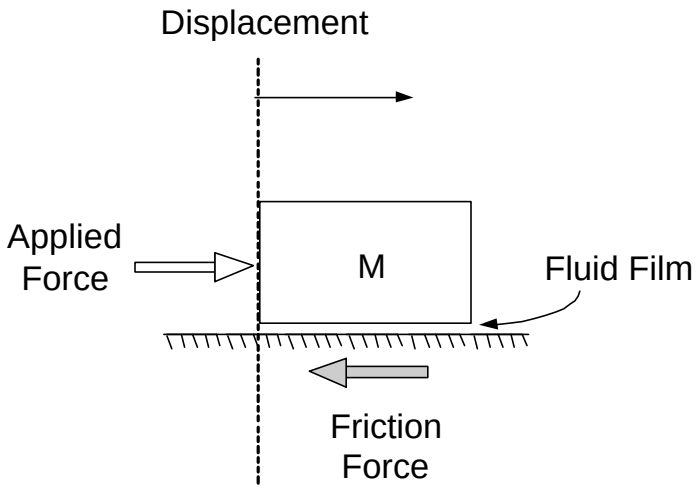

(a) Forces acting on a sliding mass

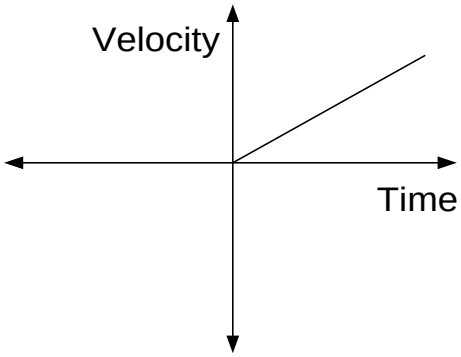

(b) Linearly increasing velocity profile

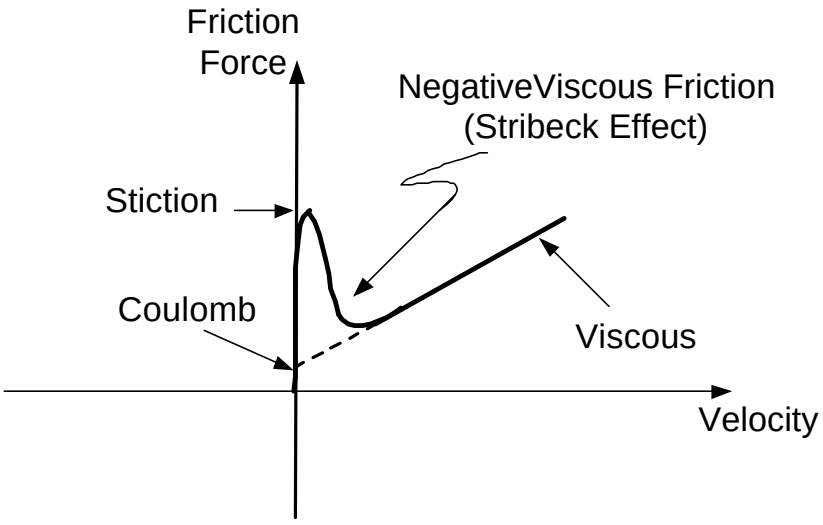

(c) Friction force vs velocity

Figure 3.1 Velocity profile and Friction force for a sliding mass

Most of the spool type valves involve three or four sliding surfaces (lands) with hydrodynamic fluid lubrication between the spool surface and valve. Due to the sliding motion between the spool and valve, the aforementioned friction characteristics are inherently present between the spool lands and valve surface, but are independent of the area of contact.

The most common fault in spool valves is a net increase in the friction force due to

the build-up of contaminants in the fine clearance space between spool and valve. Since the friction characteristics comprise of static, Coulomb and viscous friction it follows that a change in any one of them would indicate a progressing friction fault in the system. The objective of the fault simulator is to simulate the case of increase in any one or all of the friction components.

Figures 3.2 (a), (b), (c) depict the three possible scenarios of increase in friction force when plotted as a function of velocity. The possible build up of contaminants in the spool and valve clearances cause a binding between the spool land and valve thereby requiring an increased effort to initiate motion. The fault simulator can simulate this condition of increased stiction in the valve by applying an opposing force of constant magnitude, which the solenoid force should overcome to initiate motion. By changing the value of the opposing force, increasing levels of stiction can be simulated. This scenario is shown in Figure 3.3 (a), as a simulated stiction fault at very low velocities.

The presence of contaminants can cause an increased metal on metal friction or sliding friction in the valve. This increase in Coulomb friction force which has a constant magnitude and is only a function of the sign of velocity can be simulated by adding a bias force for all velocities on the fault simulator. This results in the viscous friction being offset by the added magnitude of Coulomb friction, as shown in Figure 3.2 (b). Also, the presence of contaminants can abrade the spool surface and cause the clearance to increase thereby causing more oil flow or leakage flow across the lands of the spool. This results in a corresponding increase in viscous damping at higher velocities. Increasing the opposing force on the valve spool in proportion to the velocity the fault simulator can simulate the effect of increased viscous damping. This scenario is shown in Figure 3.2 (c) as a simulated increase in the slope of viscous friction curve by the fault simulator.

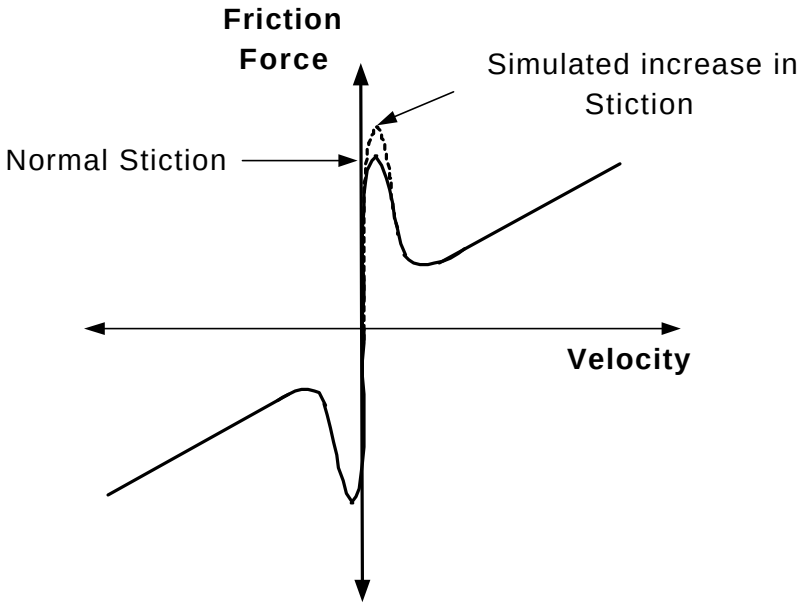

(a) Simulated increase in Static friction

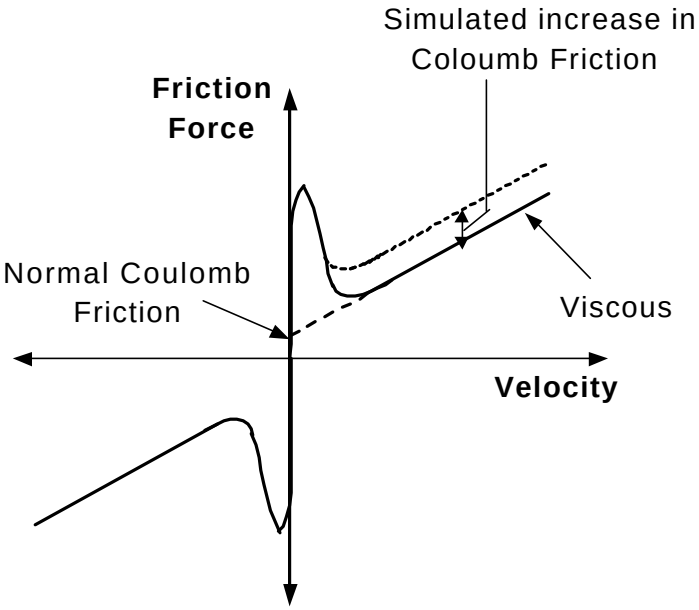

(b) Simulated increase in Coulomb friction

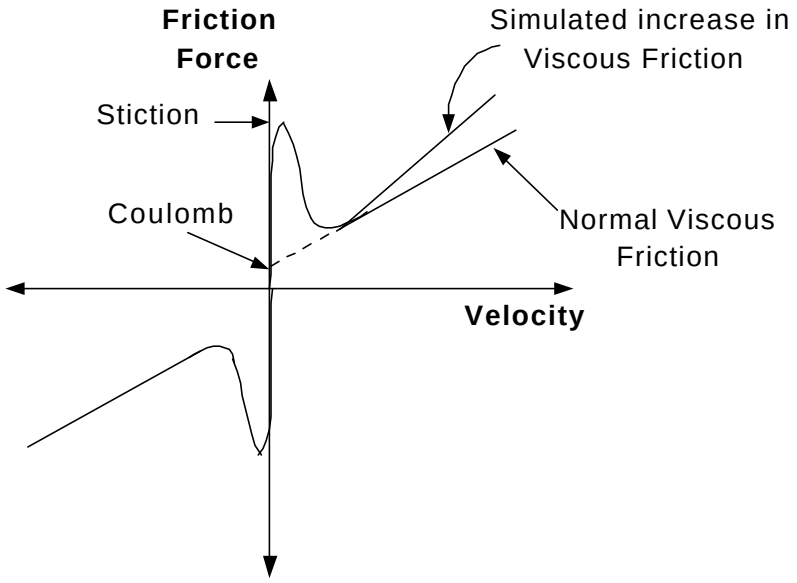

(c) Simulated increase in viscous friction

Figure 3.2 Normal and simulated increase in Friction

From the foregoing discussion it is evident that to observe the dynamics of friction, especially during the lower regions of velocity when the friction curve changes from static to sliding friction, the valve spool should be moved with slowly increasing velocity to accurately capture the significant friction phenomenon. Moreover since the effect of viscous friction is more pronounced at higher velocities, the spool velocity should also be able to incorporate this range of interest in its travel. The best way to do so would be to move it with a linearly increasing velocity that allows a wide enough window, to accurately capture the dynamic friction characteristics at very low velocities and steady state viscous friction at higher velocities.

In order to move the spool with linearly increasing velocity in presence of the nonlinearities and disturbances, and at the same time maintain the correct magnitude of friction faults, a feedback control of force and velocity was imperative. The next two sections will describe the control scheme for velocity and force control. Since both the variables are to be controlled on the same system an inherent coupling exists between them and an interaction between the two control systems is imminent. The interaction of

the two control systems is discussed in section 3.4.

3.2 Control System for Position Control

For the fault simulator to simulate the friction faults as a function of velocity, velocity control is necessary. This can be achieved indirectly through closed loop position control. The closed loop arrangement for position control of the valve spool is shown in Figure 3.4. A linear velocity profile is a first order polynomial in time which is obtained by differentiating the displacement signal; hence it follows that the displacement should be essentially a second degree polynomial of time. For example, a squared displacement waveform of the type $x = A(t - t_0)^2$ when differentiated gives a linear velocity profile of the type $\frac{dx}{dt} = 2A(t - t_0)$, as shown in Figure 3.3 (a), (b). It is seen that the slope of the parabolic displacement waveform goes from negative to positive with the slope being zero at the reversal point. This condition of zero velocity normally occurs in the spool type valves when the spool is about to begin its stroke or is reversing its direction about a particular point. Since the friction characteristics (stiction) are multi-valued at very low velocities (Figure 3.3 (c)), assuming arbitrary positive or negative values, it poses a very challenging proposition for control. This was one of the important considerations in developing the control algorithm to simulate friction characteristics at low velocities.

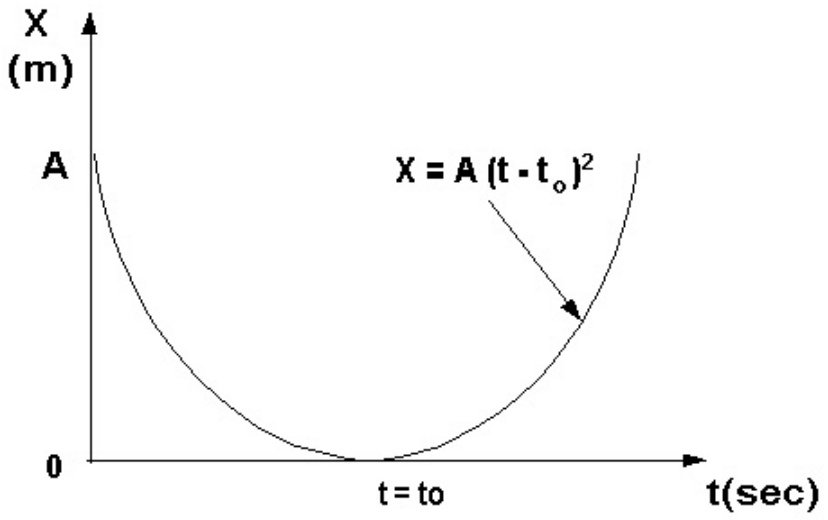

(a) Parabolic displacement profile

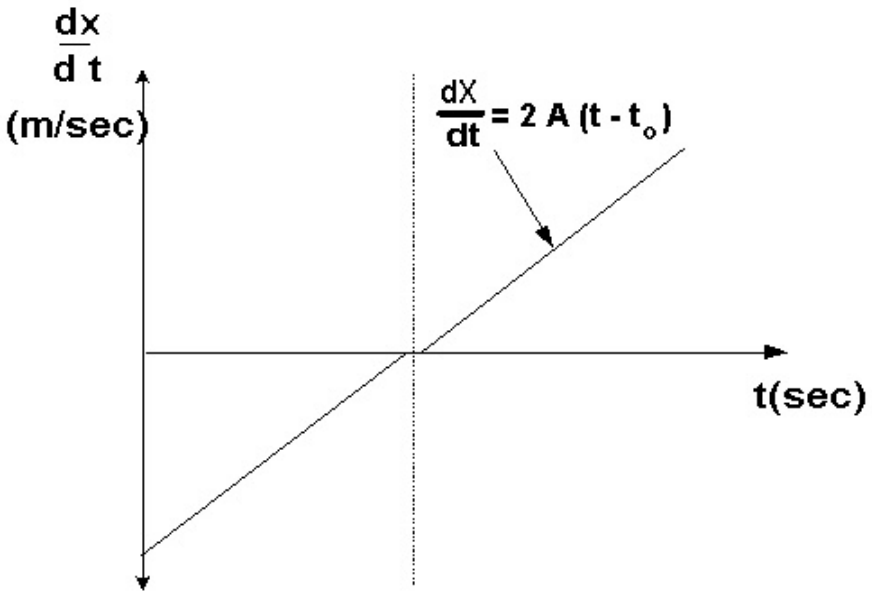

(b) Linear velocity profile

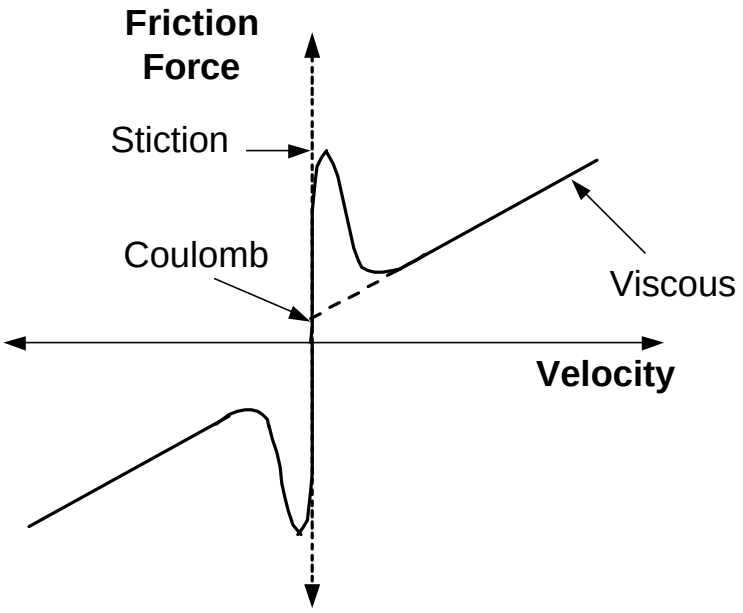

(c) Normal friction characteristics in the valve

Figure 3.3 Spool position, velocity and friction force profile

The parabolic waveform used as a desired input signal for position control is shown in Figure 3.3 (a). An LVDT connected to the valve accurately measures the valve position, and the resulting signal is compared to the desired signal from which an error signal is generated. In the closed loop control system shown in Figure 3.4, Controller A outputs the necessary voltage V, to Solenoid A, which generates the required force F_{Sol} to drive the valve spool to desired position by correcting for any external disturbances. The force disturbance shown in Figure 3.4 is in fact the force or load produced by the fault simulator.

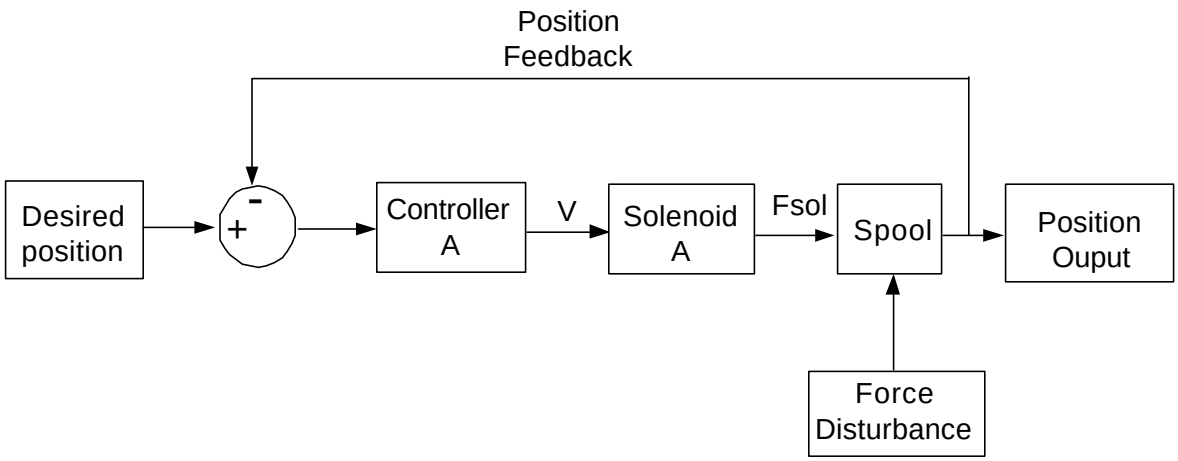

Figure 3.4 Closed loop position control system

3.3 Control System for Force Control

As outlined in the previous section, the position control algorithm used spool position feedback to drive the valve spool using Solenoid A with a linearly increasing velocity profile. The second control algorithm to be developed was that of generating the desired friction characteristics using Solenoid B. As the Solenoid A moves the spool with a linearly increasing velocity profile the desired frictional force to be simulated was generated in Solenoid B by means of a look-up table.

As shown in Figure 3.5, the input signal to the fault simulator is the velocity of the spool and output signal is the friction force on the valve spool. The algorithm implemented in the friction model was a simple lookup table that determines the magnitude of the desired friction force based upon the corresponding velocity. For example, when the spool is reversing direction, the velocity at reversal would be near zero. This velocity corresponds to a certain magnitude of stiction force in the look-up table which was used as the desired friction force for the fault simulator. The force transducer measures the force generated by the Solenoid B and is compared to the desired force signal based on which an error signal is generated. Controller B outputs the required control signal to Solenoid B to

generate the desired friction characteristics. The friction force generated by the fault simulator depends upon the combination of the inherent friction characteristics of Solenoid B and the friction model. The selection of friction model determines the shape and magnitude of the friction curve which is discussed in the next section.

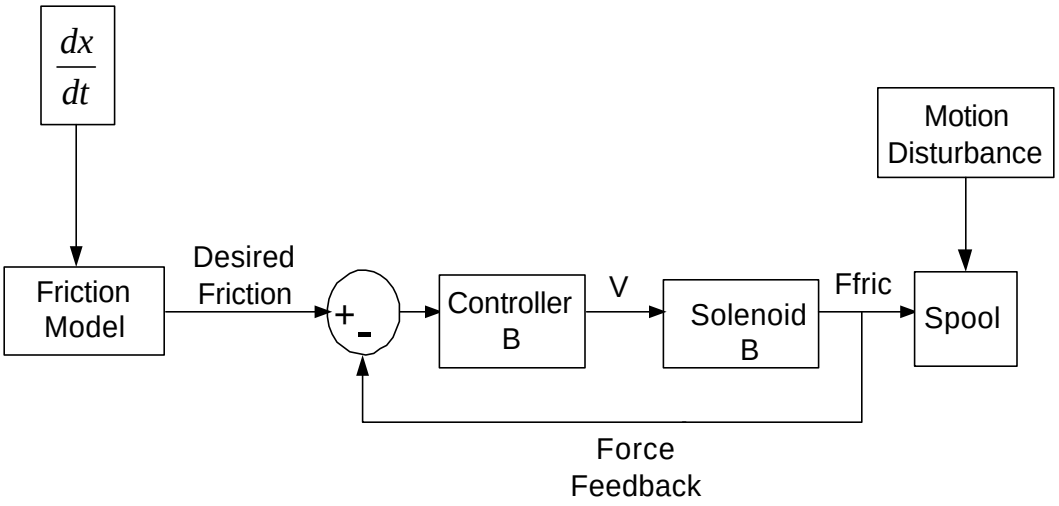

Figure 3.5 Closed loop force control system

3.4 Friction Model

An important consideration in the design of the fault simulator is the friction model. Friction modeling has been an intriguing and a challenging proposition for control engineers as the loading conditions, lubrication, materials and other factors make it difficult to model the problem at hand using a general friction model. The friction model developed should closely represent the actual friction characteristics of the system, which are a function of the sign and absolute value of velocity.

Since this research was primarily concerned with artificially introducing increased friction in the valve, it was desired for the friction model to be able to incorporate the desired values of stiction, Coulomb and viscous friction defined by the user. The friction model should be flexible enough to accommodate changes in any one of the friction

characteristics while keeping the others constant or to incorporate a change in all three components.

The friction model used for this research had a similar structure to the Karnopp [1985] model but used the velocity of the valve spool in real time as an input signal to the model, as depicted in Figure 3.6 (a). The model used in this research utilizes the information on velocity of the spool to output the desired friction force specified by the user based upon a look-up table. The look-up table is activated for two different velocity bands as shown in Figure 3.6 (a); a lower velocity band which activates the stiction characteristics and the higher velocity band which activates the Coulomb and viscous friction models.

In spool valves stiction occurs at very low velocities or near zero velocities; generally when the spool is about to begin its motion or when reversing the direction. It occurs because the applied force is unable to overcome the friction force thereby preventing the motion of the spool. For the fault simulator to simulate an increase in the Static friction, it should apply an equal and opposite force equal to that of Solenoid A in addition to the inherent stiction in the valve (Equation 2.2). In the case of conventional on/off solenoid valves, the solenoid force is highly nonlinear and varies as the armature position changes for the same value of current. Hence simulating stiction at the desired position in conventional solenoid on/off valves is very difficult. In contrast, proportional solenoid valves have a constant force output for a particular value of current irrespective of the position of armature in the air gap as outlined in Section 2.2. This property of proportional valves was used in the current research, to simulate stiction at any desired position of valve spool.

The procedure adopted to simulate stiction in the proportional valve was as follows: As shown in Figure 3.6 (b), when the spool velocity reaches a certain minimum value, (in lower of the two velocity bands shown) the current in Solenoid A is fed back to Solenoid B. Assuming that the force-current characteristics of both the solenoids are identical, the

force generated by Solenoid B should be equal to that of Solenoid A for the same value of current. Since the forces in both the solenoids are of the same magnitude, they cancel out each other resulting in no net force on the valve spool. Due to the absence of any driving force the spool is stalled at the desired location, thus achieving the same effect as of stiction at low velocities.

Once the force in Solenoid B reaches a certain predetermined/ desired level of static friction, as shown in Figure 3.6 (b), the model switches from static to sliding friction model. This is implemented using a logic function, that compares the measured value of stiction to the desired value (Fs), and outputs a logic zero when both are equal thereby cutting off the current to Solenoid B as shown in Figure 3.6 (b). The value of Fs determines the amount of static friction force simulated in the valve. As soon as the current to Solenoid B is cut off, the force due to Solenoid A accelerates the spool thereby increasing its velocity. When the velocity of the spool reaches a certain magnitude, i.e. the setting on the high velocity band, the friction model switches from a static to sliding (Coulomb and viscous) mode as shown in Figure 3.6 (a).

In the sliding mode, Coulomb friction is modeled as a constant that depends on the sign of velocity as shown in Equation 3.1.

$$F_{ca} = K_c \ \text{sgn}\left(\frac{dx}{dt}\right) \qquad (3.1)$$

By changing the value of gain K_c in Equation 3.1, varying levels of Coulomb friction can be simulated.

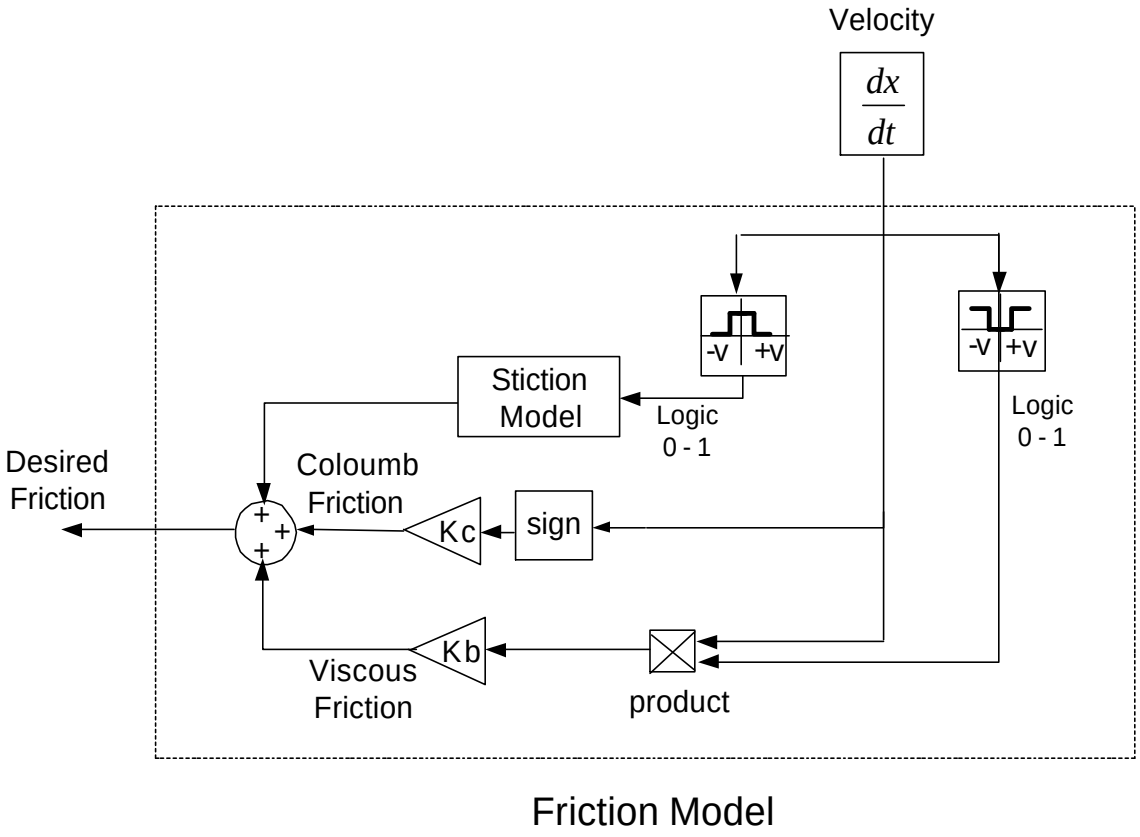

(a) Friction Model for inducing artificial friction in spool valve

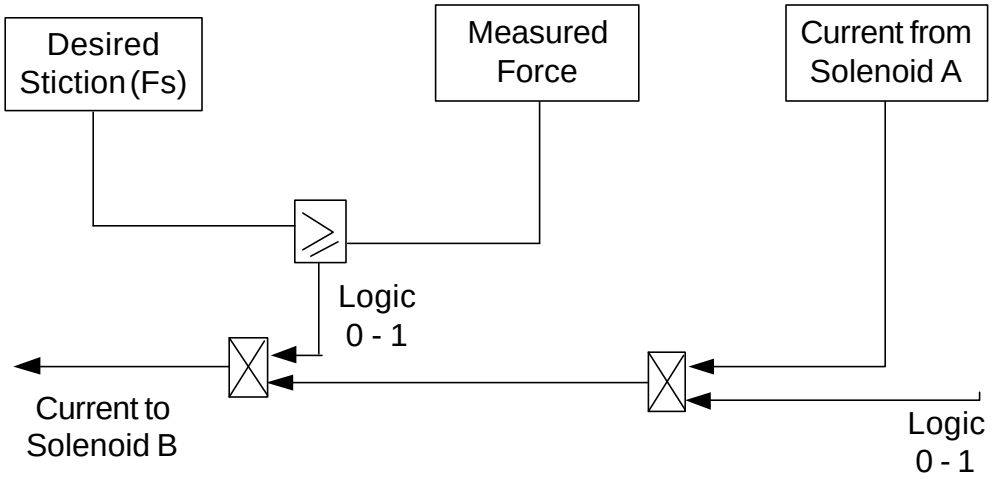

(b) stiction algorithm

Figure 3.6 Fault Simulator algorithm

The damping force is a linear function of velocity and is modeled by incorporating a constant of proportionality K_v, as shown in Equation 3.2. Keeping the velocity of the spool unchanged, an increase in damping force can be achieved by increasing the value of K_v which has the effect of increasing the slope of the friction curve as depicted earlier in Figure 3.2 (c).

$$F_{va} = K_v \frac{dx}{dt} \tag{3.2}$$

The desired friction force generated by the friction model is a combination of the stiction, Coulomb and viscous forces and forms the reference input for the force control algorithm. The force generated by the Solenoid B was superimposed on the existing friction characteristics in the valve spool thereby increasing the total friction force on the valve spool. This model does not model the transition region from stiction to sliding friction as the time taken from slip to stick would be in the same range as the dynamics of the solenoid. Thus, even though this model may not be able to simulate the profile of the friction curve during the transition period, it does represent the transition time by virtue of the solenoid dynamics.

3.5 Control system interaction

In the normal configuration two proportional solenoids on opposite sides of the valve spool (refer Figure 2.1) are employed to achieve bi- directional position control of the spool. The fault simulator used in this research, utilizes one of the proportional solenoids as an actuator (Solenoid B) to output the desired friction force on the valve spool. As mentioned in the previous sections, since the force and velocity control systems are acting on one system; i.e. the spool, the control action of one system will tend to act as a disturbance input to the other system.

Consider Figure 3.7; Controller A tries to control the spool position by compensating for any force disturbances imposed on the spool due to the fault simulator.

This disturbance is desirable as it is a means by which the change in friction characteristics of the valve can be observed and the reliability of a CMS assessed. The valve spool was deliberately forced to move in a parabolic waveform which enhanced the inherent friction forces and also enabled observation of the force disturbance for the desired velocity range.

Similarly, the Controller B tries to control the force output of the fault simulator by rejecting the motion disturbance imposed on it due to the displacement of the spool. This disturbance on the fault simulator is undesirable and reducing the effects of it would be considered in Chapter4. The interaction between the two controllers is due to the fact that both of them have the spool as an common interface to control either the force or displacement.

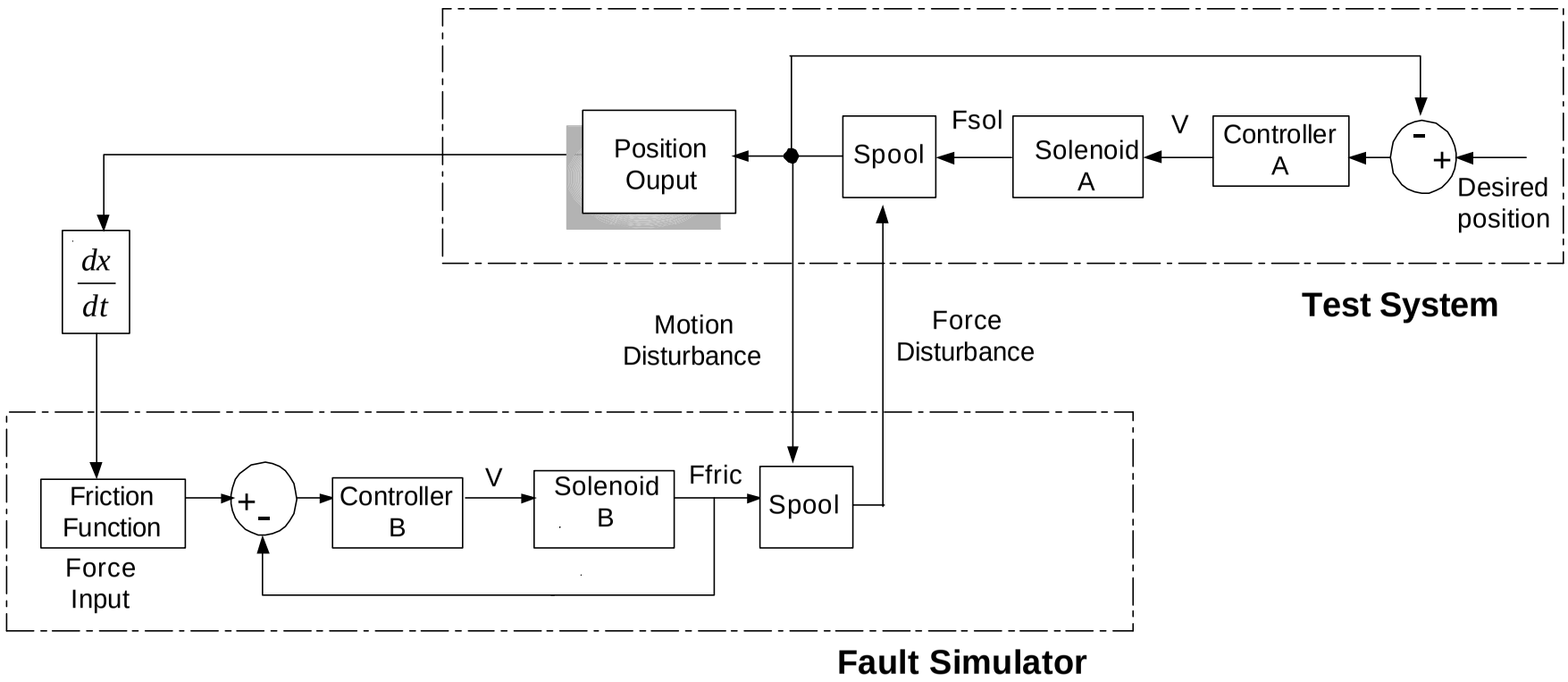

Figure 3.7 Interaction between force and postion control systems

3.6 Summary

Friction modeling helps the control designer in achieving improved performance of the plant by designing better control algorithms for friction compensation. Unlike the traditional use of friction modeling, this chapter investigated the development of a friction model for fault simulation in a proportional valve, where faults due to friction have a considerable effect. The friction model used a velocity-force look-up table, which was divided in two velocity regions; low and high velocity. Depending on the spool velocity the appropriate friction force values were output by the fault simulator.

Also, the control system design for implementing the fault simulator in a proportional valve was presented. The position control system made use of a unique waveform for forcing the spool to move with linearly increasing velocity so that the dynamics of friction at very low velocities can be easily observed and controlled. The corresponding force control algorithm ensured that the magnitude of desired friction characteristics which are a function of the spool velocity, is relatively unaffected by the disturbances due to the spool displacement.

The next chapter explains the controller design for force and position control, and the experimental results achieved using the friction model presented in this chapter.

Chapter 4

Experimental Results

Friction is an inherent phenomenon between two sliding surfaces, typically manifested in three different forms, depending upon the relative velocity between the surfaces. The friction model discussed in Chapter 3 was used to model the desired friction characteristics (static, Coulomb and viscous), by varying the magnitude and the shape of the desired friction curve. By implementing a closed loop control system, the fault simulator was used to artificially induce the friction characteristics in a PSV using the experimental setup described in Chapter 2. This chapter presents the experimental results achieved using the fault simulator to induce preset friction characteristics in the valve. The controller design for force and position control is presented along with a simple condition monitoring technique to validate the fault simulator.

4.1 General

As discussed in Chapter 1 the main objective of this research was to induce artificial friction faults in a PSV to facilitate the reliability evaluation of different CMS developed for these valves. The PSV with the spool and Solenoid A is the system in which the faults have to be simulated, and the fault simulator is any external device which induces the desired friction loading in the system. One of the innovative features of this project was to use the Solenoid B as the fault simulator which otherwise would have been a redundant component in the system. This design feature of fault simulator eliminates extraneous components otherwise required in the fault simulator and since both the solenoids are of the same rating, greatly enhances fault simulation. The friction model described in Chapter 3 was used to induce the faults over the existing friction characteristics in the PSV.

The existing friction characteristics, henceforth referred to as the “normal friction characteristics”, are the values of friction inherent in the valve. These represent the

magnitude of friction in the valve, when the valve is operating normally or is in a "healthy" condition. Many researchers have tried to estimate the friction parameters in a valve, but a recent study by Dan et al [2001] suggested at having a map of the friction characteristics over the entire length of spool travel rather than estimating it at one point. Since measuring the value of friction force was not practical, the study suggested mapping the current characteristics of the solenoid to gauge the health of the valve. The fault simulator developed in this research, used a parabolic displacement waveform described earlier in Chapter 3 and can be used to induce the faults at any particular location in the valve. A measurement of the current characteristics of the Solenoid A can provide a great deal of information regarding the type and magnitude of the fault being induced. The closed loop force control system for inducing these faults ensure a controlled insertion of the faults thereby providing a correlation of change in current to the amount of fault introduced. This particular aspect is further described in the Section 4.4.

Since the friction characteristics of the valve are indirectly contained in the current characteristics, the current in Solenoid A was measured to provide a trend of the friction parameters rather than explicitly measuring them. Solenoid B, which acts as a fault simulator, however, contains the armature which slides in the housing and thereby possesses its own friction characteristics. To introduce additional friction in the valve, it was first necessary to know the amount of static, coulomb and viscous friction in the Solenoid B, as it would contribute additional friction to that induced by the fault simulator.

As the Solenoid A drives the valve spool, it overcomes the acceleration and spring forces along with the friction in the valve. Therefore, the force measured by the force transducer, F_T , which is placed between the valve spool and Solenoid B, as shown in Figure 4.1, measures the force required to overcome the armature friction and spring forces in Solenoid B. This can be better explained with the aid of Equation 4.1.

$$F_{Sol\,A} - (M_v \ddot{x} + K_v x + F_{fric}) = F_T = F_{solB} \tag{4.1}$$

where, $F_{fric} = F_s + K_c \operatorname{sgn}\left(\frac{dx}{dt}\right) + K_b \frac{dx}{dt}$

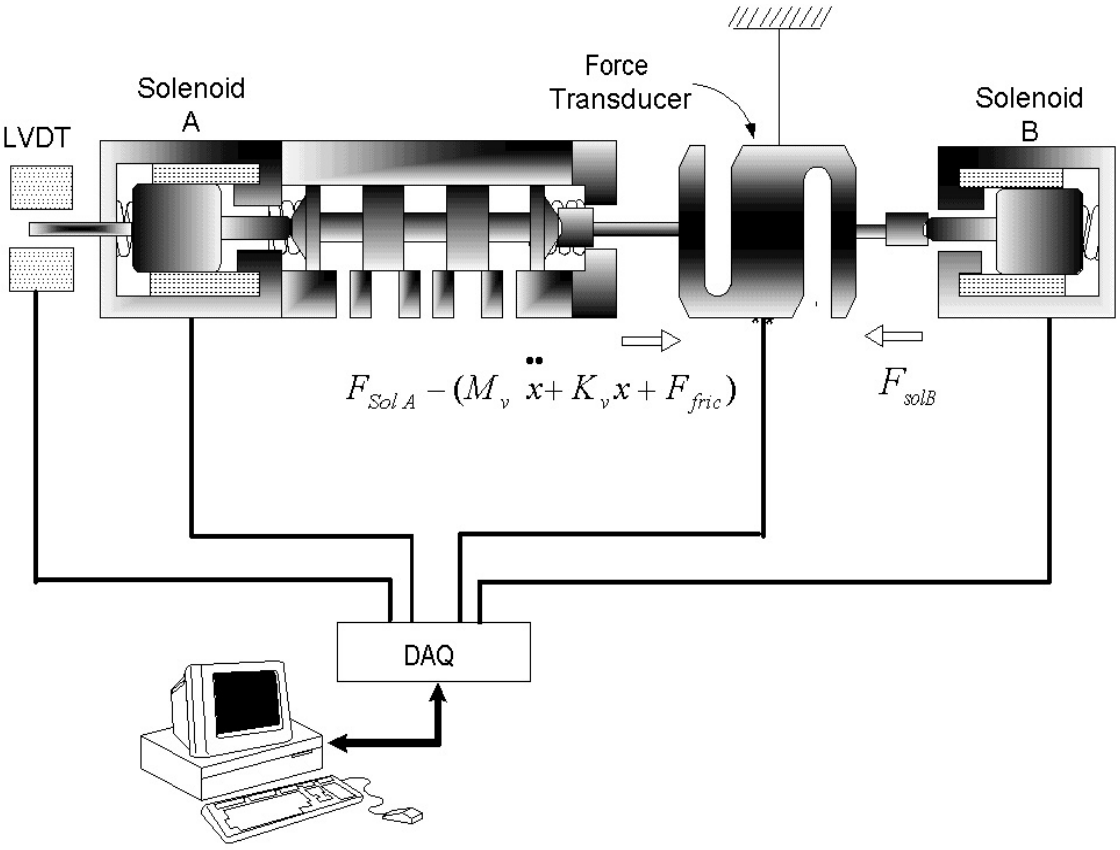

Figure 4.1 Solenoid force measurement using force transducer

The force required to overcome the spring and friction force in Solenoid B is given by

$$F_{solB} = M_a \ddot{x} + K_a x + F_{sa} + F_{Ca} + F_{Va} \tag{4.2}$$

In the above equation, the spring force in Solenoid B was measured and the spring constant was found to be 0.465 N/m. The calibration of the Solenoid spring is given in Appendix B.

To determine the amount of friction, the spool was moved along a triangular displacement waveform as shown in Figure 4.2 (a). By using a triangular displacement waveform the spool can be moved at a constant velocity thereby forcing the acceleration term in the Equation 4.2 to zero. This facilitates the determination of the friction parameters of the Solenoid B, having already determined the spring force.

The three friction terms as shown in Equation 4.2, each have unique behavioral characteristics with respect to the spool velocity and can be determined by moving the spool along a certain velocity pattern. In order to determine the Coulomb friction which is a function of the sign of velocity, the spool was moved along a triangular displacement waveform as seen in the Figure 4.2 (a), with a constant velocity of 0.5 mm/sec or displacement of 0.5 mm per 500 sample points. Since the slope of the waveform in Figure 4.2 (a) changes from positive to negative at the reversal point, the Coulomb friction also changes the sign instantly thereby causing an abrupt drop in the force characteristics as shown in Figure 4.2 (b). Of the total Coulomb friction as shown in Figure 4.2 (c) half the value is the force for the spool displacement with positive velocity and the other is due to the negative velocity. Note that by using a triangular waveform, stiction is eliminated during the reversal position by changing the spool velocity abruptly from a positive to negative value, thereby not allowing enough chance for the inter-surface asperities to lock into each other and stall the spool. The magnitude of Coulomb friction was found to be 0.17 N. This experiment was repeated at different points of spool reversal, and the average Coulomb friction was found to be 0.17 N.

The slope of the force/displacement waveform (Figure 4.2 (c) was found to be 0.4 N/m, which is due to the fact that there is negligible viscous friction in the solenoid and is entirely due to the force required to overcome the spring rate (0.45 N/m).

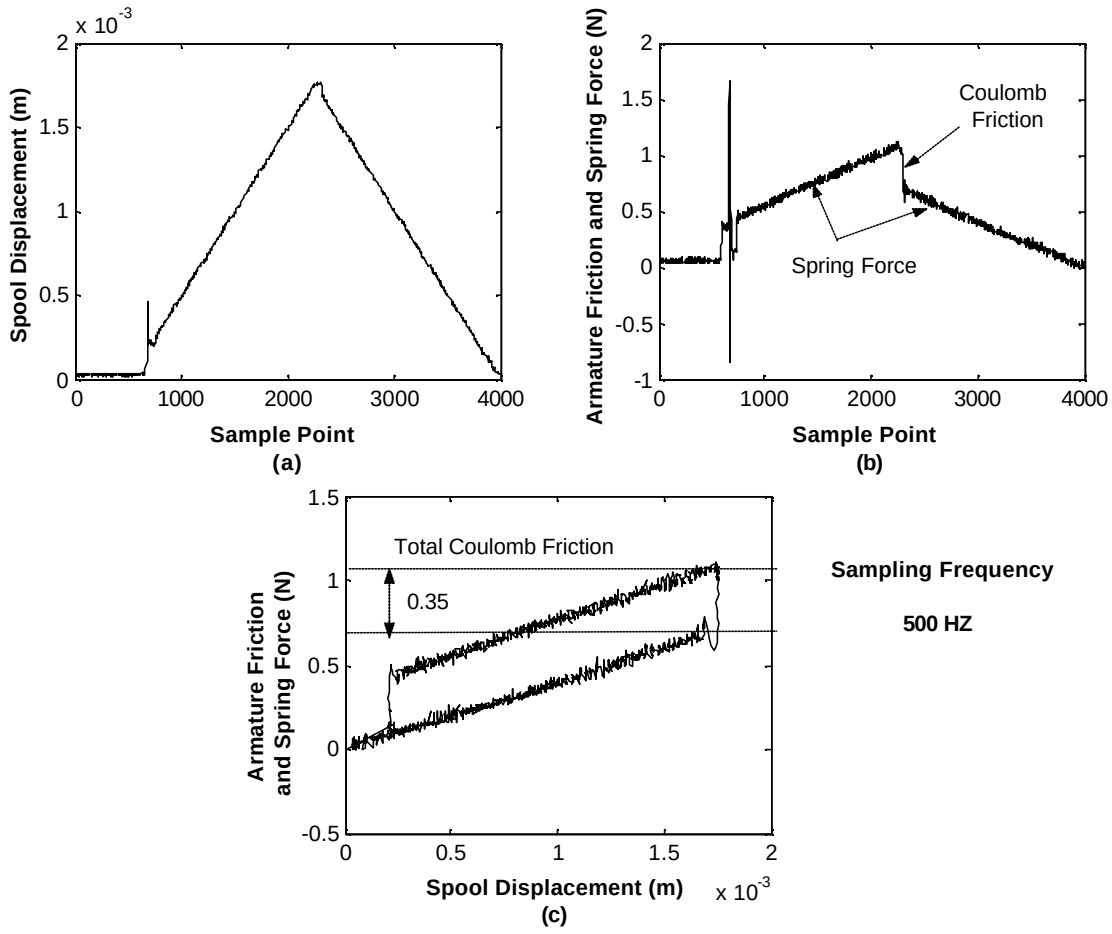

Figure 4.2 Coulomb friction estimation

viscous friction should theoretically increase as a linear function of velocity. To measure the viscous friction, ramp signals of increasing slopes were used as the displacement signal to the valve spool. By increasing the velocity of the spool for each test an estimate of the corresponding increase in damping force can be achieved which provides us with the damping ratio of the Solenoid B. The damping force was calculated from the Equation 4.2, by subtracting the spring force and Coulomb friction estimated earlier. It was found that moving the spool with velocities ranging from 0.5 mm/sec to 4 mm/sec the damping force did not exhibit any significant increase in its magnitude as shown in Figure 4.3. Hence it was decided that for further experiments the damping in Solenoid B would be considered to be negligible.

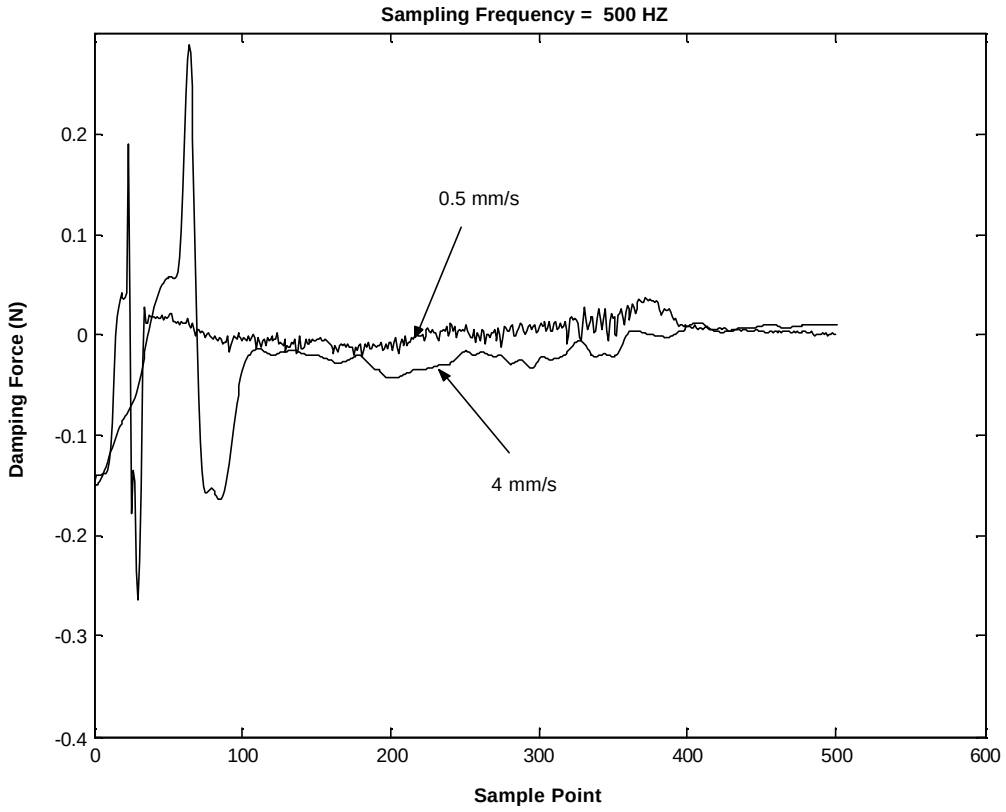

Figure 4.3 viscous friction estimation

The stiction in the valve was found difficult to estimate by simple means as the solenoid spring pre-compression was superimposed on the stiction characteristics and was difficult to estimate at any desired location. These measurements are carried out to serve as benchmarks below which no friction characteristics can be simulated by the fault simulator and hence serve as a minimum threshold above which the desired friction characteristics are induced.

The next step was to verify the effectiveness of the fault simulator to induce the faults. As described in Chapter 3, since the motion of the test system provides a disturbance input to the fault simulator and vice-versa, it is imperative to design suitable controllers for both systems to be able to induce the faults in a controlled manner. The following sections describe the controller design for the position and force control of the

test system and the fault simulator, respectively. Also, the experimental results achieved by implementing the controller are presented. The duration of all the experiments was chosen to be 6 seconds and were carried out at room temperature of 20° C.

4.2 Controller Design for Position and Velocity Control

As mentioned in Chapter 3, the input signal to the Solenoid A is the desired displacement of the valve spool, which is a parabolic displacement waveform designed to enhance the typical friction characteristics at the spool reversal point. The requirement of the controller was to make the spool follow the parabolic part of the desired displacement waveform as closely as possible to generate a linearly increasing velocity profile. This would facilitate the simulation of stiction in the low velocity region and the coulomb and viscous friction for the higher velocity regions.

There are many types of valve controllers used in the industry but the most commonly used type of controller is the PID (proportional plus integral plus derivative) controller. A typical PID controller has the following form

$$\text{Controller output} = K_p\, e_k + K_i \frac{T}{Z-1}\int e_k + K_d \frac{d}{dt}(e_k) \tag{4.3}$$

Where

e_k = Error signal at a sampling instant k,

K_p = Proportional gain,

K_i = Integral gain,

K_d = Derivative gain and

T = Sampling time

The method of determining the parameters of the controller which satisfy the performance requirements of the system is termed as “controller tuning”. One of the popular methods of tuning the industrial process controllers was suggested by Zeigler and Nichols [1942]. The procedure adopted was as follows:

1. In the closed loop system shown in Figure 4.4, the controller gains are set such that the integral and derivative gains for Equation 4.3 are set to zero and the proportional gain is increased from zero to a critical gain at which the system exhibits sustained oscillations.
2. Such a system is termed as a marginally stable system and the corresponding controller gain as the critical gain (K_{cr}) the oscillation period as P_{cr}. Thus both the critical gain and oscillation period are determined experimentally.
3. The Controller gains are empirically set to

$$K_p = 0.6 * K_{cr} \tag{4.4}$$

$$K_i = 2 * K_p / P_{cr} \tag{4.5}$$

$$K_d = 0.125 * K_p * P_{cr} \tag{4.6}$$

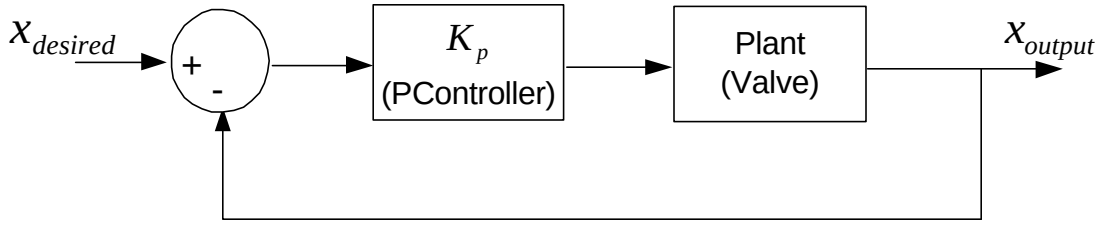

Figure 4.4 Closed loop system with only proportional control

Figure 4.5 shows the critical gains and oscillation period obtained by the above procedure at different spool positions. The natural frequency of the valve from the

manufacturer specifications is 50 Hz, which is in the same range as of the oscillation period depicted in the Figures 4.5 (a-d) of 0.025 sec. The controller gains were calculated by using the empirical formulas given by Equations 4.4-6, and their values are tabulated in Table 4.1. It was observed that the integral gain was much higher than the other two gains which is due to the characteristic drawback of the Zeigler-Nichols method which was originally developed for systems with larger time constants. Thus when used with electro-mechanical systems with smaller time constants the integral gain often tends to have a very large value which could make the system unstable.

The Zeigler –Nichols method served as a reference point for tuning the proportional and derivative gains to achieve the desired dynamic response. Based on the system response the integral gain was tuned to achieve a satisfactory steady state response.

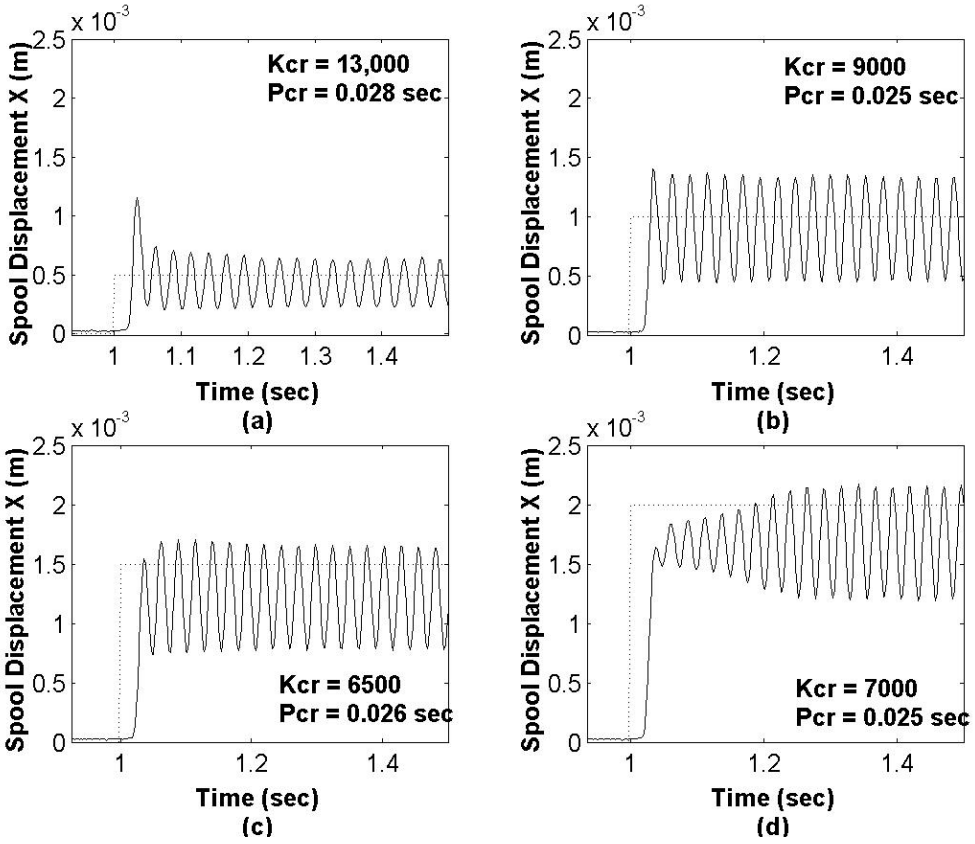

Figure 4.5 Critical gains for different spool positions

x / Gains	0.5	1	1.5	2
K_{cr}	13,000	9,000	6,500	7,000
P_{cr}	0.028	0.025	0.026	0.025
K_P	7,800	5,400	3,900	4,200
K_I	5,57,142	4,32,000	3,12,000	3,36,000
K_D	27.3	16.875	12.675	13.125

Table 4.1 Controller gains using Zeigler Nichols method

The final gains of the controller were tuned starting with the values in the above table and were decided based on the gains which gave a satisfactory velocity profile and minimal lag between the desired and actual spool position. Since the measured displacement signal is associated with noise, it was observed that the derivative control had a destabilizing effect on the system making the system response to be jagged. Hence it was decided to use a simple PI controller by dropping the derivative control. Moreover, since hydraulic systems have inherent damping present in them due to the lubricating oil between the clearance passage of spool and valve body, the derivative controller could be safely dropped.

The PI controller was subsequently tuned until a satisfactory response was obtained as shown in Figure 4.6 (a). The final gains of the PI controller were adjusted to $K_p = 3000$ and $K_i = 80{,}000$. As seen in the Figure 4.6 (a), the spool position exhibits an overshoot during the initial step response but due to the integral action follows the parabolic or squared part of the waveform quite accurately which is evident from the minimal error between the desired and actual spool position. The input signal was designed such that the velocity of the spool linearly increases from - 5mm/sec to + 5mm/sec in 1.02 seconds.

Figure 4.6 (b) shows the velocity profile for the spool displacement indicated in Figure 4.6 (a). The two abrupt peaks at 1.4 and 2.8 seconds are due to the differentiation of the leading edge of the step input for the spool displacement. The linear velocity region, where the spool velocity increases from – 5 mm/sec to + 5mm/sec, was used as an input signal to the fault simulator for simulating the friction characteristics. The spool velocity signal was obtained by differentiating the displacement signal measured in real-time and a low pass third order Butterworth filter with the cut off frequency of 20 HZ was used to obtain a relatively noise free velocity signal shown in Figure 4.6 (b).

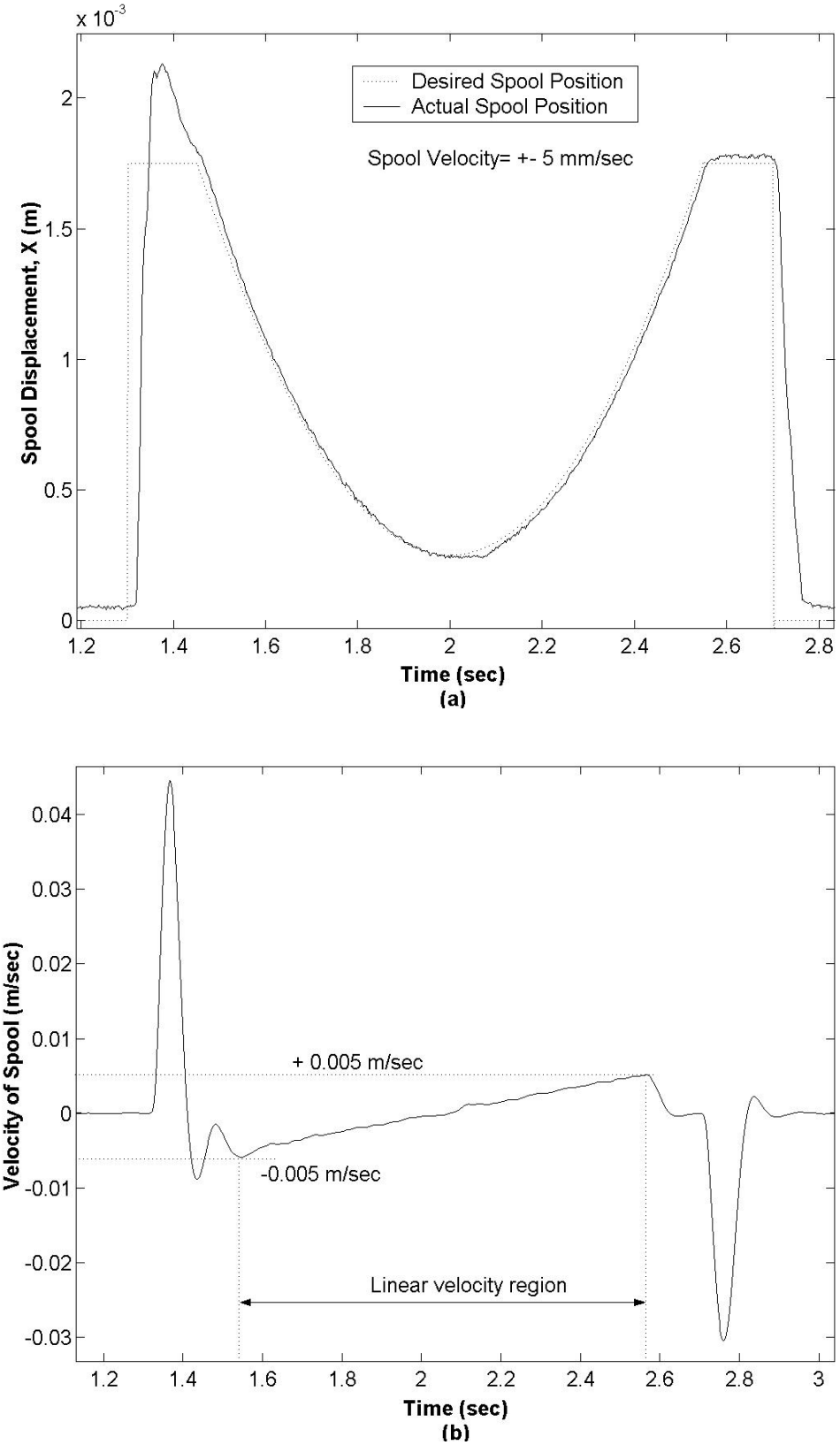

Figure 4.6 Spool position and velocity profile using a PI controller

One of the drawbacks of using a higher order filter was the introduction of a time lag in the velocity signal. As seen in Figure 4.6 (a), the spool reversal at 0.25 mm occurs at 2 sec, whereas in the velocity profile (Figure 4.6 (b)), the signal passes through the region of zero velocity at 2.025 sec. This indicates that filtering the signal introduces a delay of 0.025 sec. The input signal to the fault simulator is the velocity of the valve spool, based on which the fault characteristics are simulated. Thus it was imperative to use filtering and have a clear velocity signal which otherwise would have resulted in difficulties in designing the force controller. The velocity band used in the fault simulator for simulating friction was adjusted such that the velocity signal was processed earlier by the amount equal to the filtering time delay. In order to test the effectiveness of the controller at higher velocities, the spool displacement waveform was modified to produce spool velocities of +- 7 and 10 mm/sec. Figure 4.7 depicts the three displacement waveform used to produce the desired velocity profiles of 5, 7 and 10 mm/sec and the controller was found to be effective in closely following the spool displacement in the desired velocity range. Spool velocities greater than 10 mm/sec were not feasible as there was a considerable phase lag between the desired displacement and actual waveform

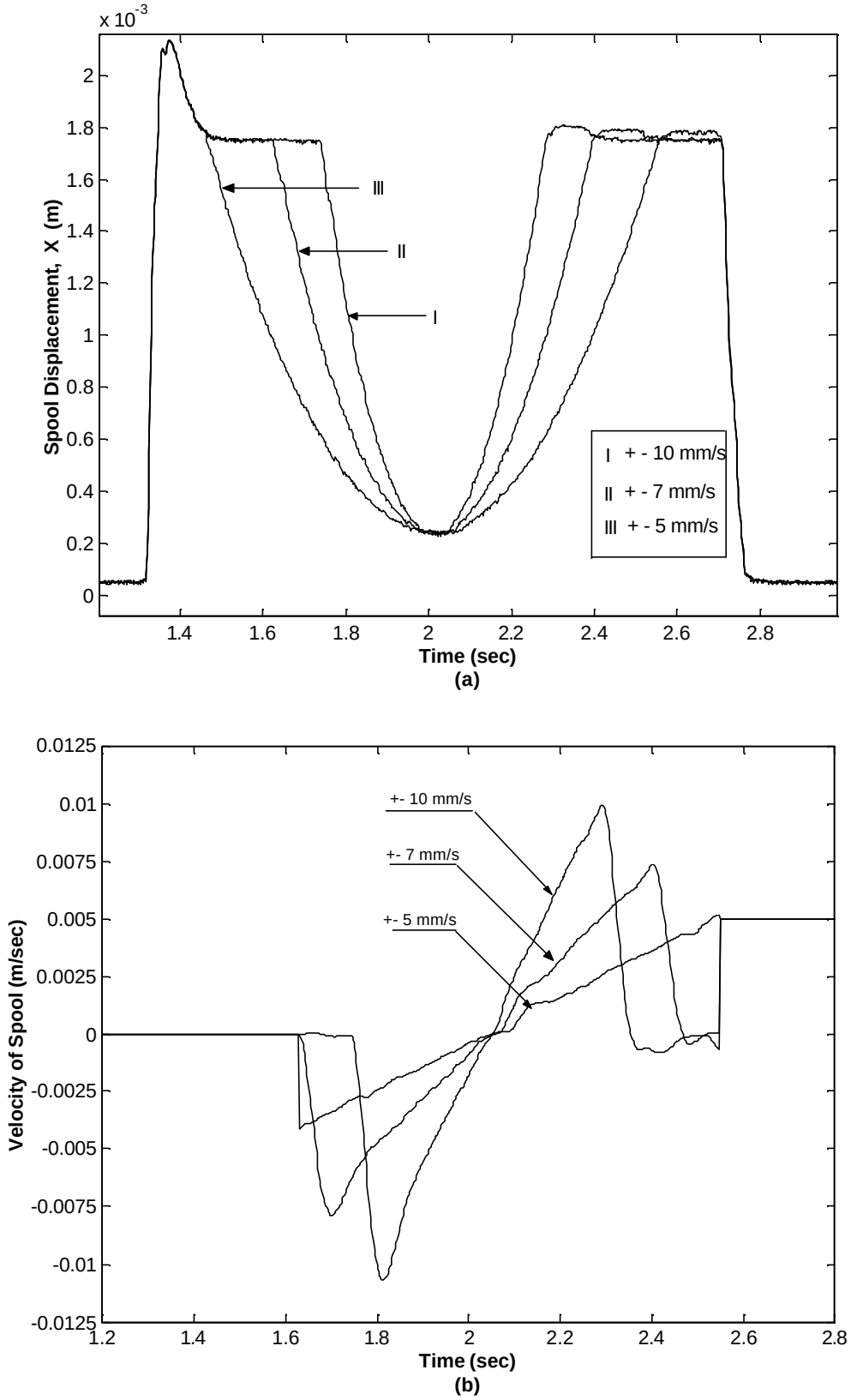

Figure 4.7 Measured spool displacement and velocity profile

4.3 Controller Design for Force Control

As mentioned in the previous section, the linear velocity region shown in Figure 4.6 (b) is used a reference signal by the fault simulator, for the different friction characteristics. The classical friction curve, as discussed in Chapter 3, is a function of linearly increasing spool velocity, and is symmetrical about the point of zero velocity. Hence, if the friction characteristics for only one direction of spool velocity, e.g. + 5mm/sec of Figure 4.6 (b), can be simulated then the friction characteristics for the reverse direction would be an inverted mirror image of the friction characteristics in positive velocity region.

This particular aspect of the friction characteristics was employed to simulate the desired friction characteristics only in the positive region of spool velocity. i.e. only unidirectional friction forces were induced in the valve using Solenoid B as the actuator. Moreover since the force transducer is located between the Solenoid B and the valve spool, it can measure the force exerted by Solenoid B on the valve spool, which in this case measures the friction forces induced on the valve by the fault simulator. This facilitates the closed loop control of the friction characteristics for the valve. In all the experiments for inducing the fault characteristics, a current amplifier with an output/input gain of unity was used to drive the Solenoid B, rather than using the conventional voltage amplifier. This was because the force produced by the solenoid is proportional to the input current and hence could be easily controlled by directly controlling the amplifier current to the solenoid.

4.3.1 Removing Bias of Force Transducer

As shown previously in Figure 4.1, when Solenoid A drives the valve spool, the force acting on the force transducer is that required to overcome the friction and spring forces of Solenoid B. The force measured by the force transducer as Solenoid A drives the spool through the parabolic displacement waveform is depicted in Figure 4.8 (a). Since the output of the force transducer is fed back to the fault simulator algorithm, there will

always exist a bias force which the force controller tries to compensate. Since the friction characteristics are to be induced in the linear velocity region, any force signal other than that produced by the fault simulator will tend to act as a bias on the friction characteristics to be simulated. Hence it was necessary to separate the bias force and the force characteristics due to simulated friction faults.

This was achieved by measuring the force from the transducer with Solenoid A driving the spool along a parabolic displacement waveform. These force characteristic are termed as the 'normal' force (F_{normal}) characteristics as they represent the force measured by the transducer during the normal operation of the valve as indicated in Figure 4.8 (a). The normal friction characteristics are then stored in a Matlab file which are recalled during the real-time simulation to be subtracted from the measured force, as shown in Figure 4.9. This procedure negates the effect of the bias signal due to the 'normal' force, thereby giving a net zero force as an feedback signal to fault simulator, as depicted in Figure 4.8 (b). The force signal to the fault simulator algorithm is now due only to those friction characteristics induced by the Solenoid B. This results in better control over the friction characteristics as the force controller is not required to compensate for the bias force and can be used for only for the control of friction characteristics.

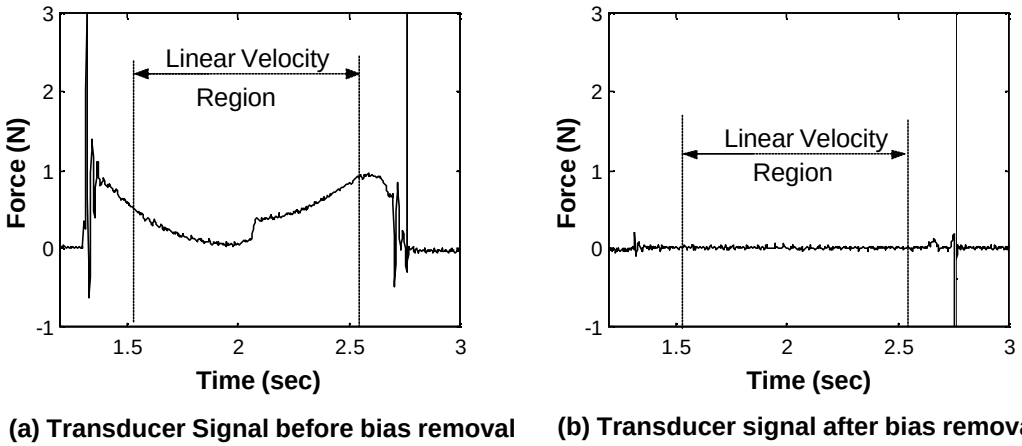

Figure 4.8 Normal force characteristics before fault simulation

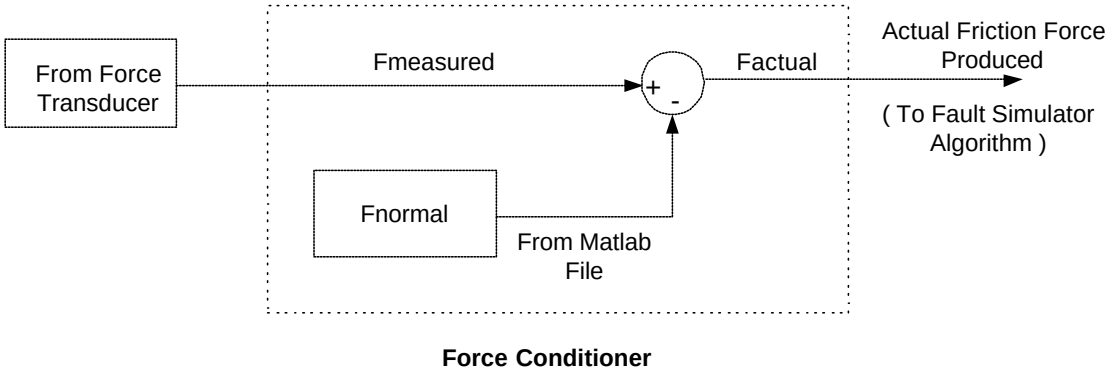

Figure 4.9 Force conditioning algorithm

This conditioned force is used in the feedback element of the fault simulator algorithm as shown in the Figure 4.9. The desired friction characteristics (static, Coulomb and viscous) were generated using the velocity of the spool as the reference signal, as depicted in Figure 4.10 below. The generation of Static friction is described in the next section as well as by the design of the controller to accurately produce the Coulomb and viscous friction.

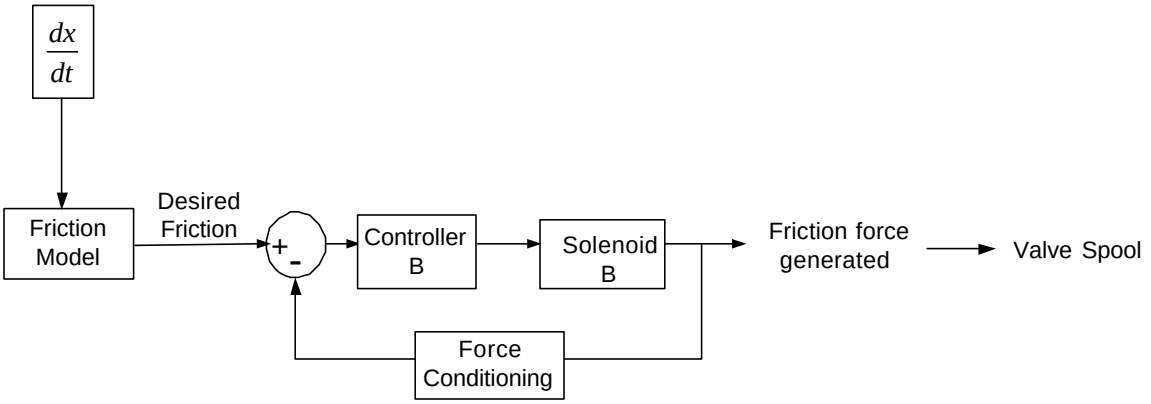

Figure 4.10 Fault simulator employing force conditioning in feedback loop

4.3.2 Static Friction /Stiction

Stiction is the resistive force between two sliding surfaces, which prevents any motion between them. The applied force must be greater than the static friction, to initiate motion of the body. Thus to simulate stiction at any desired position along the spool displacement, the spool must first be brought to rest or the velocity should be low enough for the spool and valve surfaces to “stick”, implying no relative motion between the sliding surfaces. Different magnitudes of stiction can then be simulated by applying an equal and opposite force on the spool. By varying the magnitude of the opposing force, the effect of various magnitude of stiction force can be simulated.

In summary the two requirements for inducing the stiction characteristics are,

a) A region of zero velocity implying no displacement of the spool and
b) Producing a force of the same magnitude as that generated by Solenoid A to prevent any motion of the spool from the zero velocity position.

The region of zero velocity was attained by moving the spool using the parabolic displacement wave form discussed earlier. During the reversal point, the inherent stiction in the valve causes the spool to stick momentarily causing a zero velocity band in the

otherwise linear velocity profile.

In order to generate the same magnitude of force as that of Solenoid A, it was decided to use the Solenoid B to generate the opposing force on the valve spool. This was achieved by measuring the current in the Solenoid A and using a current amplifier to amplify the measured current signal to Solenoid B. In carrying out this experiment the presumption was that the current-force characteristics of both solenoids were identical, giving exactly the same amount of force output for each value of current. If the current passing through both the solenoids is of the same value, the forces generated are also identical resulting in no net force on the valve spool.

Before proceeding with the aforementioned setup it was first necessary to know the force-current relationship of the solenoids with respect to the spool displacement. Normally in proportional solenoids the force is proportional to the current up to a certain spool displacement. It was desired to know the range of spool displacement for which the force-current relationship is proportional so as to have an idea regarding the range for which static friction can be simulated.

4.3.2.1 Force-Current-Displacement characteristics of a PSV

For a proportional solenoid, the force developed by the solenoid should be proportional to the input current irrespective of the armature displacement. This implies that in the working range, i.e. for the maximum spool displacements, the force/displacement characteristics would represent constant lines of force for increasing displacement of valve spool. The desired amount of force can be obtained for any spool displacement by passing the required amount of current through the solenoid coil.

The solenoid was tested for its force-current characteristics, by locking the armature in position against a force transducer and applying a voltage input to the solenoid coil. Force output tests with currents rising up to 2 amperes were carried out for 10 different armature positions over the 3 mm stroke length. The resulting 3 dimensional plot

is shown in Figure 4.11 (a). This plot confirms that the force generated by the solenoid is proportional to the coil current and does not change significantly over the normal operating range of the valve. The plot of the force-displacement characteristics in Figure 4.11 (b), suggests that by passing the same current in both the solenoids the solenoid force acting on both the sides of the valve spool can be balanced, thereby possibly stalling the spool at any desired location between 0-3 mm of its travel.

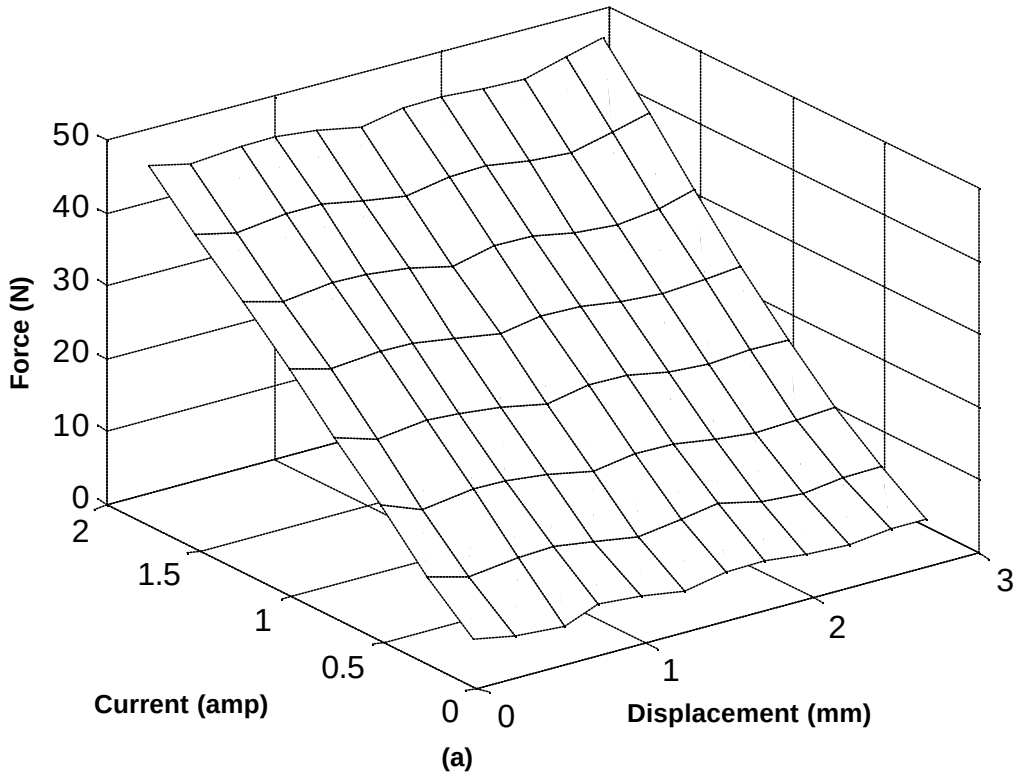

(a)

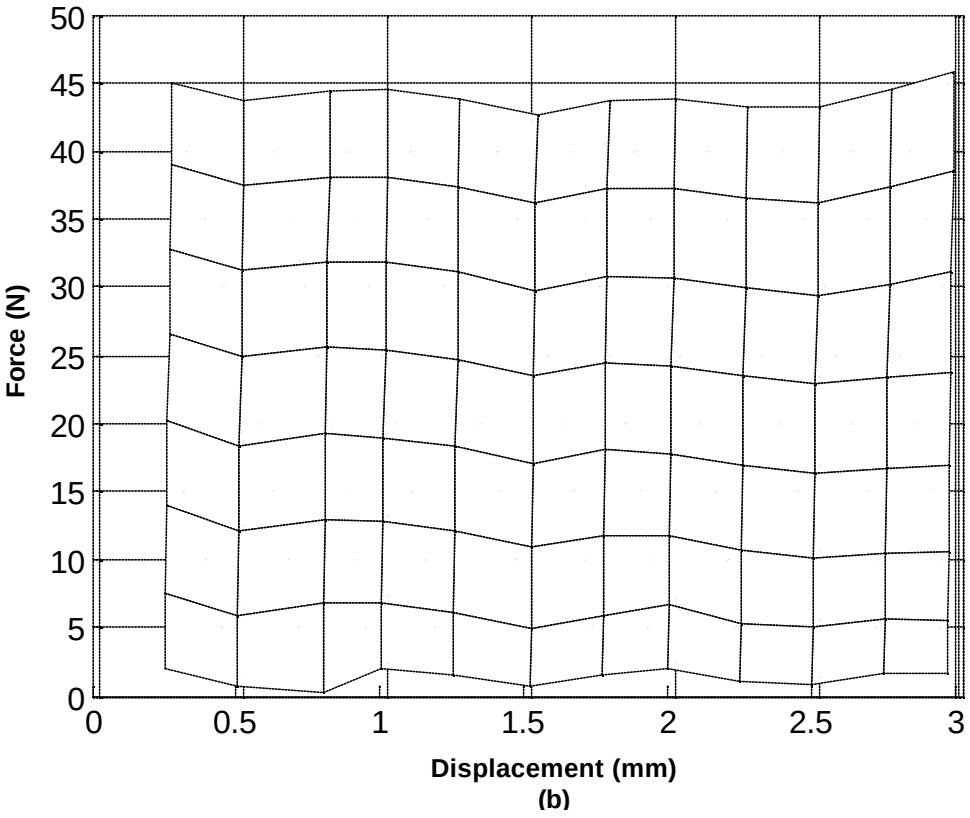

Figure 4.11 Force -Current- Displacement characteristics of Proportional Solenoid

It was noted during the experiments that the pre-compression of the valve spring which was @ 2.5 mm, caused an unbalance in the spring forces as the valve spool was displaced to either side of the center position. Since the spool is centered in the valve body by the spring forces, the spring forces balance each other only at the centre position . As the spool moves to either side of the center position, one of the springs is compressed while the other is decompressed. This causes an imbalance of forces away from the centre position, such that the force applied by the spring under compression is $2K_a x$ until the pre-compression length and is equal to $K_a x$ thereafter.

Thus, at any desired position, if the current in both the solenoids is the same, the spool should be stalled in absence of the centering springs. But due to the imbalance in spring forces at other than centre position, the valve spool is pushed by the compression

spring until the spring forces balance each other. Theoretically the spool should be pushed back to the centre position, but due to the presence of friction and other non-linearities like hysteresis, the spool can reside at a new position in between centre position and the desired location of stalling, depending on the magnitude of the non-linearities. At the moment of the stalling and just before the compression spring pushes back the spool, the friction forces are zero and the interaction of the solenoid and spring forces acting on the valve spool can be given by Equation 4.7,

$$F_{SolA} = 2K_a x + F_{Sol\mathbf{B}} \tag{4.7}$$

If forces in both the solenoids are the same, the spring force of $2K_a x$ still remains unbalanced in the above equation and causes the spool to accelerate in the reverse direction and reach a new position other than that desired. Thus in order for the Solenoid B to stall the spool it should generate only enough force to balance the above equation. In other words the difference in the force generated by Solenoid A and B should be equal to $2K_a x$ to balance the spool as shown in Equation 4.8.

$$F_{SolA} - F_{Sol\mathbf{B}} = 2K_a x \tag{4.8}$$

Since the force generated by the solenoid is proportional to the input current, it follows that the above force balance equations can also be written in terms of their current components, i.e.,

$$i_{SolA} - i_{Sol\mathbf{B}} = i_{2K_a x} \tag{4.9}$$

Thus if the force required to overcome the spring force, $2K_a x$, can be measured in terms of the equivalent current, as shown in Equation 4.9, the current required in the Solenoid B, for the force balance on the valve spool can be calculated as

$$i_{SolB} = i_{SolA} - i_{2K_a x} \tag{4.10}$$

In order to measure the current required to overcome the spring force $2K_a x$, a map of the solenoid current vs. spring displacement was obtained by feeding a ramp input signal to the Solenoid A and measuring the corresponding current in the solenoid using a current meter. The spring displacement was measured using the LVDT integral to the Solenoid A. The arrangement used for measuring the spring current is illustrated in Figure 4.12. A polynomial function of fifth order was used to fit the Current-Displacement curve and is used as a look-up table which outputs the current for the corresponding input displacement. The polynomial function used is given by Equation 4.11.

$$i_{2K_a x} = 1.7\text{e+}013 * x^5 - 1.5\text{e+}011 * x^4 + 5.2\text{e+}008 * x^3 - 8\text{e+}005 * x^2 + 1\text{e+}003 * x + 0.087 \tag{4.11}$$

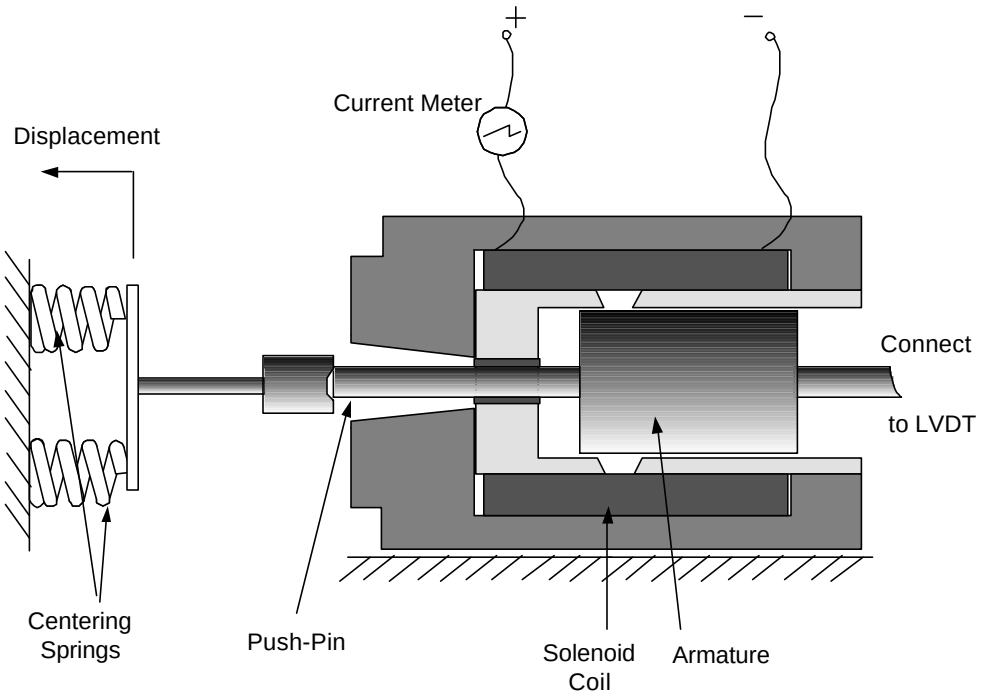

Figure 4.12 Experimental setup for main spring current-displacement characteristics

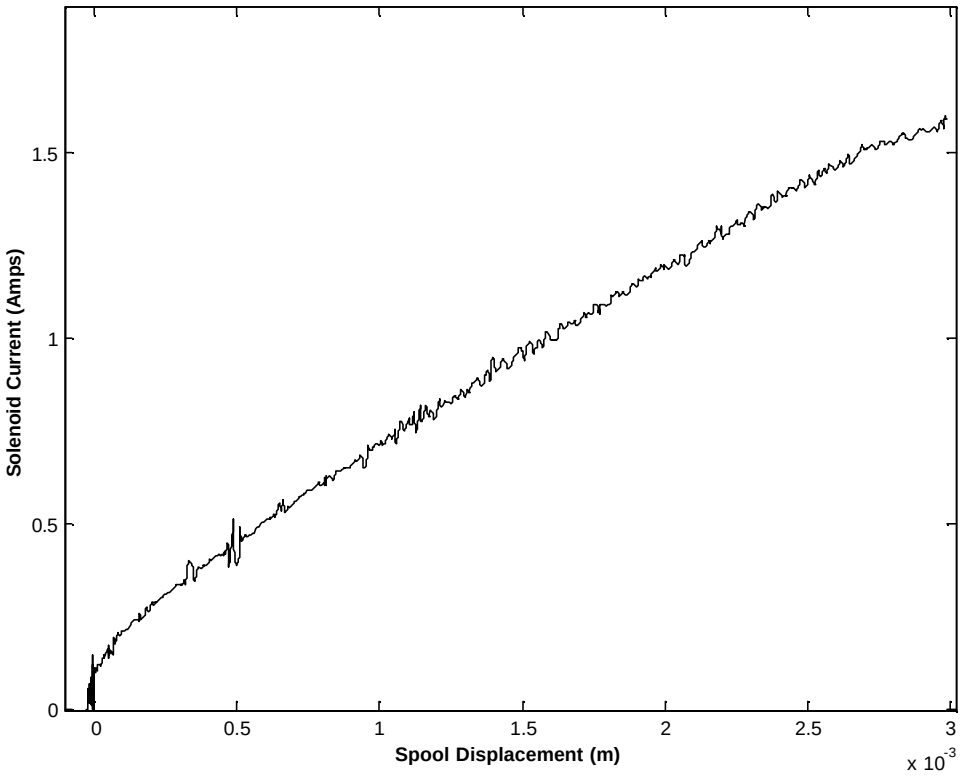

Figure 4.13 Main spring Current-Displacement characteristics

This spring current-displacement map was incorporated in the stiction part of fault simulator algorithm by subtracting it from the current given to Solenoid B as shown in the Figure 4.14. The stiction algorithm would output the current to solenoid B only when both the logic are true, i.e. the measured stiction should be less than the desired and at the same time the velocity of spool should be within the velocity band set for the stiction algorithm. The limit for the velocity band for stiction was set to 0.5 mm/sec, to account for the fact that the interlocking asperities between the sliding surfaces are elastic in nature and deform under load. This velocity band allowed small enough velocities up to 0.5 mm/sec during sticking. Since the stiction algorithm employs logic functions to switch off the current to Solenoid B when the desired level of stiction is achieved, no separate controller was required for controlling the magnitude of stiction.

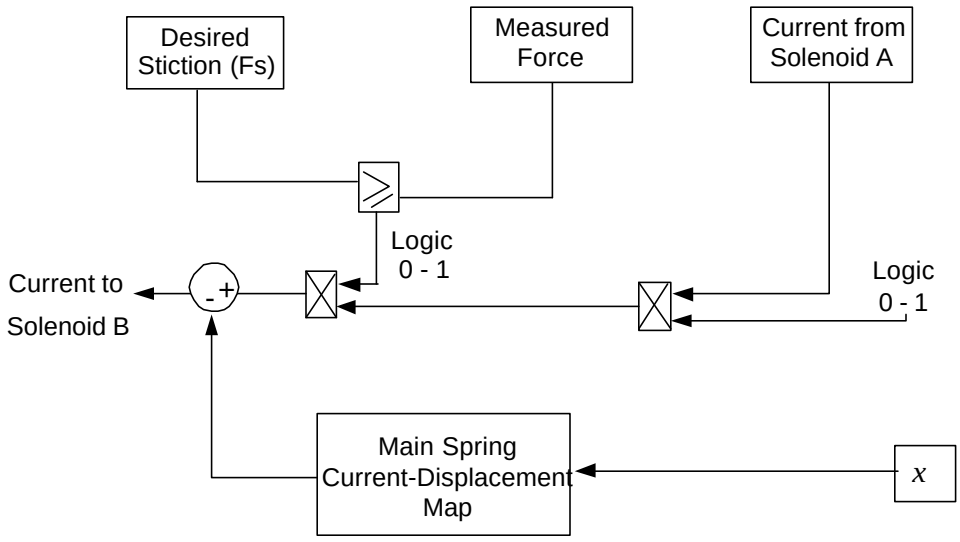

Figure 4.14 Current-displacement map of main spring for generating stiction

Figures 4.15 and 4.16 depict the experimental results for two cases of stiction conditions induced in the valve. In the first scenario, as shown in Figure 4.15, the limiting or maximum stiction was induced in the valve causing the spool to stall at the desired

location. As seen in Figure 4.15 (a), the valve spool follows the desired spool trajectory until the reversal position where the stiction fault is induced by the fault simulator. Due to the high value of stiction, Solenoid A was unable to generate enough force to move the spool causing the spool to stall at 0.25 mm. Also it can be observed from the velocity profile of the spool in Figure 4.15 (b), that ideally the spool velocity should linearly increase from -5 mm/sec to +5 mm/sec if the spool follows the desired displacement profile. But due to the induced stiction fault the velocity increases only from -5mm/sec to zero at the reversal position, where the stiction prevents any further noticeable increase in velocity. The value of the stiction force induced was 40 N.

It can be seen from Figure 4.15 (a) that after 2.3 sec, the spool is pushed back to the centre position by the fault simulator causing a negative spool velocity as seen in Figure 4.15 (b). This was attributed to the fact that as the current in the Solenoid A reaches the saturation value, the corresponding increased current in Solenoid B, develops more force than estimated to hold the valve spool at desired location. This was due to the non-linearities of both the Solenoids at higher values of current and force. It can be seen from Figure 4.15 (c) that the maximum value of stiction which results in stalling the spool was 40 N.

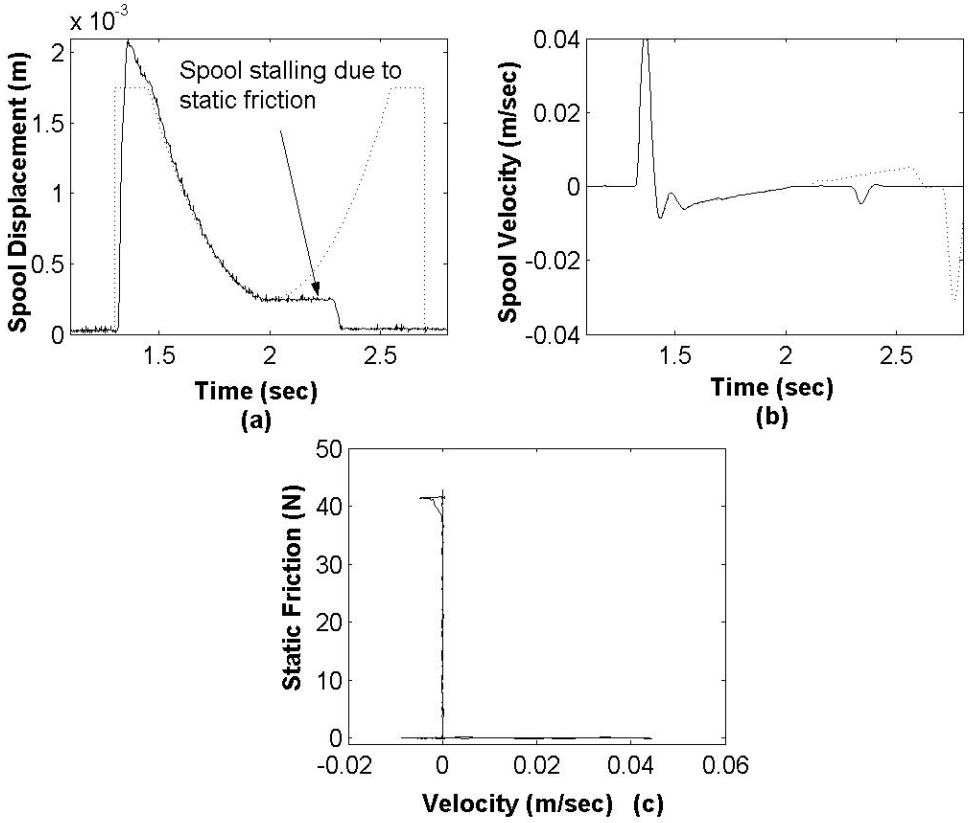

Figure 4.15 Maximum static friction induced in a PSV

In the second scenario, the induced stiction was limited a certain magnitude which was implemented using the algorithm depicted in Figure 4.14. The three magnitudes of stiction induced were 10, 5 and 2 N as shown in Figure 4.16 (a), (b) and (c). When the force developed by Solenoid A is greater than the induced stiction spool motion is initiated. During the time period when stiction is induced, the position controller increases its control output to compensate for the induced disturbance by increasing the current to Solenoid A. When the force developed by Solenoid A overcomes the induced stiction spool motion is initiated and the position controller moves the spool back along the desired trajectory, as depicted in Figure 4.17. But this is accompanied by an overshoot of the spool position, since the force required to keep the spool in motion is less than that required to initiate motion. The overshoot in spool position is related to the amount of induced stiction and increases as the magnitude of stiction force is increased. It can be

observed from Figure 4.17 that as the magnitude of induced stiction is increased from 2 N to 10 N, the corresponding overshoot in spool position is also increased, with the maximum overshoot being for the static friction of 10 N.

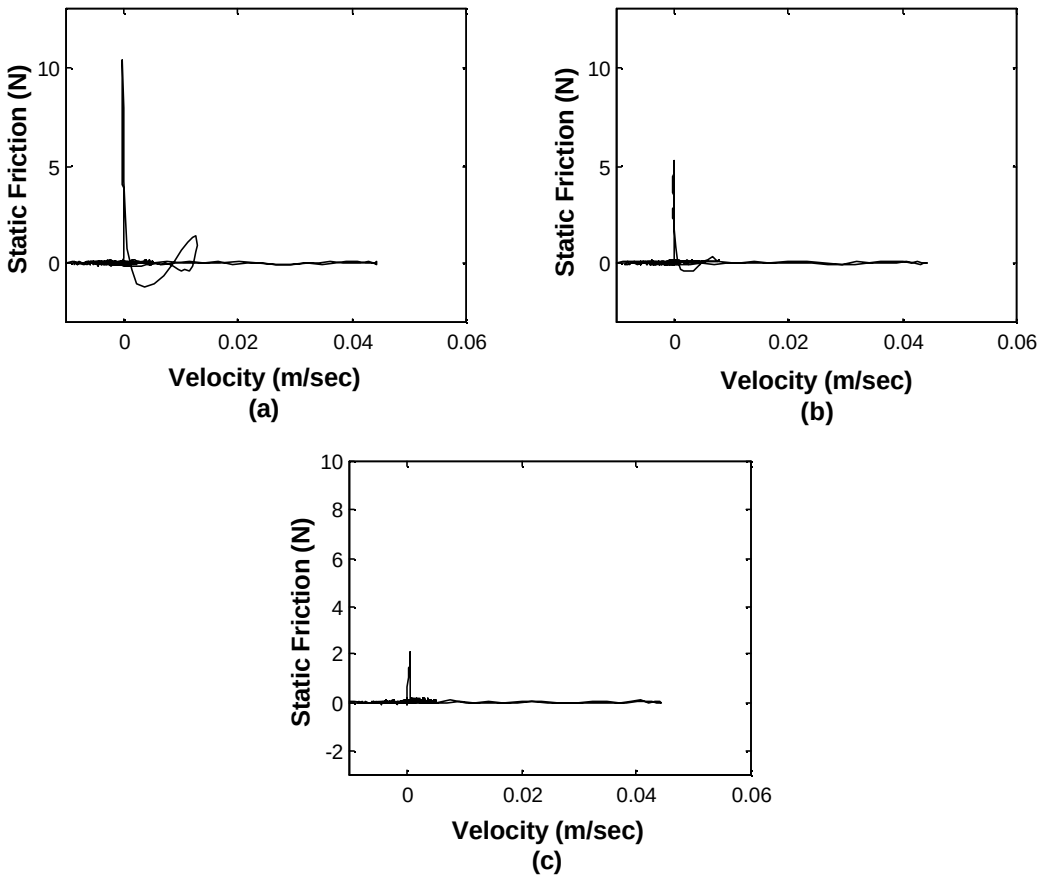

Figure 4.16 Different magnitudes of stiction induced in a PSV [(a) 10N, (b) 5N, (c) 2N]

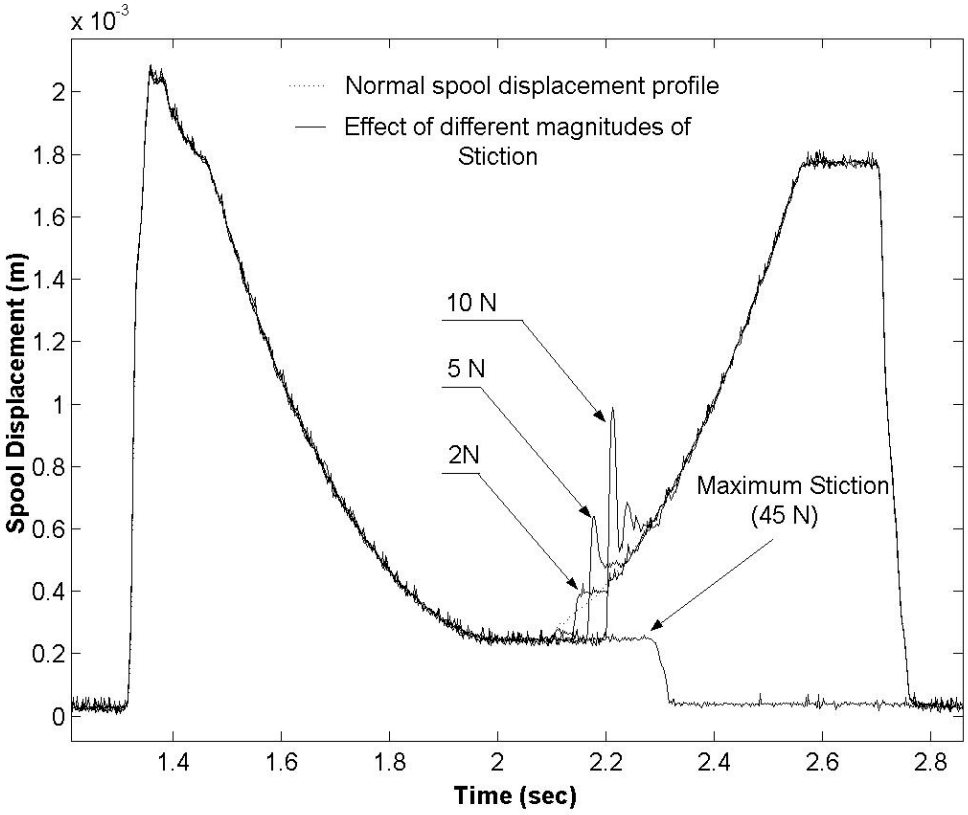

Figure 4.17 Effect of different magnitudes of static friction on spool displacement

4.3.3 Sliding Friction

As mentioned in Chapter 3, when the velocity of the spool reaches a certain magnitude, the velocity band for stiction algorithm outputs logic zero thereby switching off the current to Solenoid B as shown in the Figure 4.14. The threshold of velocity band was set at 0.05 mm/sec and was decided based upon on the fact that the interlocking asperities are elastic in nature and deform under load. This velocity band allowed small enough velocities up to 0.05 mm/sec during sticking and as the velocity increases beyond the threshold the asperities break allowing the surfaces to slide. The fault simulator algorithm switches from a stick to slip mode, when velocities greater than 0.05 mm/sec cause the velocity band for sliding friction to output logic 1. This activates the algorithm for sliding friction, where the desired Coulomb and viscous friction values can be set.

The force controller used for inducing the increased coulomb and viscous friction employs a PI controller. The desired friction force is a function of the spool velocity which contains some noise as well as the force measured from the transducer contains the sensor noise it was observed that the derivative controller could make the system unstable and hence was not used in the controller. Moreover in the controller design for position control by Zeigler –Nichols the system should be excited such that the control variable exhibited sustained oscillations for determining the empirical parameters. But it was difficult to achieve the same for the force controller, since the position controller driving the spool always tried to compensate for any force disturbance imposed by the fault simulator. Hence the gains of the PI controller for force control were adjusted experimentally until the design satisfied the following criteria:

1. The response of Solenoid B should be fast enough to reach the desired value without any negative overshoot of the spool position. Negative overshoot implied that the friction force applied by the fault simulator should not result in the spool being pushed in a direction opposite to its path of travel. This was an important consideration for designing the controller, since a failure to control the negative overshoot implied that the friction force could push the spool in the reverse direction of its travel, which was not possible practically.
2. The controller should be able to maintain the desired steady state value by compensating for the motion disturbance imposed by the spool.

Using the above criteria the final gains of the controller were adjusted to $K_p = 1.4$ and $K_i = 10$. The PI controller with these gains was used for all subsequent experiments carried out to induce the coulomb and viscous friction.

4.3.3.1 Coulomb Friction

Coulomb friction represents a constant magnitude of force opposing the motion of spool and is dependent on the sign of the spool velocity. The Coulomb friction force was

represented by a step function, which was activated when the signal input to the sliding friction algorithm is set to logic 1 as described previously in Chapter 3 (Figure 3.6 (a)). A closed loop force control system using current as the control signal ensures that the desired coulomb friction force is simulated. The Coulomb friction inherent in the Solenoid B was estimated by the procedure outlined in Section 4.1 and was found to be 0.15 N. In all the experiments for inducing Coulomb friction the closed loop control induces only those values desired by the user. Thus for all the experiments it was thought to be of convenience for the user to interpret the results as biased by an magnitude of 0.15 N instead of explicitly including it in the desired value.

Figure 4.18 shows the experimental results of the measured Coulomb friction as a function of the spool velocity, with the velocity threshold set to 0.05 mm/sec and desired coulomb friction values of 0.5, 1, 1.25 and 1.5 N. It was observed that the Solenoid B was able to attain the steady state values without any negative overshoot of the valve spool position and also exhibited fast response time of 0.03 sec. The desired and measured values of coulomb friction for 0.5,1 and 1.25 N, as shown in Figure 4.19 (a-c), also indicate there was no overshoot of the measured values which ensured that the characteristics did not exhibit an alias stiction.

For values of coulomb friction greater than 1.5 N, a negative overshoot of the spool position occurred, which indicated the controller settings were satisfactory only for inducing Coulomb friction values up to 1.5 N. A set of 15 experiments carried out in a period of three days indicated the results were highly repeatable. In some experiments due the drifting of the sensors, especially the force transducer which is highly sensitive (0.1 N), the ‘normal force characteristics’ had changed which caused a small error in the results (2%).

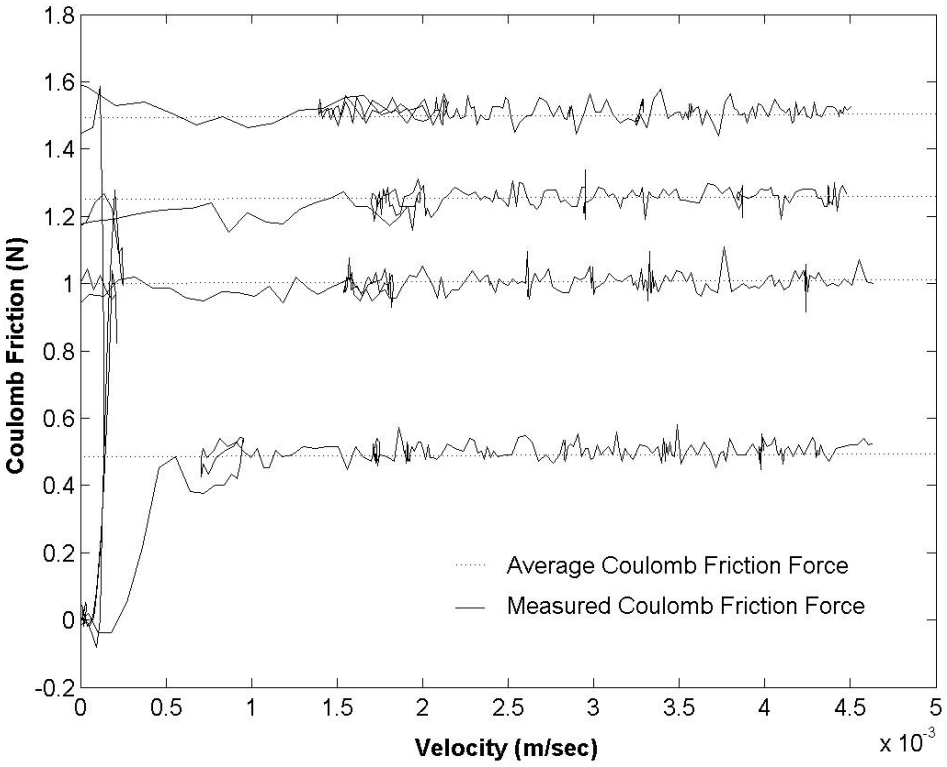

Figure 4.18 Simulation of increased coulomb friction in a PSV using Fault Simulator

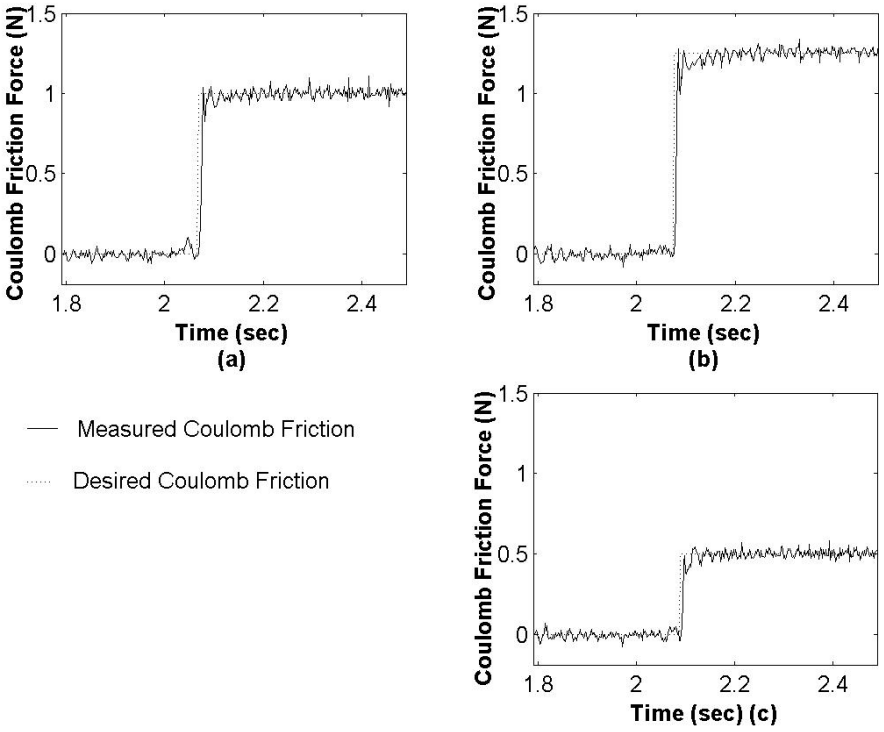

Figure 4.19 Desired and measured coulomb friction [(a) 1N (b) 1.25 N (c) 0.5 N]

4.3.3.2 Viscous Friction

Viscous friction is that component of the classic friction model, which changes in direct proportion to the velocity of the spool. The ratio of the viscous friction force to the velocity is commonly known as the damping co-efficient, and is mainly dependent on the viscosity and the temperature of the oil. Due to oil contamination, the viscosity of oil tends to increase which in turn increases the damping co-efficient. The fault simulator was used to simulate this condition of increased damping co-efficient by increasing the force applied by the Solenoid B in proportion to the spool velocity. By linearly increasing the velocity of spool, the effect of the damping co-efficient on the viscous friction force can be clearly observed at higher velocities.

Since only unidirectional friction forces were simulated; only the 0 to +5mm/sec part of the linearly increasing velocity profile was used for inducing the desired viscous friction characteristics. When the velocity of the spool crosses the velocity threshold for sliding friction (0.05 mm/sec), the product of the spool velocity and the desired damping co-efficient was used as the desired input to the PI controller. The controller employed the modified force feedback from the transducer, as described earlier in 4.1.1, to control the desired damping co-efficient.

Figure 4.20 (a) depicts the desired and actual response of Solenoid B which was used to simulate the effect of viscous friction. The desired values of damping friction co-efficient that were simulated were 10, 50, 100 and 300 N-sec/m and can be that as the desired damping co-efficient is increased, the slope of the measured viscous friction was able to track it accurately. The ability of the controller to track the desired damping force is best observed when plotted as a function of velocity as shown in Figure 4.20 (b). It can be seen that as the velocity was increased linearly from 0 to 5 mm/sec, the corresponding damping force induced also increases from 0 to 0.05, 0.23, 0.5 and 1.5 N for curves IV, III, II and I respectively. This corresponds to a gradient of 10, 50, 100 and 300 N-sec/m respectively which were the desired values of damping induced.

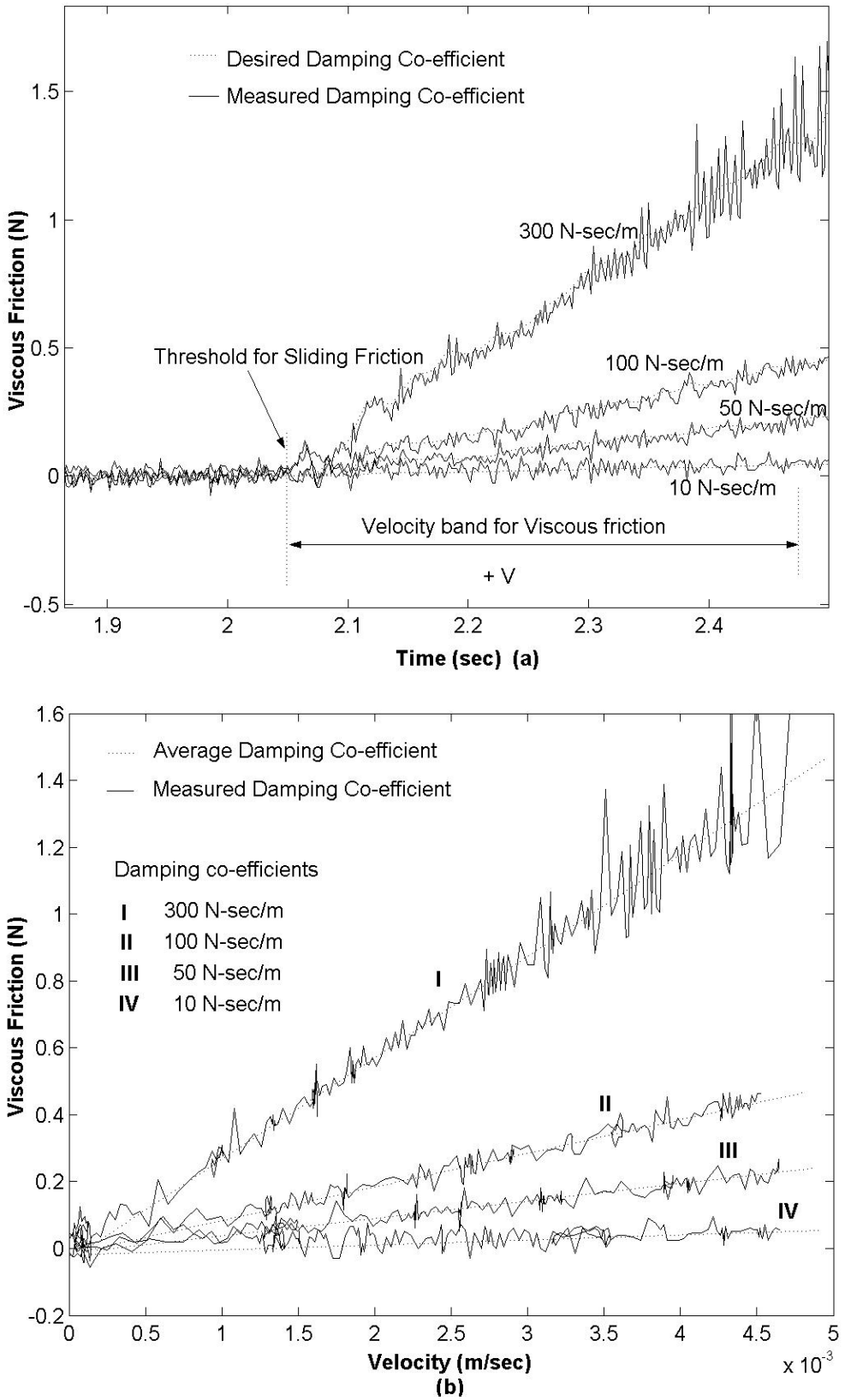

Figure 4.20 Simulation of increased damping co-efficient in a PSV using Fault Simulator

4.3.3.3 Combined friction

The ability of the fault simulator to produce the individual components of the classical friction curve, i.e., Static, Coulomb and viscous friction, was presented earlier. This section examines the ability of the fault simulator to amalgamate the three friction components to produce the effect of the classical friction force in the PSV.

Most mechanical systems exhibit either static and sliding friction or only sliding friction, depending upon the level of boundary lubrication prevailing between the contact surfaces [Armstrong, 1994]. If the lubricant provides little or no boundary lubrication, the classical friction curve with static and sliding friction is obtained. With substantial boundary lubrication and with certain additives in lubricant the static friction can be reduced to the level of sliding friction. Based on this observation, two cases that were simulated; one in which the Static friction is greater than the Coulomb friction and other in which the level of Static friction is same as that of sliding friction.

Figure 4.21 depicts the case where only the Coulomb and viscous friction were induced in the valve to simulate the case where the static friction is reduced to the level of sliding friction. After the spool reversal position, when the velocity is greater than 0.05 mm/sec, a Coulomb friction of magnitude 1 N and viscous friction of damping co-efficient 50 and 100 N-sec/m were induced in the valve. It can be observed that the Coulomb friction instead of being a step function appears to be a curve, which is due to the rise time of the solenoid of 0.03 sec. Moreover, it appears that one of the curves tend to lag behind the other , which was attributed to the vagaries of the sampling instant due to difference in sampling time due to which one of the step functions for Coulomb friction is initiated later than the other.

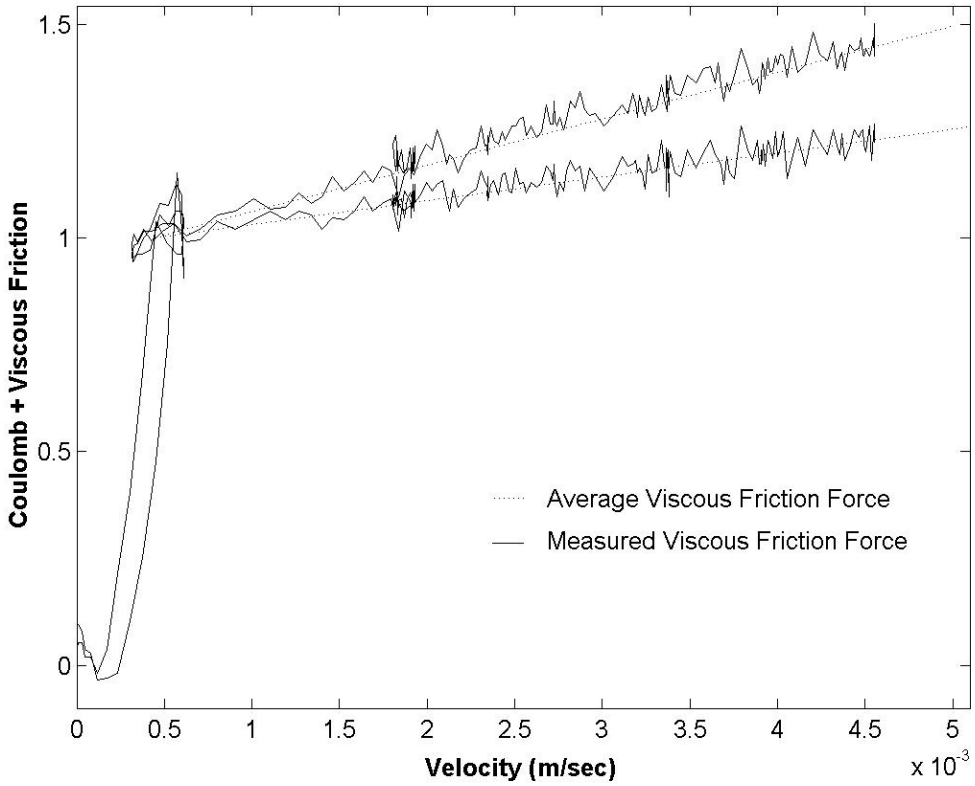

Figure 4.21 Simulation of increased Coulomb and viscous friction in a PSV

The second case where the stiction is greater than the sliding friction is depicted in Figure 4.22. The magnitude of static and Coulomb friction was kept at 1 N each, while three different damping co-efficient values of 50,100,300 N-sec/m were induced in the PSV. It can be observed that the curves exhibit the characteristics similar to the classical friction curve, especially the stribeck effect wherein the friction characteristics exhibit a drop in magnitude with increasing velocity. It was observed that the velocity of spool increased marginally in the region where Static friction was induced. This effect was desirable due to the fact that in actual situations, the surface asperities of the two surfaces in contact tend to deform under the applied load and exhibits marginal increase in velocity [Dahl, 1977].

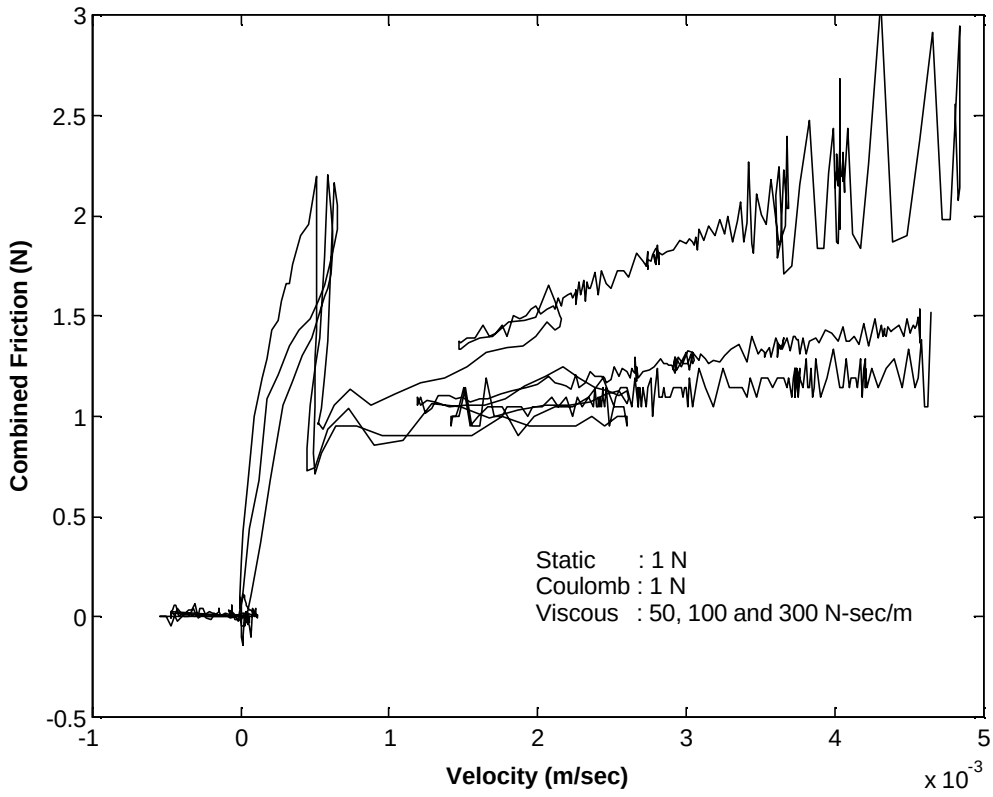

Figure 4.22 static, Coulomb and viscous friction induced in a PSV

4.4 Evaluation using a simple condition monitoring technique

The earlier sections described the ability of the fault simulator to induce different magnitudes of friction force by using a closed loop force control system using a force transducer as the feedback element. The normal force characteristics of the valve were subtracted from the force characteristics of fault simulator to obtain the net force added by the fault simulator. Though this serves as one means to measure the increase in friction characteristics it would not be a practical choice since this arrangement requires an added attachment to the valve in the form of a force transducer. For condition monitoring of any system it would be desirable to utilize the existing sensors to detect any abnormality in the characteristic variable.

This section describes a simple method of analyzing the fault simulator for its ability

to induce faults in the valve as well as serve as a rudimentary CMS. Since the input signal to the solenoid is current which is also responsible for force generation, it was deemed to be a prudent choice to select current as the candidate parameter for fault evaluation. A change in current characteristics from the normal behavior at any spool position would serve as an indication of a progressing fault. The artificial friction force induced by the fault simulator results in an increase in current drawn by the Solenoid A to drive the valve spool. These three friction components will have a unique current signature, which will determine the type of friction fault being developed. This is based on the assumption that only one type of fault i.e., friction, occurs at any given time in the valve.

Since high level of stiction in the valve generally results in stalling of the spool, it is apparent that the position control system will try to draw the full current available in order to drive the spool to the desired location. Figure 4.23 (a) depicts this particular scenario, where the fault simulator induces a stiction force as shown previously in the Figure 4.15. It can be seen from Figure 4.23 (a) that at the spool reversal position where the stiction fault has been induced, the current in Solenoid A increases rapidly and approaches the saturation limit of 2.5 amperes. As mentioned previously the most common failure is due to stiction, when the spool sticks at one position and the solenoid continues to draw full current as shown in the Figure 4.23 (a), thereby burning out the solenoid coil if used for longer periods. Such sudden increase in current characteristics could be used a fault signature for identifying the stiction faults.

Similarly, the effect of inducing stiction of different magnitudes shown previously in Figure 4.16, results in a momentary increase in current drawn by Solenoid A as depicted by the spike in current characteristics of Figure 4.23(b).

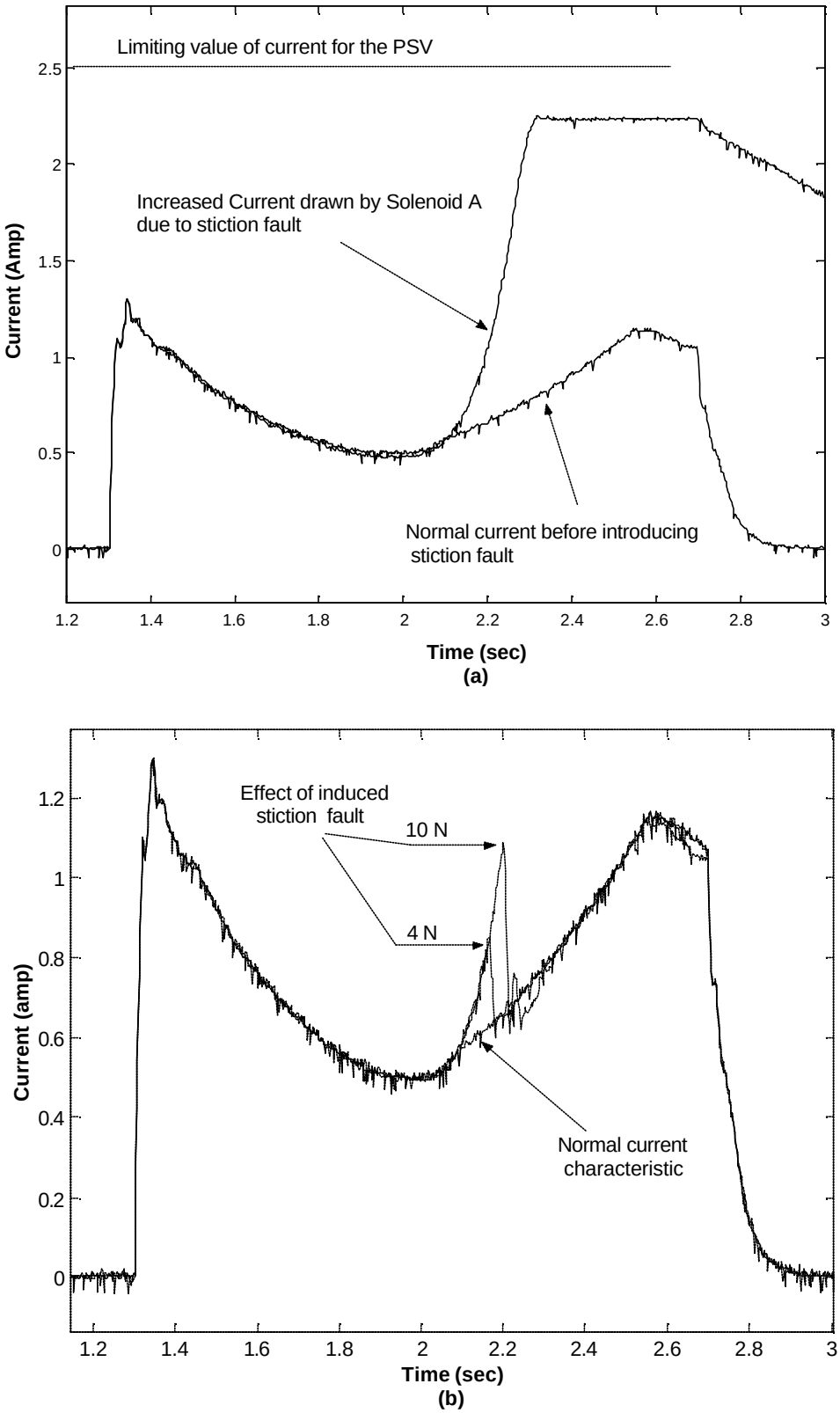

Figure 4.23 Effect of increase in static friction on the current drawn by Solenoid A

Increased Coulomb friction normally results in a step change in the force characteristics as shown previously in Figures 4.18 and 4.19. Similarly it results in a step change in the current characteristics of the Solenoid A as shown in Figure 4.24. Two different levels of Coulomb friction force, i.e., 1 and1.5 N are simulated which results in a different level of current being drawn by the Solenoid A. The current abruptly changes from the normal value to a new level, at the spool reversal position after inducing the faults. This is due to the characteristics of the Coulomb friction force which is associated with an abrupt increase after the zero velocity position. Thus an abrupt step change in current near spool reversal positions could possibly be used an indication of a change in Coulomb friction.

A change in the viscous friction is manifested by an increased slope of the viscous friction force as was shown in Figure 4.20. To overcome this increase in the force gradient, there is a corresponding increase in the current gradient of Solenoid A. Figure 4.25 depicts the change in the slope of current characteristics after the fault simulator induced a fault characteristic indicative of increased viscous friction. It was noted during the experiments that low values of viscous friction did not cause a noticeable change in the gradient of current characteristics hence higher values of viscous friction were induced in the valve. Figure 4.25 shows the gradient change due to damping co-efficient of 300 and 500 N-sec/m and it can be seen that the current gradient increases sharply after the reversal position for the 500N-sec/m case.

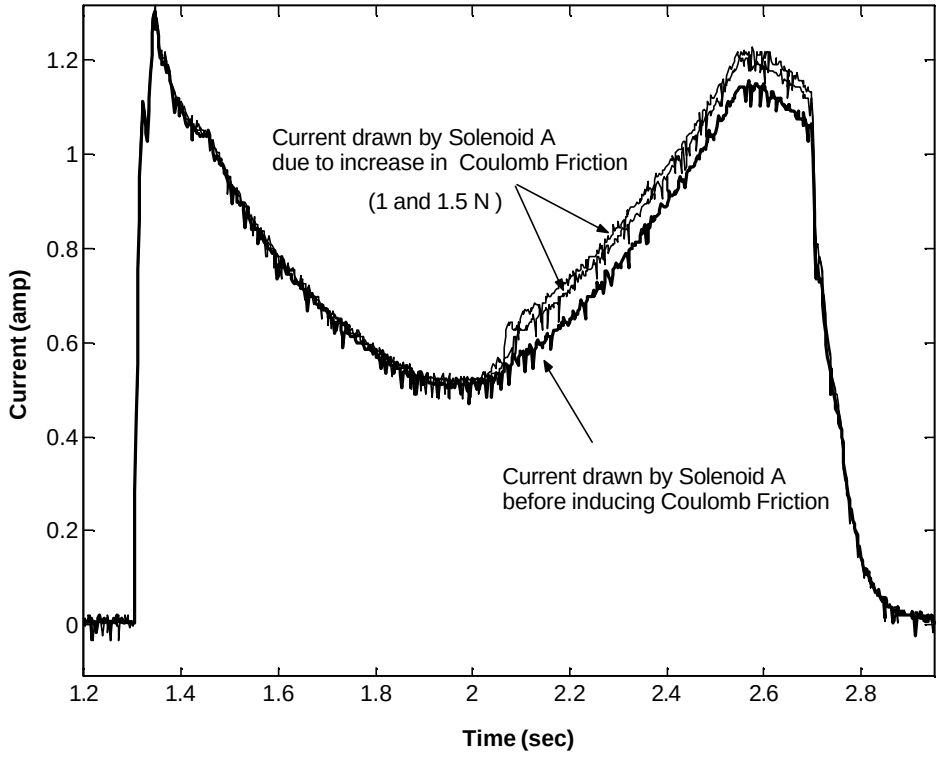

Figure 4.24 Effect of increased Coulomb friction on the current drawn by Solenoid A

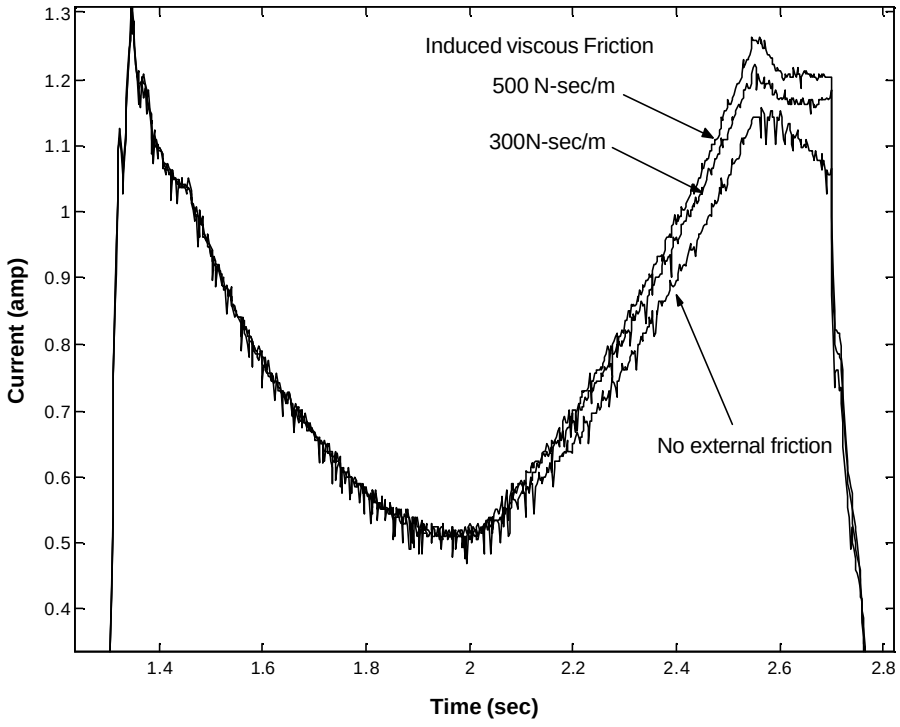

Figure 4.25 Effect of increased viscous friction on the current drawn by Solenoid A

Figure 4.26 shows the effect of combined Coulomb and viscous friction on the current characteristics of Solenoid A. Due to the Coulomb friction, the current abruptly changes to a new level after the spool reversal position and thereafter the gradient of the current characteristics increases due to the increased viscous damping. The Coulomb friction was increased to 1 N and viscous friction magnitudes of 100 and 500 N-sec/m were induced in the PSV.

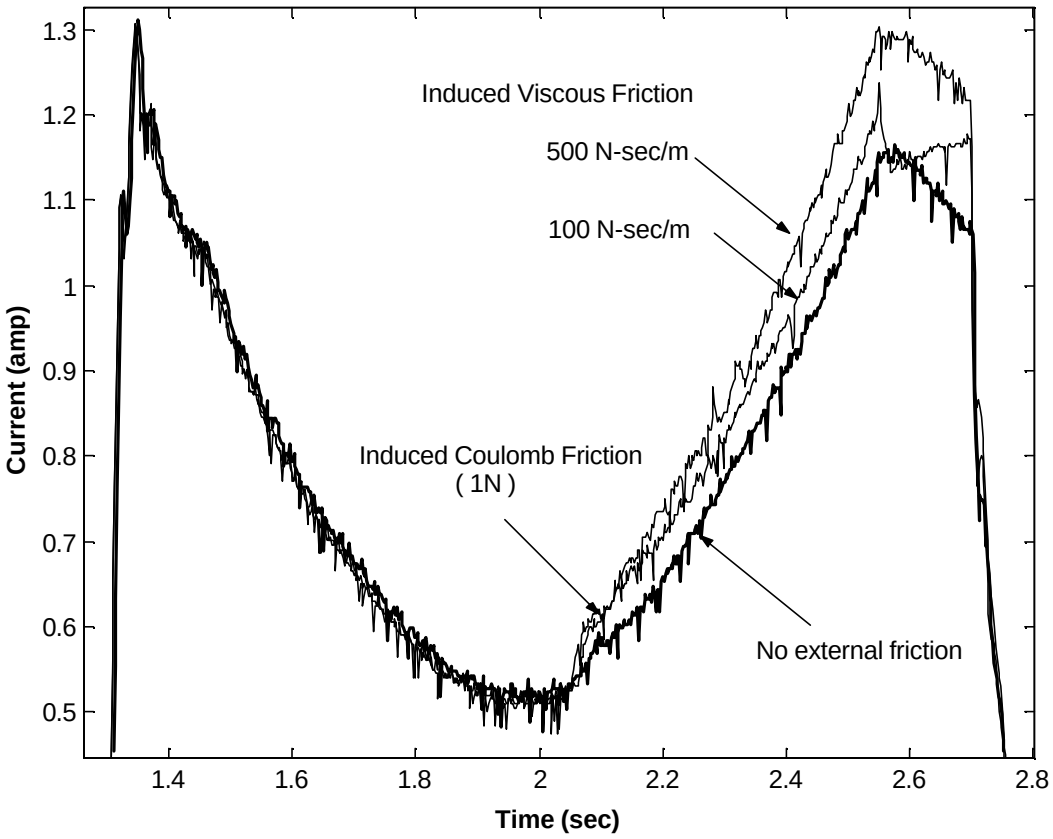

Figure 4.26 Effect of simulated increase in coulomb and viscous friction on the current drawn by Solenoid A

The effect of all the three friction components on the current drawn by Solenoid A is depicted in Figure 4.27. It can be observed that the stiction fault causes a spike in the current characteristics after the spool reversal position. This is followed by the Solenoid A drawing more current than normal to compensate for the effects of induced Coulomb and viscous friction faults. The effect of inducing higher damping co-efficient results in an

increased slope of the current characteristics after the momentary increase in current due to stiction fault.

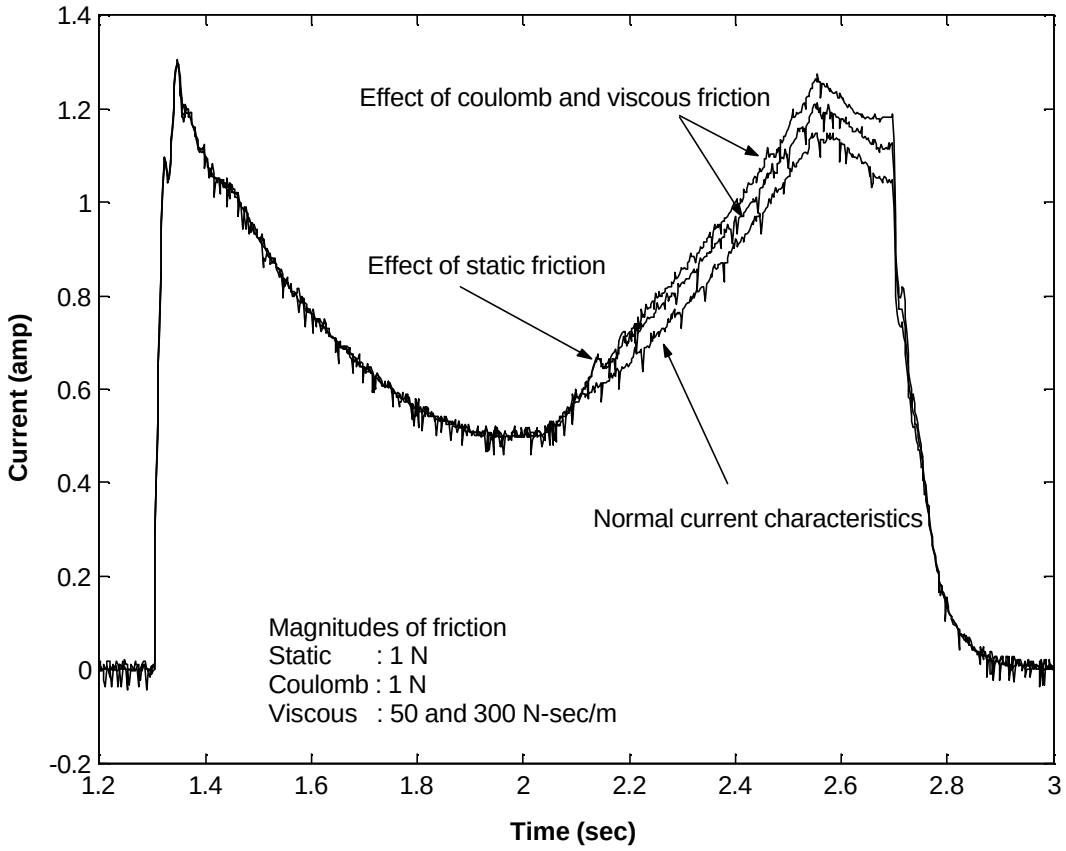

Figure 4.27 Effect of combined friction on current in Solenoid A

4.5 Summary

The ability of the fault simulator to artificially induce increased stiction, Coulomb and viscous friction was presented in this chapter. Since each of the friction characteristics exhibited unique characteristics, depending on the magnitude of the spool velocity, a position controller was designed to move the spool along a linear velocity profile. The friction faults were induced using a force controller which was designed experimentally by employing a feedback from a force transducer. The fault simulator was able to accurately induce the individual components of static, Coulomb and viscous friction as well the combination of the three thereby successfully simulating the classical friction

curve. An examination of the current characteristics of the Solenoid A was presented which provided useful information regarding the ability of the fault simulator to induce the faults. In all the cases of the faults simulated, the current characteristics depicted unique characteristics associated with each fault and can be used as a diagnostic tool for gauging the health of the valve.

Chapter 5

Conclusions and Recommendations

5.1 General

The objective of this research was to develop a non-destructive fault simulation technique for artificially inducing friction characteristics in a PSV. It was also desired that the proposed arrangement be cost effective and be able to reliably and repeatedly induce the faults in the PSV.

The hydraulic valve consisted of two proportional solenoids on opposite sides of the valve spool by which, bi-directional position control could be achieved. During the normal operation of the valve, only one of the solenoids is used at any given time, thereby rendering the other solenoid redundant. This research attempted to exploit this redundancy by using the solenoid for generating faults, thereby making the proposed arrangement cost effective. Moreover, rather than modifying the components of the valve by machining or by adding contaminants to the oil to introduce faults (which are destructive techniques), this research focused on simulating the effect of particular faults by reproducing the force characteristics that constitute the fault. Since a solenoid was used to produce the fault characteristics, this arrangement resulted in no damage to the original system and thus proved to be a non intrusive method.

Since the friction force is a function of linearly increasing velocity, one of the solenoids was used to move the spool along a parabolic displacement profile which resulted in a linearly increasing velocity map. In order to simulate the desired force characteristics, a force control system was employed on the other solenoid which used the force transducer in the feedback loop to achieve a closed loop control of the desired friction characteristics. Three types of friction characteristics (stiction, Coulomb and viscous) were induced in the valve depending upon the velocity regime of the spool.

When the valve spool reversed direction while traversing the parabolic displacement profile, the velocity of the valve spool was reduced to zero, and the spool was momentarily stopped due to its inherent stiction. At this instant, a certain amount of current was passed through the solenoid on the opposite end of the valve spool, which resulted in canceling out the driving force on the valve spool. Due to the absence of any driving force the spool was stalled at the desired location, thus achieving the same effect as that of stiction at low velocities.

At higher velocities the Coulomb friction was induced by using a step function, the magnitude of which represented the desired value of coulomb friction to be induced. The viscous friction was simulated by multiplying the velocity of the spool by a desired damping co-efficient. Since the force produced by the solenoid was proportional to the input current, a current amplifier was used for all the tests which allowed for accurate control of the desired friction force characteristics.

5.2 Conclusions

1. The fault simulator developed in this thesis is capable of accurately reproducing the friction characteristics responsible for faulty operation of a PSV. Three types of friction characteristics were induced in the valve with varying levels of friction force to represent the different magnitudes of faults. Since a high level of stiction at any location in the PSV normally results in the stalling of the spool at low velocities, experimental tests were carried out to reproduce this fault by passing the same amount of current to both solenoids in order to cancel the driving force on the valve spool. It was also observed that the centering spring force remained unbalanced for spool displacements in the working range (0-3 mm), hence an algorithm was implemented to compensate for the spring imbalance. This technique resulted in successfully stalling the spool at the desired location. In many situations the spool may or may not jam each time it passes a problem location. For example, when the spool is traveling at high speed, it may pass the problem location without difficulty.

To simulate this effect, the current to the Solenoid B was cut off after the friction force reached a predetermined level. In this way it was also possible to reproduce the conditions when static friction may not necessarily stall the spool. Both the stiction tests were induced with a high degree of repeatability and it is surmised that this technique can be used in any PSV for inducing the desired stiction characteristics.

2. The PI controller used for the fault simulator can accurately control any desired Coulomb friction value up to a magnitude of 1.5 N. It was observed that the controller was able to successfully induce the Coulomb friction characteristics up to 1.5 N without any negative overshoot of the spool position. When Coulomb friction forces greater than1.5 N were induced, the measured force exhibited excessive overshoot from the desired values which resulted in moving the valve spool in its reverse direction. A derivative controller was added to remove the overshoot, but resulted in stability problems due to the noise contained in the measured force signal and hence was not pursued further. The gains of the PI controller were readjusted to achieve a better response and it was observed that a controller with nonlinear gain structure could be used if a large range of Coulomb friction values needs to be simulated.

3. The fault simulator can induce viscous friction up to a magnitude of 300 N-sec/m. At higher magnitudes and velocities greater than 5 mm/sec an unacceptable disturbance occurs. This was observed when a damping co-efficient of 500 N-sec/m and a velocity of 5 mm/sec was reached. In this situation the fault simulator was unable to maintain a steady state value and exhibited large oscillations. Since the PI controller was designed for a certain range of force control, it was concluded that a nonlinear PI controller with a variable gain structure could be implemented to reduce the oscillations and enable a larger range of damping forces to be induced.

4. The fault simulator used in this research was capable of emulating the friction characteristics of the classical friction model. The classical friction model comprised of two friction curves which are inverted mirror images of each other about the zero

velocity region. The fault simulator utilized this concept of symmetry of the friction curve about the reversal point to induce only unidirectional frictional faults in the valve. To induce the unidirectional friction faults one of the existing solenoids in the valve was used which made the system cost effective. This otherwise would have required an expensive push-pull solenoid to generate the friction characteristics in both the directions of spool travel.

5.3 Recommendations

The fault simulator used the velocity of the spool as a reference signal for determining the type of friction to be simulated. The velocity signal was obtained by differentiating the spool position which induced considerable noise in the signal and had to be filtered out before being used for the fault simulator. The result of filtering was that it induced a delay which was undesirable. It is recommended that an accelerometer be used for future work. This would result in much less noise since the velocity signal would be obtained by integration of the acceleration signal. It was observed that a delay of 0.025 seconds resulted because of filtering. This is in the same range as the natural frequency of the valve. The delay could be of significance when simulating viscous friction at higher velocities, since the actual system velocity could be higher than that which is used by the fault simulator algorithm, making the system controller unable to produce the required damping co-efficient. Using an accelerometer would ensure that the velocity signal is not delayed and would result in better dynamic performance of the fault simulator at higher velocities.

The CMS described in this thesis was a rudimentary technique used to validate the effectiveness of the fault simulator in inducing different types of friction faults. Other CMS have been developed for PSV's which employ sophisticated algorithms like neural networks and statistical analysis for fault detection and analysis [Mourre et al, 2001]. The fault simulator can be easily integrated with these CMS to ensure better fault detection capability of the CMS and would be an interesting area for future work.

References

(1) Azzam, H., and Hazell, J., 1996, "Appraisal of Advanced Diagnostic Strategies Using a Suite of Helicopter Fault Simulations", Proceedings of Condition Monitoring and Diagnostic Engineering Management (COMADEM), University of Sheffield, UK, 43-50.

(2) Armstrong-Hélouvry, B., Dupont, P., and Canudas De Wit, C., 1994, "A survey of models, analysis tools and compensation methods for the control of machines with friction, Automatica, Volume 30, Issue 7, 1083-1138

(3) Badi, M., Engin, S., and Schonfeld, D., 1996, "Fault Classification of a Model Drive Line Using Time Domain data", Proceedings of COMADEM, University of Sheffield, UK, 43-50.

(4) Burton, R., Mourre, D., and Bitner, D., 2001, "Investigation of a Neural Network/Statistical Condition Monitoring Technique for a Proportional Valve", Proceedings of the Bath Workshop on Power Transmission and Motion Control, - PMTC 2001, University of Bath, UK.

(5) Dahl, R., 1977, "Measurement of Solid Friction Parameters of Ball Bearings", Proc. of 6th Annual Symposium on Incremental Motion, Control Systems and Devices, University of Illinois.

(6) Fey, C., 1987, "Identifying Component Wear through Metallurgical Analysis", Proceedings of the 42nd National Conference on Fluid Power, Chicago, Illinois, USA, 221-232.

(7) Haessig, D, Jr. and Friedland, B., 1991, "On the Modeling and Simulation of Friction", ASME Journal of Dynamic Systems, Measurement and Control, Vol. 113, 354-363.

(8) Haibin, W., Shiqiang, Z., and Ying, C., 2001, “Research of Hardware-In-The –Loop Simulation Testing for Offshore Platform with Bucket Foundation on Raising and Lowering”, Proceedings of the Fifth International Conference on Fluid Power Transmission and Control, Hangzhou, China.

(9) Heron, R., and Huges, M., 1986, “A Contaminant Monitor for Fluid Power Applications”, International Conference on Condition Monitoring, Brighton, UK, 57-71.

(10) Inerny, S., and Hardman, B., 2002, “Investigation of Fault Detection Algorithms Applied to a Helicopter Input Pinion Bearing ”, Proceedings of 15th International Congress on Condition Monitoring and Diagnostic Engineering Management (COMADEM), Birmingham, UK, 319-329.

(11) Karnopp, D., 1985, “ Computer Simulation of Slip-Stick Friction in Mechanical Dynamic Systems”, ASME Journal of Dynamic Systems, Measurement and Control, Vol. 107, 100-103.

(12) Khoshzaban-Zauarehi, M., 1997, "On-Line Condition Monitoring and Fault Diagnosis in Hydraulic System Components Using Parameter Estimation and Pattern Classification", Ph.D Thesis, Department of Mechanical Engineering, The University of British Columbia, Canada.

(13) Kumar, A., Kumar, V., and Hara, U., 1996, “Effective failure Analysis of Gas Turbine – A Need of Improved Monitoring System ”, Proceedings of Condition Monitoring and Diagnostic Engineering Management (COMADEM), University of Sheffield, UK, 43-50.

(14) Martin, M., 1997-2000, “ Development of Monitoring and Diagnostic Methods for Robots Used in Remediation of Waste Sites” US Department of Energy, Project Number: 60040, http://www.osti.gov/em52/final_reports/60040.pdf

(15) Martin, M., 1992, “Analysis, Design and Compensation of a Computer Controlled Hydraulic Load Simulator”, ASME winter Annual Meeting, Anaheim, CA, Paper #92-WA/FPST-5.

(16) Nandi, A., 2002, “Vibration Based Fault Detection- Features, Classifiers and Novelty Detection”, Proceedings of 15th International Congress on Condition Monitoring and Diagnostic Engineering Management (COMADEM), Birmingham, UK, 23-35.

(17) Nimegeers, C., Schoenau, G. and Burton, R., 1996, “A Computer Controlled Hydraulic Loading System for Simulating Loads”, Proceedings of the Ninth International Fluid Power Workshop, University of Bath, UK.

(18) Ohuchi, H., and Ikai, H., 1989, “Control of a Load Simulator”, Proceedings of the JHPS International Symposium on Fluid Power, Tokyo, Japan.

(19) Ramden, T., Janson, A., and Palmberg, J., 2000, "Design and Analysis of a Load Simulator for Testing Hydraulic Valves", 10th Bath Workshop on Power Transmission and Motion Control, Bath, UK, 15-18.

(20) Raw, I., and Hunt, T., 1987, “A particle Size Analyzer Based on Filter Blockage ”, Proceedings of an International Conference on Condition Monitoring, Swansea, UK, 875-894.

(21) Rosa, A., Mourre, D., Burton, R., and Bitner, D., 2000, “Estimating Parameters in a Proportional Solenoid Valve”, Bath Workshop on Power Transmission and Motion Control- PMTC 2000, University of Bath, UK

(22) Schoenau G., Burton R., and Ansarian A., 2001, “Parameter Estimation in a Solenoid Valve using the ML and OLS Techniques”, 2001, Proceedings of the 5th International Conference on Fluid Power and Transmission, Hangzou, China, pp 124-129, March 2001

(23) Tan, A., Chua, P., and Lim, G., 2003, “Fault Diagnosis of Water Hydraulic Actuators Under Some Simulated Faults”, Journal of Materials Processing Technology, 123-130.

(24) Wright, G., 2000, “Parameter Estimation of a Hydraulic Proportional Valve using Extended Kalman Filtering”, Msc Thesis, University of Saskatchewan, Canada

Appendix A

A.1 Calibration of the Data Acquisition System

The DAQ includes a data acquisition board (Keithley Metrabyte -DAS 16) and an I/O connector block. They are connected by a "ribbon cable". The DAQ has 16 single-ended (eight differential) analog input channels and 2 single-ended analog output channels, and has a sampling frequency of 200 kHz. The resolution for the analog input/output is 12 bits.

The DAQ can measure and condition the input signals which are stationary but cannot compensate for time varying effects.

A.1.1 Calibration of analog input channels

In the calibration procedure, voltages are applied to the analog input and the input voltage from the DAQ via the computer recorded. Preliminary results indicated that a DC bias and a non-unity gain existed in the DAQ. The system gain was reset to achieve a unity gain as shown in Figure A.1.1 In this figure, as in subsequent ones, the "error" is defined as the difference between the measured output voltage (after adjustment) and a "best fit" line which constitutes the "calibration equation".

The scatter of measured data with respect to the calibration best fit line falls within a region of ±0.015 V (0.15% full scale). It was observed that after the adjustment to the DAQ, the calibration best fit line was the same for all channels. In addition, tests were repeatable with no visual difference.

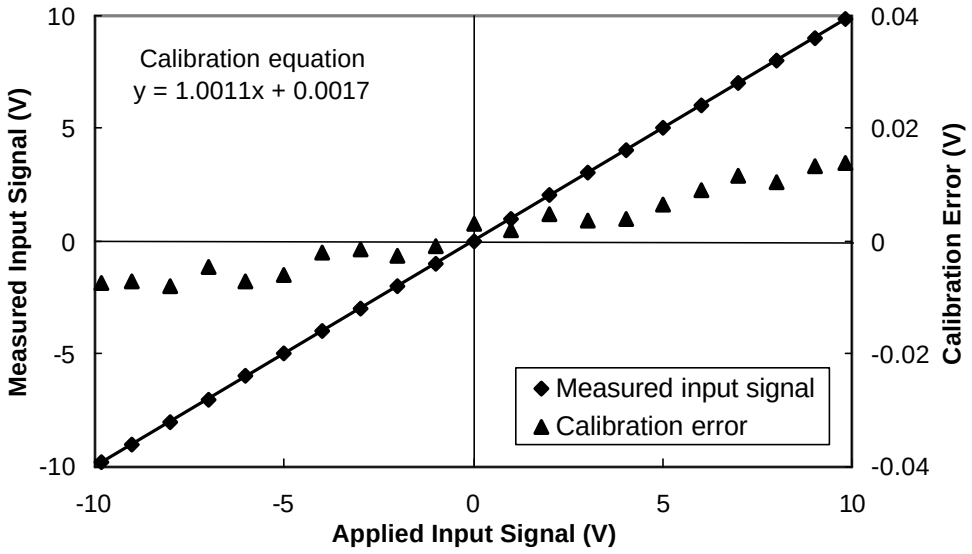

Figure A.1 Calibration of analog input

A.1.2 Calibration of analog output channels

The calibration procedure of the DAQ analog output was as follows: Voltages were generated by the computer and directed through the DAQ to each analog output channel. The output voltages were measured at the terminal end of the connector block using a highly accurate multimeter (Fluke 37, 0.1% full scale).

Similar to the input, a bias and a non-unity gain were observed. The DAQ was adjusted and the calibration procedure repeated. The results are shown in Figure A.3 along with the error. It is noted that a maximum error of 0.008 V (0.08% full scale) was observed. The test was repeated for each channel and the same calibration equation occurred. The test was highly repeatable with no visual difference in the results.

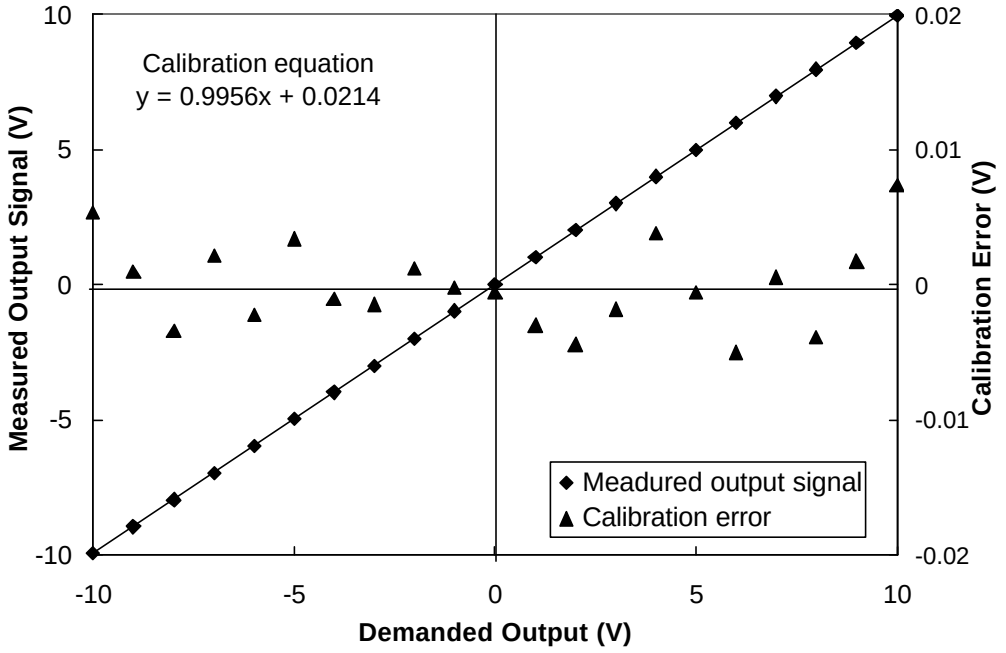

Figure A.2 Calibration of analog output

A.2 Force Transducer Calibration

In order to generate the desired friction force on the valve spool, the force generated by Solenoid B had to be measured and fed back to the computer for closed loop force control. A strain gauge type force transducer (GSE Model-5341) was installed between the Solenoid B and the valve spool, to measure the solenoid force acting on one of its end.

The force transducer has the strain gauges in a wheatstone bridge configuration. When force is applied on any of the arms of the wheatstone bridge, it changes the resistance of the strain gauge by compressing or pulling it. This causes a change in the output voltage from the bridge, which is proportional to the applied force. A series of calibrated deadweights, in increments of 0.5 lbs were applied on one end of the transducer. The output voltage was amplified by using a high bandwidth amplifier (Measurements Group- 2310 Signal Conditioning Amplifier) with the amplifier gain set to 1000.The excitation voltage to the wheatstone bridge of the transducer was set to 10 volts DC. The output voltage from the amplifier is as shown in Figure.A1.

As seen from the figure the calibration error lies with +0.002 and –0.0025 volts, which is insignificant for the tests carried out in this research. Based on the results of Figure A1, the force output for corresponding voltage was predicted using the model as shown in Figure A2. This model was used to predict the force exerted by Solenoid B on the transducer and hence on the spool of the valve. As shown in the figure, for most part the calibration error is 0.006 lbs, which was quite insignificant for this research.

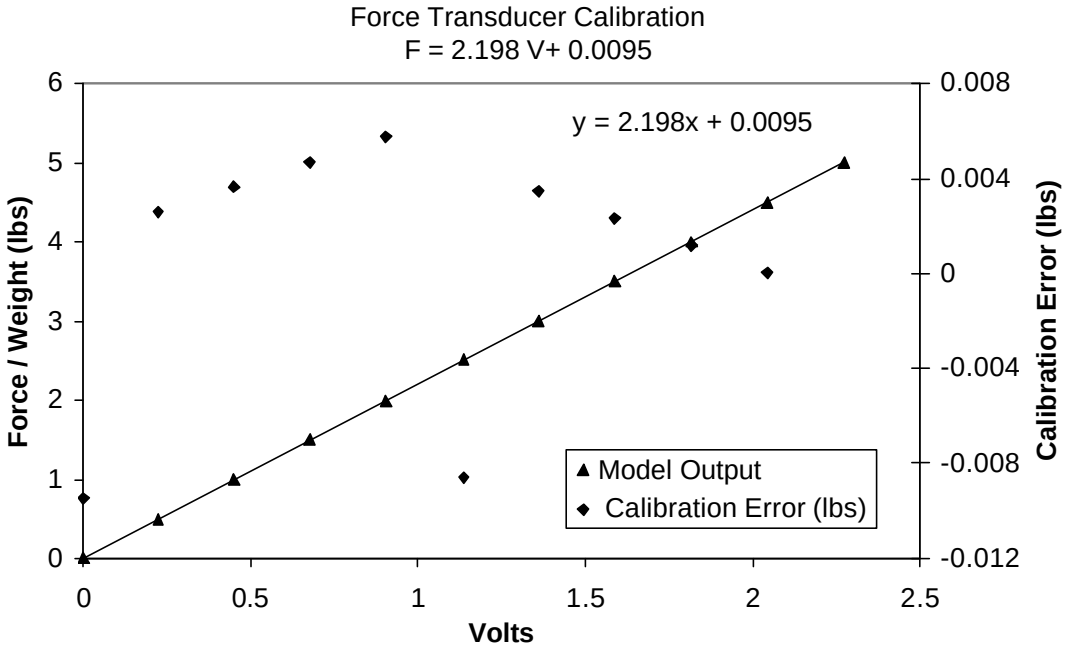

Figure A.3 Calibration of force transducer

A.3 Current Meter Calibration

The Current Probe Amplifier (Current Meter) is used to measure the current passing through the solenoid coils. An AM503 Tektronix Current Probe Amplifier comprises of a probe, which measures the magnetic flux in a current carrying conductor and an amplifier which outputs voltage proportional to the current associated with flux.

To calibrate the Current Meter the output of a signal source was fed through an power op-Amp which in turn was passed through an potentiometer having large current carrying

capacity. The probe was hooked to one of the wires into the potentiometer to measure the current passing through the circuit. A multimeter was connected in series with the circuit to accurately measure the current and compare it with the reading from the current meter, thus indicating the calibration error, as shown in figure A3.

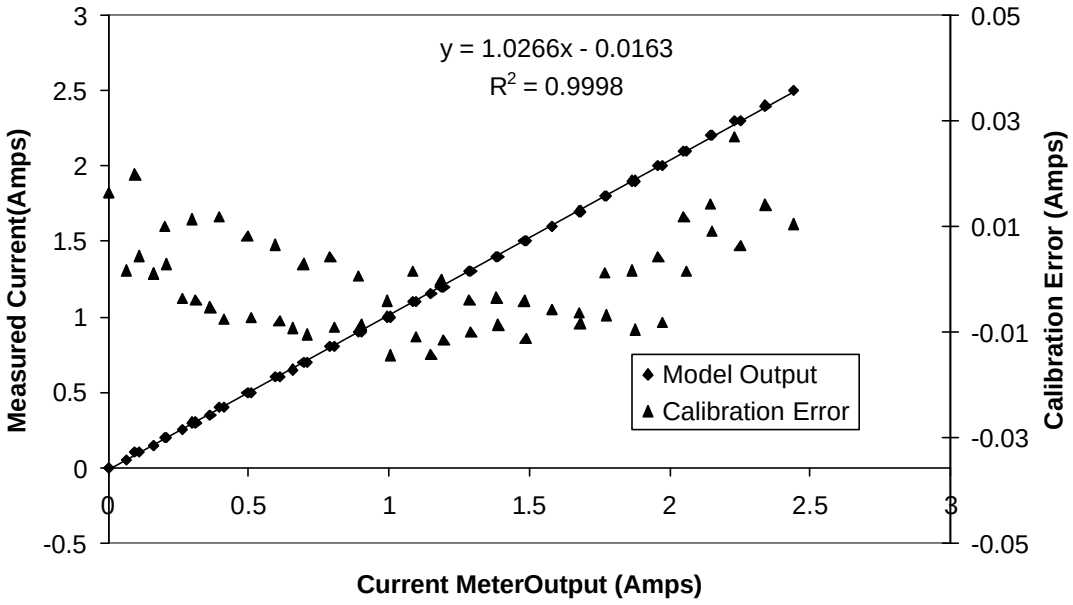

Figure A.4 Current Meter Calibration

Based on the measured current from multimeter and the reading from the current meter a model which best fits the data range and which gives minimum absolute error is selected. As shown in the figure A3, for most part of the experiment the calibration error lies within +- 0.015 amps, which was acceptable for this research as the maximum permissible current through the solenoid coil is 2.5 amps.

A.4 Calibration of LVDT

An LVDT integral to the valve was used for measuring the spool position during all the experiments doe this research. A 24 volt DC power supply was used as an excitation signal to the LVDT through a valve amplifier provided by the manufacturer.

The LVDT was calibrated by connecting the magnetic core to a micrometer which

was moved in increments of 0.25 mm and the corresponding voltage through the LVDT output measured using a high resolution Fluke multi meter. The calibration was carried out by starting from one end of the spool displacement i.e. 3mm and moving the micrometer in increments of 0.25 mm up to a maximum of 6.5 mm covering the total range of spool displacement of +-3mm i.e. 6 mm. The resolution of the LVDT was calculated as 0.312 mm/volt or 0.000312 m/volt.

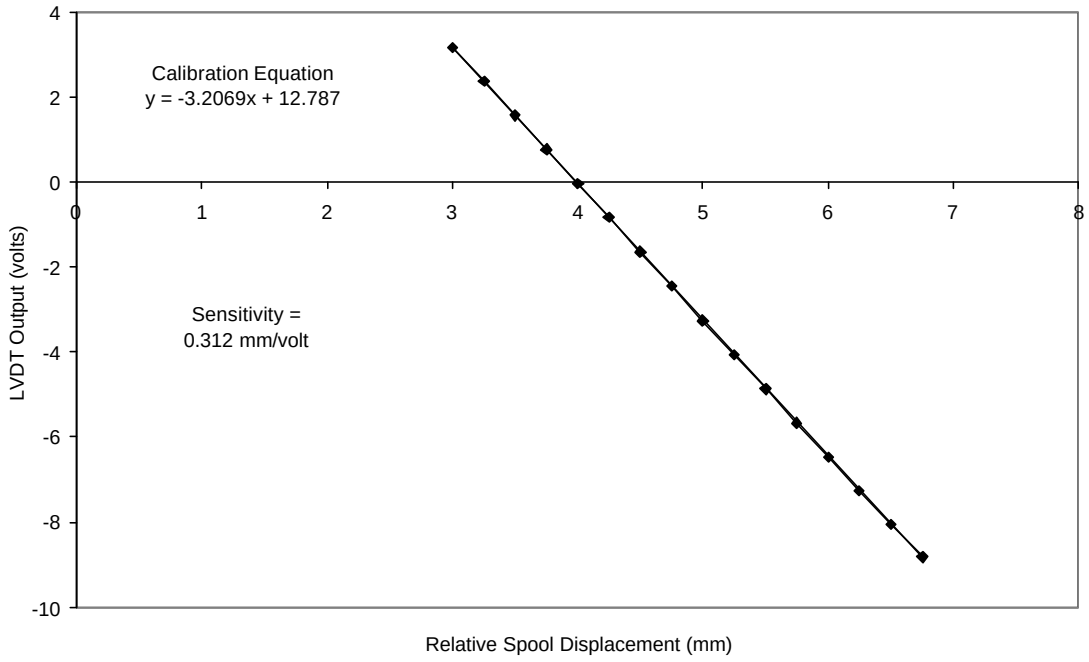

Figure A.5 Calibration of LVDT